Winter 2015

Structure-activity relationships for the water-gas shift reaction over supported metal catalysts

Kaiwalya D. Sabnis
Purdue University

Graduate School Form 30
(Revised 08/14)

PURDUE UNIVERSITY
GRADUATE SCHOOL
Thesis/Dissertation Acceptance

This is to certify that the thesis/dissertation prepared

By Kaiwalya D. Sabnis

Entitled Structure-Activity Relationships for The Water-Gas Shift Reaction over Supported Metal Catalysts

For the degree of Doctor of Philosophy

Is approved by the final examining committee:

Fabio H. Ribeiro

W. Nicholas Delgass

Jeffrey T. Miller

Bryan Boudouris

To the best of my knowledge and as understood by the student in the Thesis/Dissertation Agreement, Publication Delay, and Certification/Disclaimer (Graduate School Form 32), this thesis/dissertation adheres to the provisions of Purdue University's "Policy on Integrity in Research" and the use of copyrighted material.

Fabio H. Ribeiro

Approved by Major Professor(s): _____

Approved by: John Morgan 02/26/2015

Head of the Department Graduate Program Date

STRUCTURE-ACTIVITY RELATIONSHIPS FOR THE WATER-GAS SHIFT REACTION OVER SUPPORTED METAL CATALYSTS

A Dissertation

Submitted to the Faculty

of

Purdue University

by

Kaiwalya D. Sabnis

In Partial Fulfillment of the

Requirements for the Degree

of

Doctor of Philosophy

May 2015

Purdue University

West Lafayette, Indiana

To my parents, wife and rest of the Sabnis family

ACKNOWLEDGEMENTS

My journey as a graduate researcher for the past four and a half years has been very rewarding and fulfilling. I can proudly say that I have a sense of accomplishment from my time here at Purdue, and it has been possible due to the support I received from lot of people.

I am highly grateful to my parents (Late Mr. Dilips Sabnis and Mrs. Nalini Sabnis) for their love and support. They've made innumerable sacrifices to provide for their children and I could not thank them enough. I also thank rest of the Sabnis family for their belief in me and their unceasing encouragement. I owe a lot to my wife, Maithili, for the love and the moral support she has provided me throughout the course of my PhD. Our 'long distance' relationship has endured a lot for the past four years, but it was her confidence in me that has helped me succeed.

I have been immensely fortunate to have been advised by Prof. Fabio Ribeiro and Prof. W. Nichloas Delgass for my doctoral research. Prof. Ribeiro always ensured the availability of resources and means to achieve the best possible results. He has taught me to be meticulous and rigorous while performing experiments, which I believe are the qualities of an ideal experimentalist. His expertise in kinetic measurements and carbide

synthesis ensured that my projects are on the correct path. I thank him for giving me the opportunities to present my research work at number of reputed conferences. A true scientist has to think outside the box and critically analyze the data in hand. This was taught to me by Prof. Delgass. His passion towards research is truly inspirational. To summarize, my advisors have been instrumental in my success as a researcher. It feels proud to be the part of the 'Michel Boudart Academic Tree', and I am sure that all the other students advised by Prof. Delgass and Prof. Ribeiro resonate the similar feelings.

I would also like to thank Prof. Bryan Boudouris and Dr. Jeffrey Miller for being a part of my thesis committee. Prof. Boudouris provided me with valuable advice on written communication during my qualifying examination, which has helped me along the way. All the X-ray absorption experiment and the data analyses performed during the course of my PhD would have been impossible without the help and the guidance provided by Dr. Miller. His insights about the data have led to some very important conclusions from my research.

I would also like to extend my gratitude towards previous and current water-gas shift group member. I am grateful to Dr. Damion Williams and Dr. Mayank Shekhar for teaching me how to perform the kinetic experiments and data analysis and Dr. Jorge Pazmino and Dr. Wen-Sheng Lee for teaching me the catalyst synthesis methods used throughout my research. Dr. Paul Dietrich and Dr. Shane Bates have helped me with all my X-ray absorption experiments at Argonne National Laboratory. Dr. Fred Sollberger and I have had very fruitful collaborations while working on the correlation between the

aqueous phase reforming and the WGS reaction. I thank Dr. Cem Akatay for the beautiful and very informative electron microscopy images of the catalysts studied. I am very grateful to Yanran Cui for all the help he provided with the kinetic experiments. I also thank Dr. David Taylor and Dr. Yury Zvinevich for their help with troubleshooting various experimental units. Dr. Dhairya Mehta deserves a special mention for always being there as a sounding board for my ideas in research. I thank rest of the Ribeiro group members for their help and support when needed.

There have been times when research and coursework has led to frustrations, and it would have been impossible to sail through without the company of friends I have made here. My roommates and my very dear friends, Atish and Aniruddha have always been there for me in the time of need. Time spent with Dhairya, Harshavardhan, Karthikeyan, Anand, Krishnaraj, Anshu, Anirudh, Sumeet, Shankali and Ashish will be cherished forever.

Thank you very much, everyone!

TABLE OF CONTENTS

Page

Page

LIST OF TABLES

Table Page

LIST OF FIGURES

Figure Page

Figure Page

Figure Page

Figure Page

Figure Page

ABSTRACT

Sabnis, Kaiwalya D. Ph.D., Purdue University, May 2015. Structure-Activity Relationships for the Water-Gas Shift Reaction over Supported Metal Catalysts. Major Professors: Fabio H. Ribeiro and W. Nicholas Delgass.

The Water-Gas Shift (WGS) reaction ($CO + H_2O \rightarrow CO_2 + H_2$) has significant impact on the energy issues as it plays a pivotal role in hydrogen generation. Higher conversions can be achieved at lower temperatures, but lower temperatures result in lower reaction rates, so high performance catalysts are desired to speed up the reaction. The overall goal of this work is to develop a model-based approach to catalyst design that we call *Discovery Informatics,* which involves building a database with sufficient chemical and information diversity to allow identification of active sites, to model the kinetics and identify descriptors of the kinetic parameters. High throughput kinetic experiments and *in situ* characterization techniques are used in tandem to derive structure-activity relationships for various catalytic systems.

The first study focuses on WGS catalysis over molybdenum carbide (Mo_2C) and different transition metals supported on Mo_2C. A kinetic analysis was used to identify the descriptor for the promotion in the WGS rate over Mo_2C caused by metal promoters. The unsupported Mo_2C was prepared by temperature programmed carburization of

ammonium heptamolybdate in presence of 15% CH_4/H_2. Au was deposited using deposition precipitation and Pt, Pd, Ni, Cu and Ag by incipient wetness impregnation. High temperature reduction of molybdenum supported on Multi-Walled Carbon Nanotubes (MWCNTs) was used as an alternative route for Mo_2C synthesis, obviating the use of methane. The kinetic measurements were done in a plug-flow reactor configuration with CO conversions less than 10% at 7% CO, 8% CO_2, 22% H_2O, 37% H_2 at 1 atm total pressure. *In situ* X-Ray Absorption spectroscopy was used to study the interactions between admetals and the Mo_2C support and to observe the working state of the catalysts. The WGS rate per gram over Mo_2C (3×10^{-7} mol H_2 (g cat)$^{-1}$ (s)$^{-1}$) is comparable to that of commercially used $Cu/ZnO/Al_2O_3$ catalyst at 120°C. This rate is promoted by the addition of Pt (6 times), Au, Pd (4.5 to 5 times) and Ni (3 times) and is unaltered by Cu and Ag. The increase in the WGS reaction rate upon addition of Pt, Pd, Au and Ni on Mo_2C is accompanied by an increase in H_2O order and a decrease in CO order, and a decrease in apparent activation energy. The enhancement in the rate and the kinetic parameters depend on type of admetals. Hence, the dominant active site is modified from the Mo_2C support to the admetal surface or admetal-Mo_2C interface. Adsorption strength of CO, which increases as the CO reaction order decreases, is identified as a descriptor for WGS reaction over Metal/Mo_2C. *In situ* EXAFS over fresh Au/Mo_2C indicates that the carburization pretreatment at 600 °C leads to irreversible re-dispersion of Au nanoparticles. Pt, however, assumes a stable structure that is unaltered by temperature or the exposed gas mixtures after such treatment over Pt/Mo_2C. Thus, strong adhesive interaction between admetals and carbide support is observed. Similarity of apparent kinetic parameters measured at 120°C suggests that Pt/Mo_2C and

Pt/Mo/MWCNT possess active sites of similar chemical nature. The importance of Pt or Pt-Mo_2C contact sites towards the WGS reaction rates is de-convoluted from the contribution of Mo_2C support sites by the use of a series of Pt/Mo_2C/MWCNT catalysts. For a constant amount of Pt (1.5%), the WGS rate per gram of catalyst at 120°C increases only by a factor of 2.1, with a change in Mo weight loading from 2% to 20%. On the other hand, for a constant amount of Mo (10%), the WGS rate per gram increases by a factor of 8.2 with a change in the Pt weight loading form 0.5% to 5%.

In a follow-up study, the dependence of the WGS rates over Mo_2C and the Pt-modified unsupported Mo_2C on the residual oxygen content was studied with temperature programmed reduction (TPR). It was observed that the passivated form of Pt/Mo_2C could be activated for WGS at 120°C by a relatively milder reduction pretreatment at 300°C in 25% H_2/Ar, opposed to the 600°C carburization. Such activation could not be successfully performed for the Pt-free unsupported Mo_2C. The 300°C reduction rendered a Mo_2C catalyst an order of magnitude lower WGS rate per gram at 120°C as opposed to the Mo_2C subjected to the 600°C carburization. Presence of Pt leads to an enhancement in oxygen removal from Mo_2C for a given reduction pretreatment. Based on the TPR and the Oxygen uptake-H_2 titration experiments, the hydrogen spillover mechanism is proposed as a means of low temperature activation of Mo_2C based catalysts in presence of Pt admetal. A high activity Pt/Mo_2C catalyst with practically viable activation procedure has been reported.

In the last study, experiments were performed for the elucidation of role of a secondary metal promoter (cobalt) towards enhancement of the WGS rates over Pt supported on multi-walled carbon nanotubes. A series of PtCo/MWCNT bimetallic catalysts were synthesized. Compared to the monometallic Pt, WGS turnover rate (TOR) at 300°C was enhanced by an order of magnitude at the Co:Pt ration of 3:1. Selective leaching of CoO_x (metallic Co and CoO) phases that are not alloyed with Pt was performed with a dilute solution of acetic acid. The TOR after the leaching treatment decreased 20 times. X-ray absorption studies confirmed that the PtCo alloy was not severely affected by the leaching process. The formation of PtCo alloy was concluded to be inconsequential towards promotion in WGS TOR. The interface sites between CoO_x and the PtCo alloy particles are suggested to be the active sites for WGS.

CHAPTER 1. INTRODUCTION

In the beginning of 20th century, the Haber's process emerged as an economical route to fix atmospheric dinitrogen, in form of ammonia, which is used to produce synthetic nitrogen fertilizers. The Haber's process involves a stoichiometric reaction between nitrogen and hydrogen. Hydrogen obtained from the electrolysis of water was used for this process during the course of its development. As the scale of ammonia production escalated with the demand for fertilizers, steam reforming of natural gas (methane) proved to be the most economical source for hydrogen required in the process.

$$CH_4 + H_2O \leftrightarrow CO + 3H_2 \quad (1)$$

The carbon monoxide (CO) produced in the process of reforming needs to be removed, to obtain hydrogen with high purity, for its downstream use in the ammonia synthesis. The Water-Gas Shift (WGS) process is employed as the purification step for hydrogen [1,2]. It is a reaction between CO and water, which produces hydrogen and the CO is oxidized to CO_2.

$$CO + H_2O \leftrightarrow CO_2 + H_2 \quad (\Delta H = -41.2 \text{ kJ/mol}) \quad (2)$$

Along with the ammonia synthesis process, WGS is an integral part of other industrial processes that require pure hydrogen, such as methanol production and hydroprocessing of crude oil in refineries. In addition, WGS can be potentially used in H_2 fuel cell applications, where high purity of hydrogen is required. In light of the growing

importance of hydrogen economy, WGS plays a pivotal role in hydrogen production and has a significant impact on the energy issue. The WGS reaction is moderately exothermic and conversions are equilibrium controlled. The equilibrium constant decreases with increasing temperature [3]. Accordingly, high conversions are favored at low temperatures and are not affected, significantly, by changes in total pressure. The reaction is reversible and the forward rate is inhibited by the reaction products, H_2 and CO_2. Thus, today, the industrial WGS process takes place in a series of adiabatic converters where the effluent from the reformer system is converted in two WGS reactors (High Temperature Shift and Low Temperature Shift converters, respectively), with the second WGS reactor at a significantly lower temperature in order to shift the equilibrium towards the favored hydrogen product .

Owing to its high importance and possible impact, WGS reaction has been one of the vastly studied reactions in the field of heterogeneous catalysis [4–10]. One can find a common theme for the motivation of the abundant research still undertaken for WGS, which is, developing a catalyst that does not suffer from the drawbacks of the Fe_2O_3-Cr_2O_3 and the $Cu/Zn/Al_2O_3$ catalysts viz. pyrophoric nature, lengthy activation and high volumes [11]. The general motivation for the fundamental catalysis studies with WGS concurs with the overarching goals of the research in the field of heterogeneous catalysis [12] i.e. development of highly active and very selective catalysts for important chemical processes, to achieve minimization of cost and waster production. This objective invokes the study of the catalysts on a molecular level. A physicochemical characterization of the catalysts performed to understand its performance towards a certain reaction leads to the

establishment of structure-activity relationships. Such relationships have been fruitful for development of better heterogeneous catalysts by improving the understanding of the underlying mechanism.

The overall goal of the present research work is to develop a model-based approach to catalyst design that is called *Discovery Informatics,* which involves building a database with sufficient chemical and information diversity to allow identification of active sites, to model the kinetics and identify descriptors of the kinetic parameters [13]. Thus, WGS has been used as a probing tool or a test bed for discovery of catalyst descriptors, which provide vital insights in the fundamental catalysis over a wide variety of heterogeneous catalysts.

On a specific level, the first three chapters describe the study of WGS over molybdenum carbide catalysts modified by supporting various transition metals. Unsupported and supported molybdenum carbide catalysts were synthesize and used as supports for metals such as Pt, Pd, Au, Cu, Ni and Ag. These catalysts were shown to be superior to the commercial $Cu/Zn/Al_2O_3$ catalysts in terms of the WGS rates. By the use of WGS reaction kinetics in tandem with various spectroscopic techniques, the potential active sites were identified.

The last chapter pertains to the elucidation of the role of a secondary metal promoter (cobalt) towards the enhancement of WGS rates over supported Pt catalysts. A series of catalysts with varying metal to promoter ratio were prepared and characterized.

Overall, this dissertation has been an attempt to demonstrate how the reaction kinetics can be used in tandem with the catalysts characterization to understand the working mechanism of the catalysts under reaction conditions.

CHAPTER 2. WATER-GAS SHIFT CATALYSIS OVER TRANISITON METALS SUPPORTED ON BULK MOLYBDENUM CARBIDE

2.1 Introduction

Transition metal carbides (TMCs) such as Mo_2C, WC, TiC etc. are formed by the incorporation of the carbon atoms into the metal lattice. These materials possess unique physical properties such as high tensile strength and high melting points, and are therefore used as refractory materials and in cutting tools [14]. The electrical and thermal conductivities of these materials are close to those of pure metals, and so are the crystal structures. Additionally, these materials have been shown to display intriguing catalytic properties. In one of the early observations of the catalytic activity of molybdenum carbide (Mo_2C), Sinfelt and Yates reported that during the process of ethane hydrogenolysis, the carburization of the molybdenum catalyst lead to an increase of the reaction rate over time and the formation of the molybdenum carbide was confirmed with X-ray diffraction [15]. Levy and Boudart showed that tungsten carbide (WC) could catalyze isomerization of neo-pentane to isopentane [16], a reaction that was known to be catalyzed by only platinum and iridium [17]. It was therefore concluded that the surface electronic properties of tungsten were modified by the incorporation of carbon, to resemble that of platinum. These early findings were then followed by numerous studies which have shown that carbides of molybdenum and tungsten exhibit catalytic activities for several chemical reactions viz. ammonia synthesis [18], carbon monoxide

hydrogenation [19], methane reforming [20], hydrodesulphurization [21] etc. The turnover rates for such reactions under reducing environments were equal to or more than the metals catalysts such as Pt, Pd and Ru, and these materials were deemed to be the cheaper replacements for the noble metal catalysts.

Among the plethora of investigations that followed, Patt et al [22] studied the Water-Gas Shift (WGS) reaction ($CO + H_2O \rightarrow CO_2 + H_2$) over unsupported Mo_2C and reported that the WGS reaction rates normalized by the amount of catalyst over Mo_2C were comparable to commercially used low temperature WGS catalyst, $Cu/ZnO/Al_2O_3$. Schweitzer et al. [23] used high surface area Mo_2C as a supporting material for Pt nanoparticles to study WGS catalysis. It was shown that the WGS reaction rate normalized by total moles of Pt was higher compared to the most active oxide supported Pt catalysts such as Pt/CeO_2, Pt/TiO_2 etc. This study has laid the groundwork for the potential application of Mo_2C as a support for making high activity WGS catalysts.

To gain insights into the high WGS rates over Mo_2C and metals supported over Mo_2C, here, a detailed kinetic and spectroscopic investigation of Metal/Mo_2C systems has been performed. Passivated, unsupported Mo_2C, synthesized via temperature programmed carburization in presence of a CH_4/H_2 mixture, was used as a support for making supported Pt, Pd, Au, Ni, Cu and Ag catalysts. Variation in the WGS reaction kinetic parameters with admetals was used to predict a potential descriptor for the promotion of WGS rates over Mo_2C by deposition of admetals. In coherence with the study by

Schweitzer et al [23], the superiority of the Metal/Mo_2C systems over the oxide supported catalysts has been confirmed. We have performed in situ X-ray absorption spectroscopy (XAS) to observe the working state of the catalysts during WGS reaction. The high resolution Scanning Transmission Electron Microscopy (STEM) microscopy combined with Electron Energy Loss Spectroscopy (EELS) was used to understand the morphology and qualitatively determine the composition of the supported metal particles over Mo_2C.

2.2 Experimental Methods

2.2.1 Catalyst Synthesis

The unsupported Mo_2C was synthesized by temperature programmed carburization of ammonium heptamolybdate precursor [$(NH4)_6Mo_7O_{24}\cdot 4H_2O$; 81-83% as MoO_3] from Alfa Aesar in a fixed bed reactor system with 0.5 grams of the precursor loaded in a quartz reactor tube over a quartz plug. The precursor was exposed to pure H_2 (75 sccm) and the temperature was ramped to 350-370 ºC at 4 ºC/min and was soaked at this temperature for 10 h. The temperature was further ramped to 600 ºC at 3 ºC/min while the gas was switched to 15% CH_4/H_2 (75 sccm) mixture. The reactor was maintained at this temperature for 3.5 to 4 h. It was then cooled to RT under the flow of Ar and then passivated in a flow of 1% O_2/Ar. The oxygen concentration in the passivation mixture was progressively increased to 20% and the Mo_2C support was ultimately exposed to air. Passivation was performed in order to avoid the spontaneous combustion of the freshly synthesized Mo_2C upon exposure to the ambient air. The passivated Mo_2C was used as a support for the synthesis of Metal/Mo_2C catalysts.

Au/Mo_2C was prepared using the deposition precipitation method. Chloroauric acid ($HAuCl_4 \cdot 3H_2O$, Sigma) was added to deionized water along with the support material. Appropriate amount of 1 N Na_2CO_3 solution was added drop wise to maintain a pH of 2.6 for 6 hours of stirring. Additional Na_2CO_3 was then added to bring the pH near 6.6 and the solution was stirred for another 4 hours. The mixture was then centrifuged, washed and dried. Atomic absorption spectroscopy was performed on each sample using an AAS, Perkin-Elmer AAnalyst 300 instrument. Prior to AAS measurements, the catalysts were digested in 2 mL/1 mL/100 mg = aqua regia/HF/catalyst in a Nalgene® amber high-density polyethylene bottle for at least 3 days and this solution was then diluted to the desired concentration for the AAS measurement. Concentrations of Au were determined by comparing results to those of known standards.

Incipient wetness impregnation (IWI) was used for the preparation of Pt, Pd, Ni, Cu and Ag supported on passivated Mo_2C. The precursors used were aqueous solutions containing appropriate amounts of Chloroplatinic acid ($H_2PtCl_6.6H_2O$, Sigma), Tetrammonium palladium (II)nitrate ($Pd(NH_3)_4(NO_3)_2$, Alfa Aesar), Nickel nitrate ($Ni(NO_3)_2.6H_2O$, Sigma), Copper nitrate ($Cu(NO_3).3H_2O$, Alfa Aesar) and Silver nitrate ($AgNO_3$, Alfa Aesar) for Pt, Pd, Ni, Cu and Ag respectively. The solutions were added drop-wise to the solid catalyst while it was stirred to enhance the mixing. The catalysts were then dried overnight at room temperature and reduced in presence of pure H_2 at 450 ºC for 3 hours and passivated using the method mentioned above. All the metal loadings were kept between 1.5 and 2%. The $Cu/Zn/Al_2O_3$ catalyst was obtained from Süd-

Chemie in form of pellets. The pellets were crushed and sieved to size between 125 to 250 microns, before loading in the reactor.

2.2.2 Kinetic Measurements

The details of the kinetic measurement apparatus are described elsewhere [24]. The WGS reaction rates were measured under differential conditions i.e. CO conversion was kept below 10% the products of the WGS reaction (CO_2 and H_2) were also co-fed. The appropriate amount of each catalyst was loaded, so that the WGS kinetics could be measured at 120 ºC for all the samples. Since the catalysts were prepared over the passivated Mo_2C, prior to the kinetic measurement, each catalyst was subjected to temperature programmed carburization up to 600 ºC at 3 ºC/min, to bring back the carbide surface in its native form by the removal of oxygen from the surface. After this pretreatment, reactors were cooled under Ar to 120 ºC and were exposed to the WGS reaction mixture (Standard conditions, 6.8% CO, 21.9% H_2O, 8.5% CO_2, 37.4% H_2, and balance Ar) with a flow rate of 75.4 sccm. The $Cu/ZnO/Al_2O_3$ catalyst was reduced using a previously reported procedure [25], i.e. at 200 ºC in 5% H_2/Ar and was tested at 140 ºC. The catalysts were stabilized for a period of ~20 hours, which was enough for the initial deactivation to occur and a stable CO conversion value to be reached. The apparent reaction orders were then measured over the stabilized catalysts by varying the partial pressures of one component at a time over the range of 4–21% CO, 5–25% CO_2, 11–34% H_2O, and 14–55% H_2. To determine the apparent activation energy, the temperature was varied over a range of 30°C, with the concentrations maintained at standard conditions.

After the measurements were complete, the catalysts were passivated at room temperature.

2.2.3 Catalyst Characterization

The bulk structures of the Mo_2C and Metal/Mo_2C catalysts were determined by X-ray diffraction (XRD) using a Scintag X2 diffractometer with Cu Kα radiation. Samples were scanned through 30-90° (2θ) with scanning rate 2° min^{-1}. The BET surface areas were measured using nitrogen adsorption isotherms (Micromeritics ASAP 2020). Samples were degassed at 250 °C for at 5 to 6 h before N_2 adsorption.

CO Temperature programmed desorption (TPD) was performed over Mo_2C and metal/Mo_2C catalysts using Micromeritics Autochem 2920 II coupled with an Agilent 5975C mass selective detector (MSD). Prior to CO adsorption, all the samples were carburized in presence of 15% CH_4/H_2 (50 sccm) at 600°C (3°C/min) for 4 hours. The sample cell was then purged with Helium at 600°C for 30 minutes. The pretreatment was followed by CO adsorption at RT by flowing a 5% CO/He (50 sccm) mixture for 1 hour. The sample temperature was then linearly increased at 10°C /min in presence of He (30 sccm). The CO desorption response was recorded with the mass selective detector.

In order to observe the effect of the temperature programmed carburization pretreatment over the supported metal nanoparticles (Au and Pt), X-ray absorption measurements were made on the insertion device beam line of the Materials Research Collaborative Access

Team (MRCAT) at the Advanced Photon Source, Argonne National Laboratory. Scans at the Au L_{III} edge (11.919 keV) and the Pt L_{III} edge (11.564 keV) were performed in fluorescence mode for Au/Mo_2C and Pt/Mo_2C catalysts. In situ experiments were performed in 1 in OD quartz tubes connected to Ultra-Torr fittings with welded ball valves (for gas inlet/outlet and sealing) and Kapton windows. The catalyst mass was calculated to give an absorbance (μx) of approximately 2.0, with an edge step (Δμx) between 0.4 and 1.5. The samples were pressed into wafers which were kept at a 45º angle with the X-ray beam inside the in situ reactor, and the fluorescence detector was kept perpendicular to the length of the reactor tube. The scans were collected over the freshly prepared samples (over passivated Mo_2C) at RT under air. The catalysts were then subjected to the aforementioned high temperature carburization pretreatment in presence of 15% CH_4/H_2 at 600 ºC and then cooled to 130-140ºC. At this point, the samples were exposed to the WGS reaction mixture (7% H_2O, 8% CO, 7% CO_2, 44% H_2 and balance Ar). After a period of 1 h, the samples were cooled to RT and were passivated. XAS scans were collected at each stage viz. after the carburization, during WGS and after the passivation. XAS spectra were analyzed with the WINXAS3.1 software package. Phase shifts and backscattering amplitudes were obtained from Au foil for Au-Au. Standard procedures based on WINXAS 3.1 software were used to extract the EXAFS data. The coordination parameters were obtained by a least square fit in *q*- and *r*-space of the isolated nearest-neighbor, k^2-weighted Fourier transform data-ray absorption near edge (XANES) spectra were normalized and obtained using standard background subtraction methods. The XANES were energy calibrated with the known edge position of the first peak in the first derivative of the simultaneously obtained foil spectrum. The edge

positions for each of the catalysts were determined from the maximum of the first peak in the first derivative of the XANES of the sample.

STEM and EELS analyses were carried out using the dedicated aberration-corrected STEM Hitachi HD-2700C at 200 kV equipped with a modified Gatan Enfina ER spectrometer hosted at the Center for Functional Nanomaterials, Brookhaven National Laboratory. The convergence angle and the ADF collection angles were 28 mrad and 64-341 mrad, respectively. The Enfina spectrometer entrance aperture was set to 3 mm resulting in EELS collection angle of 26.7 mrad and an energy resolution of 0.35 eV as measured from the full width at half maximum (FWHM) of the zero-loss peak. The EELS spectra for Mo, Pt and Au were collected at the $M_{4,5}$ edges. The EELS dwell time was varied between 0.1–0.3 seconds to avoid beam induced structural changes. The step size for line-scans and mapping was varied between 1-3 Å. The core-loss intensities were extracted by extrapolating the background using a power-law model and subtracting it from the acquired signal. Data processing was carried out using Gatan Digital Micrograph.

2.3 Results

2.3.1 WGS reaction kinetics

Due to the reversibility of the WGS reaction, the apparent activation energy and the reaction orders with respect to CO, H_2O, H_2 and CO_2 were fitted to a power rate law expression of the form:

$r = A \exp(-E_{app}/RT) [CO]^a [CO_2]^b [H_2]^c [H_2O]^d (1 - \beta)$,

Where r is the overall rate, $\beta = ([CO_2] [H_2])/ (K_{eq} [CO] [H_2O])$ is the approach to equilibrium, A and E_{app} are the apparent pre-exponential factor and activation energy for the forward rate, a, b, c, d are forward reaction orders, and K_{eq} is the equilibrium constant for the WGS reaction. The detailed WGS kinetic data (apparent reaction orders, WGS rates per total moles of metal) are shown in Table A.1. All the data were measured at 120 ºC. The WGS reaction rates per gram of the catalyst and the apparent activation energies are reported in Table 2.1. The WGS reaction rate per gram of catalyst over Mo_2C at 120 ºC (0.3 μmol H_2 $(g.cat.)^{-1}s^{-1}$) was 1.5 times higher than that for the commercial $Cu/ZnO/Al_2O_3$ catalyst (0.2 μmol H_2 $(g.cat.)^{-1}s^{-1}$), measured under the standard gas composition. The effect of deposition of each metal over Mo_2C was quantified in terms of the promotion in the WGS rate per unit surface area of catalyst measured at 120 ºC i.e. the WGS rates per unit surface area over these supported metal catalysts were compared to the Mo_2C support. The WGS reaction rate per unit surface area of catalyst at 120 ºC varies between 4.6×10^{-9} mol H_2 m^{-2} s^{-1} for Mo_2C support and 2.9×10^{-8} mol H_2 m^{-2} s^{-1} for 1.5% Pt/Mo_2C. Ag (4.9×10^{-9} mol H_2 m^{-2} s^{-1}) supported on Mo_2C exhibited WGS rate per unit surface area of catalyst at 120 ºC that was similar to the rate over Mo_2C. Cu (7.7×10^{-9} mol H_2 m^{-2} s^{-1}) showed some improvement by a factor of 1.6. Ni promoted the WGS reaction rate per unit surface area over Mo_2C by a factor of 3.3 (1.5×10^{-8} mol H_2 m^{-2} s^{-1}).The extents of promotion were higher for the noble metals. Pd/Mo_2C and Au/Mo_2C exhibited the WGS reaction rate of 2.2×10^{-8} mol H_2 m^{-2} $s^{-1}$and 2.5×10^{-8} mol H_2 m^{-2} s^{-1}. Deposition of Pt lead to promotion by factor of 6.3 (2.9×10^{-8} mol H_2 m^{-2} s^{-1}). It should be noted that the extents of promotion in the WGS reaction rates per unit surface area of

catalyst aren't the highest achievable values. There can be a further promotion achieved by adding higher amounts of rate promoting metals. The comparison made here should be used to assess the efficacy of the admetals, when similar amount (in grams) of each admetal is added to Mo_2C.

Table 2.1 WGS rate per gram at 120^0C under 6.8% CO, 8.5% CO2, 21.9% H2O, 37.4% H2, and balance Ar for Metal/Mo2C catalysts, Mo_2C and $Cu/Zn/Al_2O_3$ catalyst

Catalyst	WGS Rate at 120°C/10^{-7} mol H_2 (g. cat.)$^{-1}$ s^{-1}	WGS Rate at 120°C/10^{-9} mol H_2 m^{-2} s^{-1}	E_{app} / kJ(mol)$^{-1}$ (±3)
1.5 % Pt/Mo_2C	18	29	48
1.5 % Au/Mo_2C	16	25	44
1.7 % Pd/Mo_2C	14	22	63
1.8 % Ni/Mo_2C	9.5	15	70
1.5 % Cu/Mo_2C	5	7.7	84
1.9% Ag/Mo_2C	3	4.9	87
Mo_2C	3	4.6	90
$Cu/Zn/Al_2O_3$	2	3.4	76

The apparent activation energies follow a progressively decreasing trend with increasing WGS rates per unit surface area at 120 ºC (Table 1). Apparent activation energies of Cu/Mo_2C (84 kJ (mol)$^{-1}$) and Ag/Mo_2C (87 kJ (mol)$^{-1}$) were similar to that of Mo_2C support (90 kJ (mol)$^{-1}$) within error. Ni/Mo_2C, with a 3.3 times higher WGS rate per unit surface area compared to Mo_2C at 120 ºC had apparent activation energy of 70 kJ (mol)$^{-1}$, whereas Pd/Mo_2C with a promotion in the rate per unit surface area by a factor of 4.8,

had an apparent activation energy of 63 kJ $(mol)^{-1}$. Significantly lower apparent activation energies were observed for Au/Mo_2C and Pt/Mo_2C (44 and 48 kJ $(mol)^{-1}$). Figure 2.1 shows the typical Arrhenius plots for all the $Metal/Mo_2C$ systems. The WGS reaction rates in Figure 2.1 were normalized by total moles of the metal added. 1.5% Au/Mo_2C and 1.5% Pt/Mo_2C exhibit the WGS reaction rate per total moles of metal which are 2.0×10^{-2} mol H_2 (mol Au)$^{-1}$ s^{-1} and 2.6×10^{-2} mol H_2 (mol Pt)$^{-1}$ s^{-1} at 120 ºC. The WGS reaction rate at 120 ºC normalized by total moles of metal was lowest for 1.9% Ag/Mo_2C (1.5×10^{-3} mol H_2 (mol Ag)$^{-1}$ s^{-1}). The rates are normalized by the total moles of metal added, because the moles of metals exposed to the surface could not be selectively measured using chemisorption techniques since Mo_2C also adsorbs the probe molecules typically used, such as CO or H_2. Figure 2.1 also shows the change in the apparent activation energies Ag/Mo_2C to Pt/Mo_2C.

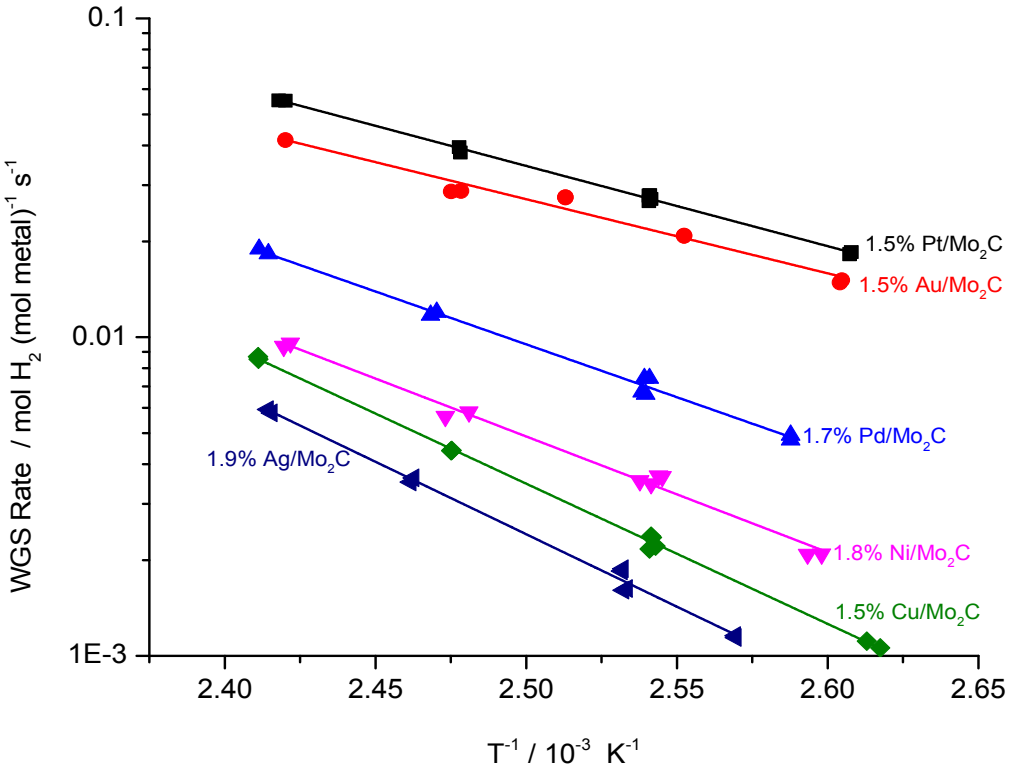

Figure 2.1 Arrhenius plots of WGS reaction rates for various metal/Mo_2C catalysts

Figure A.1 shows the representative plots (Au/Mo_2C) used for determination of apparent reaction orders with respect to CO, CO_2, H_2O and H_2. Similar plots are used for all the catalysts to measure the apparent reaction orders.

Figure 2.2 shows the correlation observed between apparent CO orders and WGS reaction rates per gram at 120ºC. The apparent CO order progressively decreases from Mo_2C (0.54) support to Pt/Mo_2C (0.05) with increase in the WGS rate per gram of catalyst.

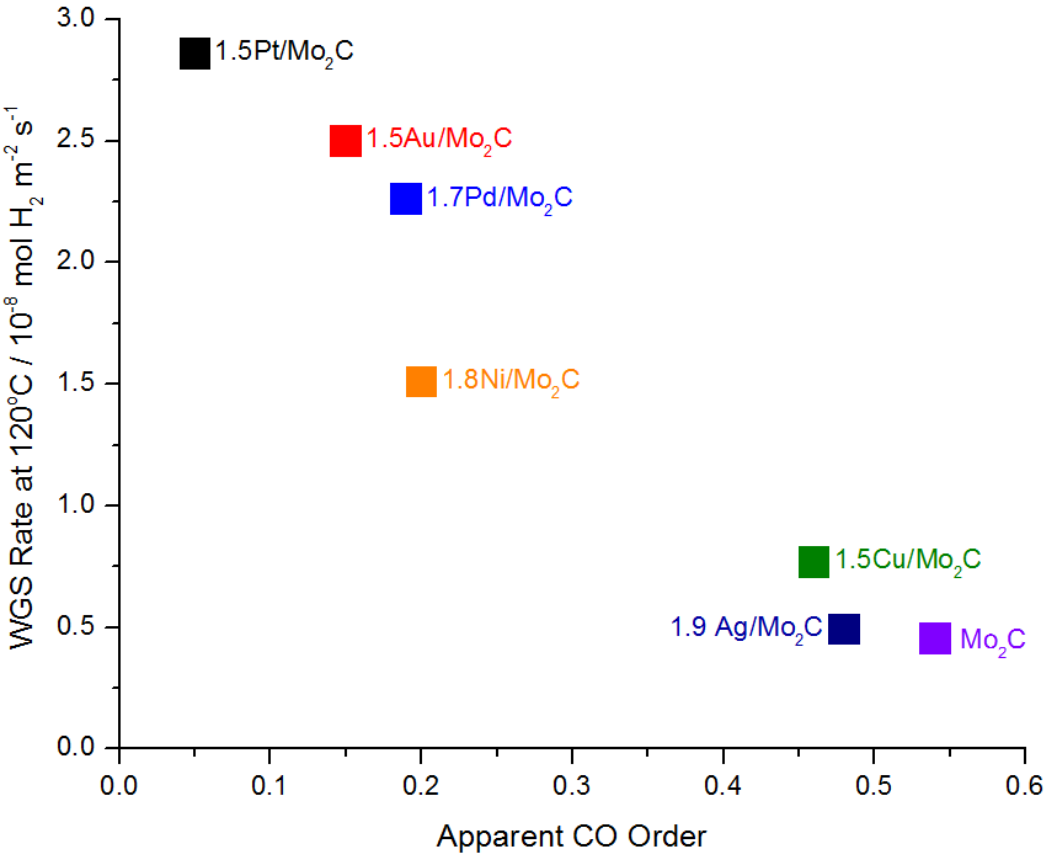

Figure 2.2 WGS rate per unit surface area at 120^0C vs. apparent CO order for various Metal/Mo2C catalysts

On the contrary, as there is promotion in the WGS rate per gram observed, the apparent H_2O order undergoes a step change from less than zero for Mo_2C (-0.09), Cu/Mo_2C (-0.04) and Ag/Mo_2C (-0.04), to 0.6 for Ni, 0.79 for Pd, 0.74 for Au and 0.76 for Pt supported on Mo_2C.

In short, the increase in the WGS reaction rate upon addition of rate promoting metals to Mo_2C is accompanied by a step change in apparent H_2O order and a progressive decrease

in apparent CO order and apparent activation energy. Also, as shown in Figure A.2, the Metal/Mo_2C catalysts tested here exhibit a compensation effect.

2.3.2 Catalyst characterization

The BET surface areas of Mo_2C and Metal/Mo_2C catalysts are listed in Table A.1. The analysis was performed on the passivated catalysts. The surface areas for all the catalysts were between 60 and 70 m^2/g, indicating that the deposited metals had a negligible effect on the surface area.

Figure A.3 shows the X-ray diffraction patterns for the unsupported Mo_2C and Metal/Mo_2C catalysts. The diffraction patterns for Pt/Mo_2C, Pd/Mo_2C, Ni/Mo_2C and Cu/Mo_2C resembled that of the Mo_2C support. There were no clearly discernable peaks for supported metals (for Pt, Pd, Ni and Cu). However, for Au/Mo_2C and Ag/Mo_2C (Figure A.4), the peaks for Au (111 at 38.2º) and Ag (111 at 38.3º) were observed for the fresh catalysts. These peaks were absent from the patterns for used Au/Mo_2C and used Ag/Mo_2C catalysts. The implications of this result will be discussed later.

Figures 2.3 and 2.4 show the normalized intensity of the CO and CO_2 signals recorded in the MSD signal plotted against the temperature during the CO TPD experiments. Peak de-convolution was performed using OriginPro 8.5.1 (Figure A.5). For CO desorption from Mo_2C, three different peaks at 52°C, 84°C and 158°C were identified. For CO desorption spectra from Ag/Mo_2C and Cu/Mo_2C, the positions of these peaks did not

change significantly compared to those for Mo_2C. For Ni/Mo_2C, the peak at ~160°C became more pronounced in relative intensity. For Pd, Au and Pt, the relative intensity of the peak at ~160°C diminished significantly compared to that for the bulk Mo_2C support. For all catalysts, 5 to 10% CO evolved as CO_2. For CO_2 evolution from Mo_2C, two peaks were assigned at 105°C and 158°C. The peak between 105°C and 110°C was observed for all the catalysts except Au/Mo_2C. The CO_2 evolution spectra for Ag/Mo_2C and Cu/Mo_2C were similar to that for Mo_2C in terms of shapes and peak positions. Ni/Mo_2C and Pd/Mo_2C exhibited a shoulder at ~205°C. Pt/Mo_2C exhibited a more pronounced shoulder at 218°C. Au/Mo_2C had a very distinct CO_2 evolution spectrum compared to that for Mo_2C. There were two peaks assigned for Au/Mo_2C, one at 123°C and a broad peak centered at 176°C.

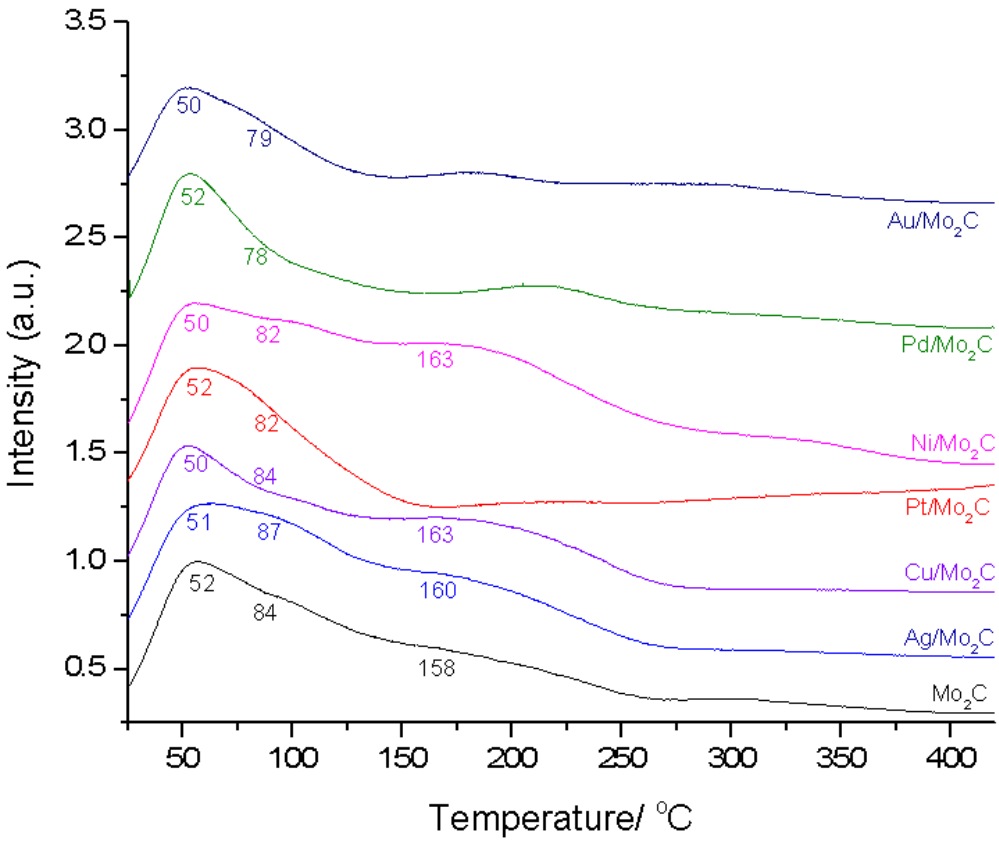

Figure 2.3 CO temperature desorption spectra for Mo2C and the Metal/Mo2C catalysts. Maximum temperatures for the de-convoluted peaks are indicated.

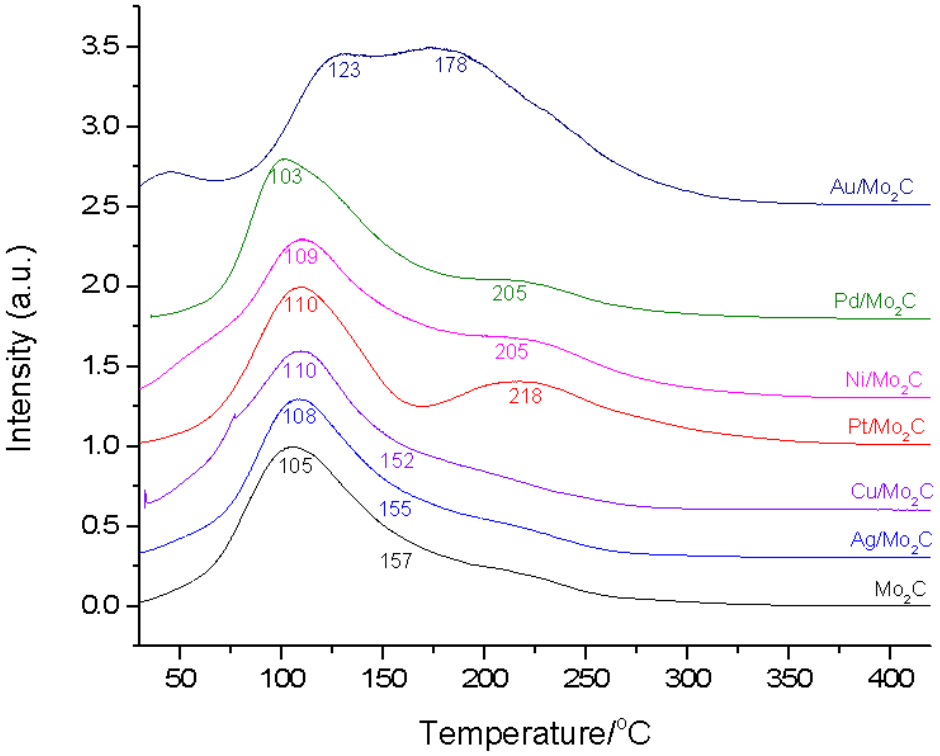

Figure 2.4 CO_2 evolution spectra for Mo_2C and the Metal/Mo_2C catalysts during CO TPD Maximum temperatures for the de-convoluted peaks are indicated.

In situ XAS was used to study the chemical states and the coordination environments of the Mo_2C supported metal nanoparticles (Au and Pt) during different treatments viz. carburization, WGS, and passivation. Figure 2.5 shows the X-ray absorption near edge structure (XANES) spectra for the Au/Mo_2C catalyst. The spectrum for the fresh catalyst resembled that of the Au foil standard, indicating that the Au was metallic in nature over the freshly prepared catalyst. The carburization did not change the oxidation state of Au, as the spectrum for the catalyst after the carburization or during WGS did not change significantly.

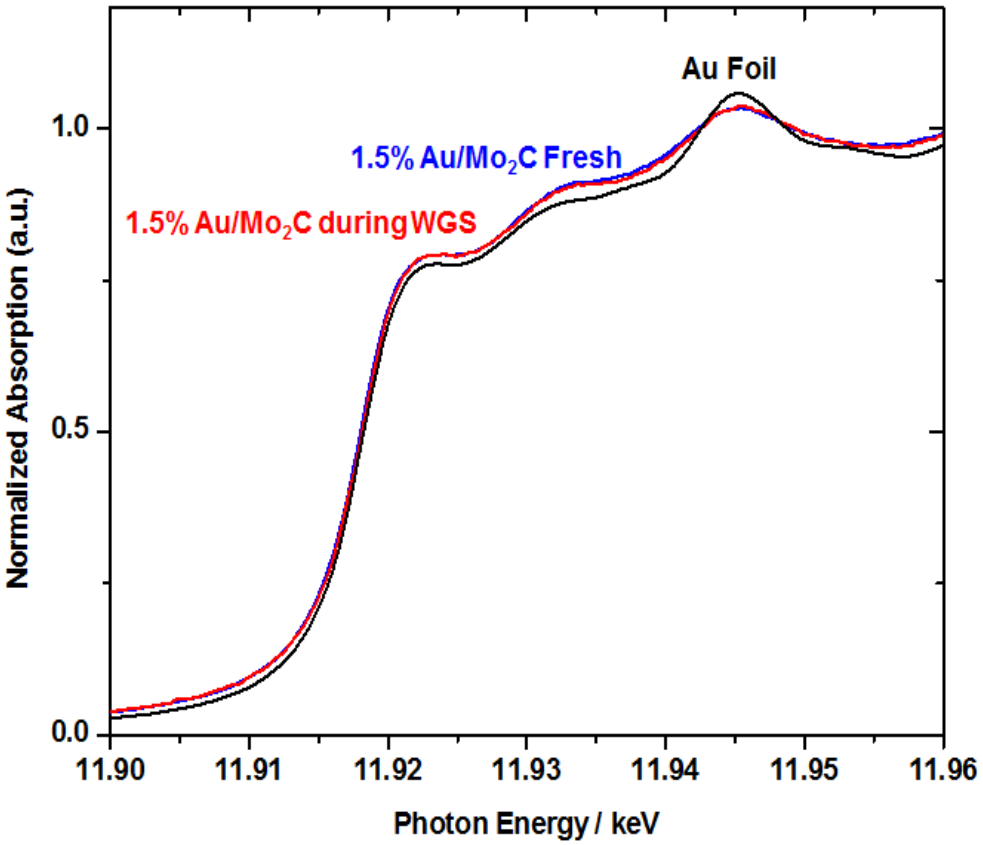

Figure 2.5 In situ Au LIII edge XANES spectrum for 1.5% Au/Mo_2C fresh (red) and 1.5 Au/Mo_2C during WGS (blue).

As shown in Figure 2.6, after the carburization, Pt was completely reduced, as evidenced by the edge energy of Pt foil (11.5640 keV) and that of Pt/Mo_2C (11.5638 keV). However, there is a significant white line shift for the Pt/Mo_2C sample after carburization and WGS (under helium, at room temperature) and also the position of the first peak appears to be shifted. These features indicate a modification in the electronic structure of the d-density of states. Such modifications in the shape of Pt L_{III} edge XANES spectra have been attributed to the formation of Pt-Mo bimetallic alloy nanoparticles [26]. Summarizing, both Au and Pt were in metallic state during and after WGS.

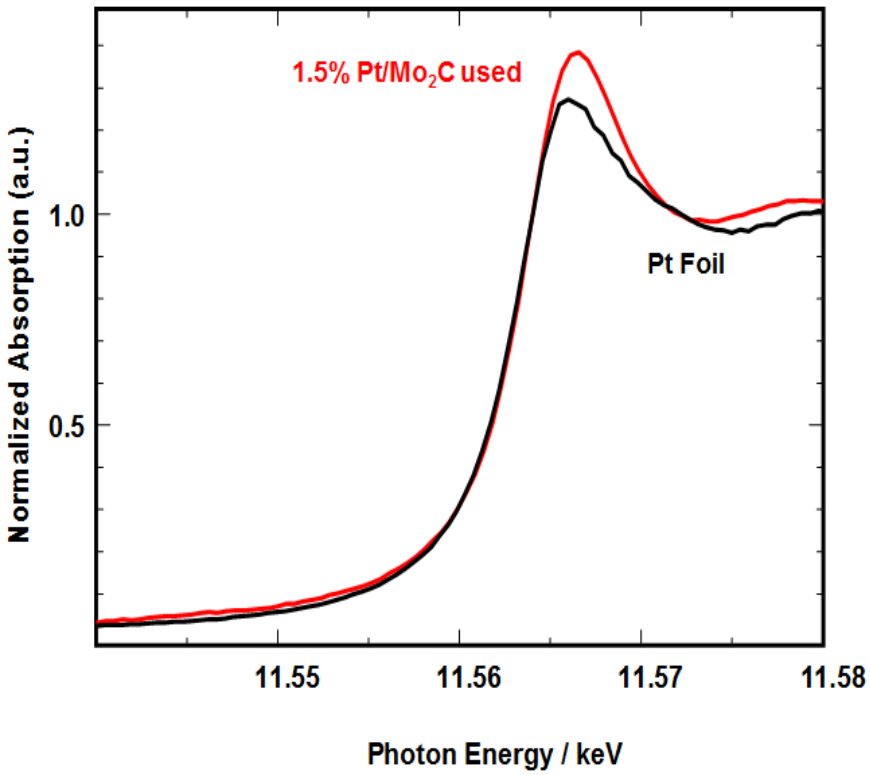

Figure 2.6 *In situ* Au L_{III} edge XANES spectrum for 1.5% Pt/Mo_2C used catalyst. The 'used' catalyst is the Pt/Mo_2C that was carburized, exposed to WGS reaction mixture at 130°C, then passivated at RT.

Figure 2.7 shows the extended X-ray absorption fine structure (EXAFS) spectra for the Au/Mo_2C catalyst, before and after the various treatments. The spectrum for the fresh catalyst is very similar to the Au foil standard. No Au-O coordination was observed for the fresh sample, again indicating that Au was in metallic state. As shown in Table A.3, the estimated Au-Au coordination number (CN) for the fresh catalyst was 11.4, which was close to 12, the Au-Au CN for bulk gold. The EXAFS particle size was determined from the previously developed correlation of coordination number with particle size [27].

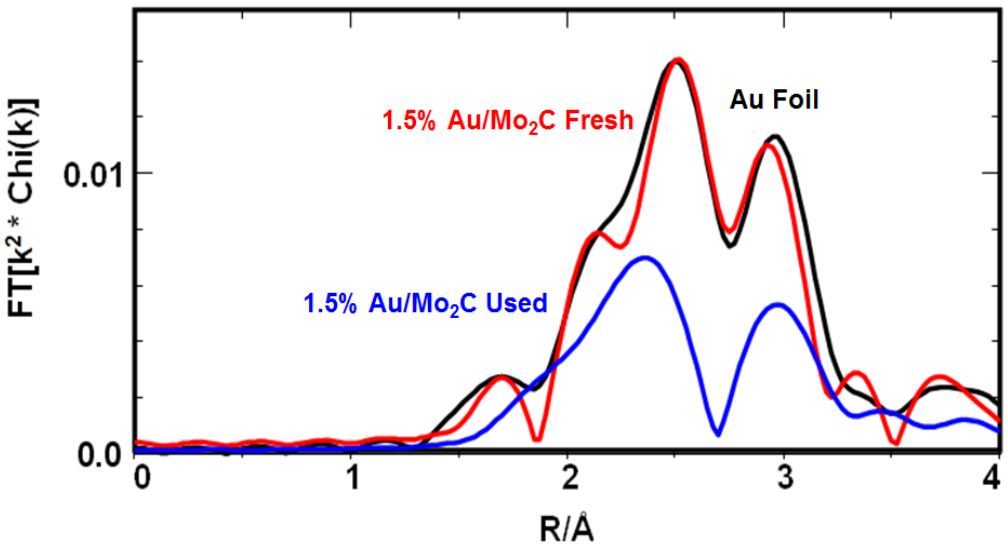

Figure 2.7 *In situ* Fourier transforms of the k^2 Au L_{III} edge EXAFS spectra for 1.5% Au/Mo_2C fresh (red) and 1.5% Au/Mo_2C used (blue). The 'used' catalyst is the Au/Mo_2C that was carburized, exposed to WGS reaction mixture at 130°C, then passivated at RT.

The estimated average particle size of Au clusters at this stage was greater than 9 nm (EXAFS offers poor precision at this particle size). This indicates that large Au nanoparticles were made when the catalyst was prepared by deposition precipitation using the passivated Mo_2C support. During the temperature programmed carburization, no change in the Au-Au CN was observed below 400 ºC (CN=10.6), but after this point, the Au-Au CN progressively decreased to 8.6 at 600 ºC. The catalyst was then cooled to 160 ºC under Helium and then exposed to the WGS reaction mixture, with no significant change in the Au-Au CN. The estimated average particle size of the Au nano-clusters significantly decreased from greater than 9 nm to about 3 nm during this process. After about 1 hour of exposure to the WGS reaction mixture, the catalyst was cooled to RT and was exposed to 1% O_2/He for passivation. After the progressive increase in the oxygen

concentration, the catalyst was ultimately exposed to air. During the process of passivation, no significant change in the Au-Au CN (and hence, the average Au particle size) was observed. Thus, the 600 ºC carburization leads to the irreversible re-dispersion of Au nanoparticles on the surface of the Mo_2C support. There was no Au-Mo coordination observed in the EXAFS (Figure 2.7), ruling out the formation of alloy nanoparticles. The results obtained using Au edge XAS were confirmed with the STEM-EELS (Figure 2.8). Bulk Mo_2C offers a poor contrast between the metal particles and the support surface, as it a relatively high Z material.

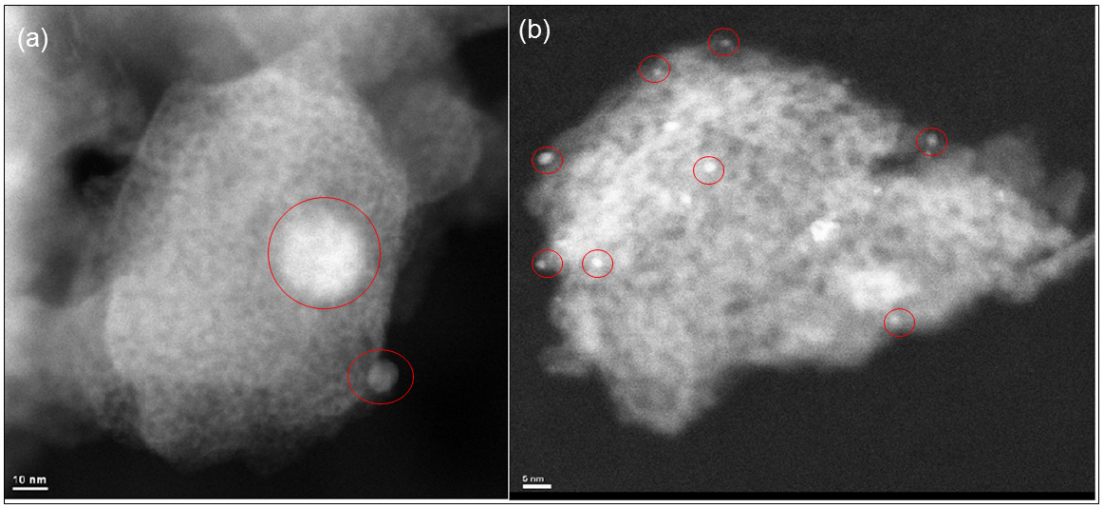

Figure 2.8 Representative HAADF-STEM micrographs for fresh (a) and used (b) 1.5% Au/Mo_2C catalyst. The gold clusters are denoted with the red circles. These images are in accrodance with the Au edge EXAFS results showing the decrease in the average Au particle size.

Nonetheless, 11 particles over the fresh Au/Mo_2C catalyst could be imaged and the number average particle size was estimated to be 11.5 ± 6.2 nm. For the used Au/Mo_2C catalyst (carburized and passivated), the number average particle size was 2.6 ± 0.7 nm,

based on the 39 particles counted. The EELS spectra shown in Figure 2.9 confirm that Mo is not present inside the Au particles, suggesting that Au-Mo alloy was not formed during carburization.

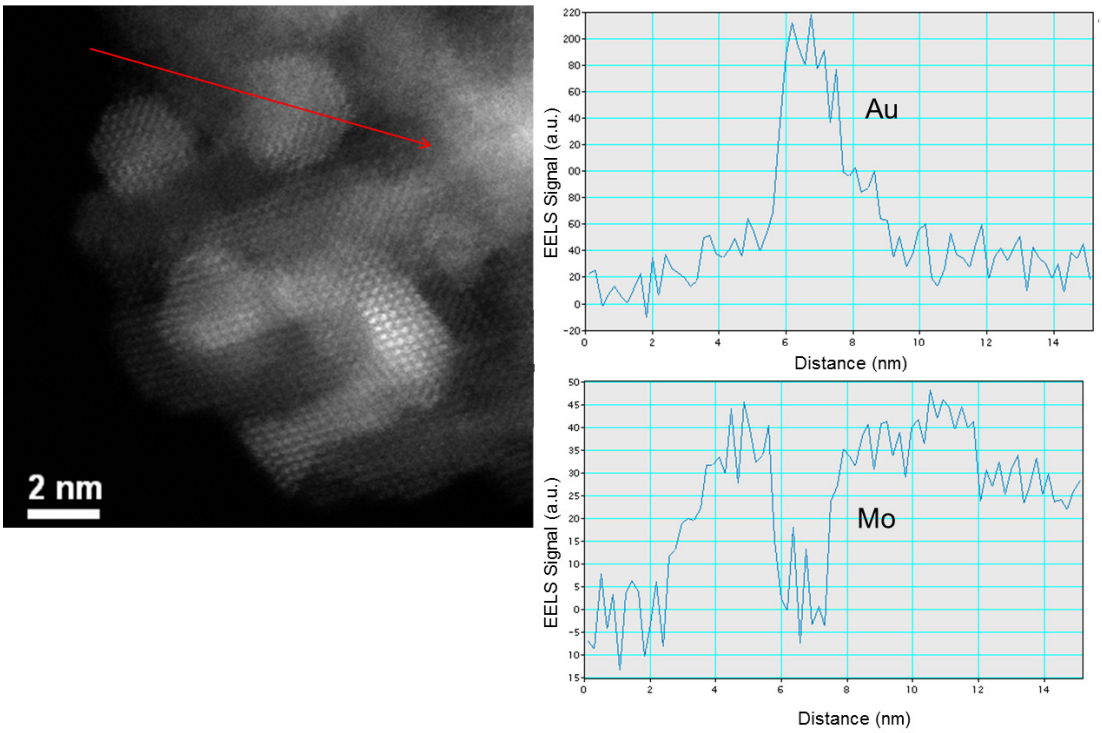

Figure 2.9 (Left) Representative HAADF-STEM micrograph of the used 1.5% Au/Mo2C catalyst used to assess the compostion of the observed particles The red line represnts the locus of the points at which the EELS scans were collected through the particle. (Right) EELS.

The state of Pt on the fresh Pt/Mo_2C catalyst was similar to what has been observed on oxide supports such as Al_2O_3, when chloroplatinic acid solution is used as a precursor [28]. Pt was in the oxidized state over the fresh catalyst, still bonded to the Cl counter ions (Table A.4). However, the EXAFS data collected after the 600 ºC carburization and

under the WGS reaction mixture at 160ºC showed no Pt-Cl coordination and Pt-Mo coordination was observed instead. Mo was included in the coordination sphere to obtain the best fit for the EXAFS data (Figure 2.10).

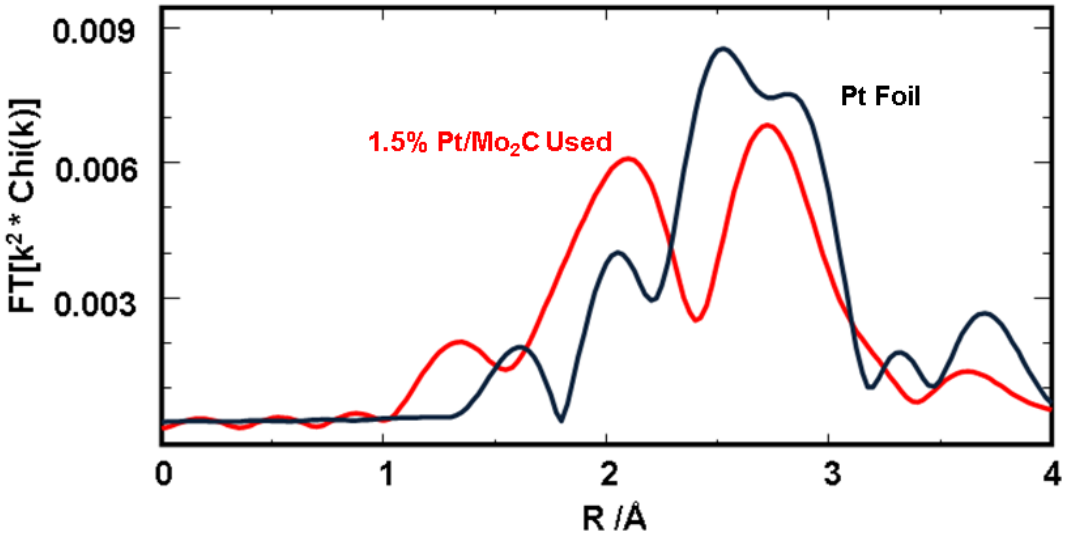

Figure 2.10 *In situ* Fourier transforms of the k^2 Pt L_{III} edge EXAFS spectra for 1.5% Pt/Mo_2C used (red). The 'used' catalyst is the Pt/Mo_2C that was carburized, exposed to WGS reaction mixture at 130°C, then passivated at RT.

The estimated Pt-Pt and Pt-Mo average coordination numbers were 6.2 and 4.1 respectively. These coordination numbers did not change significantly (Pt-Pt: 5.8, Pt-Mo: 3.7) after the catalyst was passivated at room temperature. Thus, Pt nanoparticles assumed a stable structure after carburization. The observed Pt-Mo coordination suggests the formation of alloy nanoparticles and the absence of Pt-O coordination under WGS confirms that Pt stayed in metallic state.

2.4 Discussion

2.4.1 Implications of WGS kinetics

The promotion of the WGS rate per gram with different metals was accompanied by a change in kinetic parameters. Since the enhancement in WGS reaction rate and the measured apparent kinetic parameters depend on the type of admetal, we conclude that that the kinetically relevant steps occur either on the admetal surface or the admetal-Mo_2C interface.

As discussed above, there is a clear trend that apparent activation energy progressively decreases with deposition of different metals. Consequently, the difference between the relative rates between the unsupported Mo_2C and the Metal/Mo_2C systems increases as temperature is decreased and the catalysts with lower apparent activation energies have higher relative rates. One of the possible interpretations of the compensation effect exhibited by the Metal/Mo_2C catalysts (Figure A.2) is that all these catalysts follow a similar WGS reaction mechanism [29].

For a catalytic reaction that follows a Langmuir-Hinshelwood type of mechanism, the intrinsic reaction rate is a direct function of the relative surface concentrations of the adsorbed species that are actively involved in the reaction mechanism [30]. The measured apparent kinetic parameters (activation energy and reaction orders) are hence dependent on the relative surface concentrations of the adsorbed reactive species, and they in turn are often related to the gas phase concentrations of the reaction mixture components through Langmuir isotherm equations.

For a mixture of reactant A and B (A+ B→P),

$\Theta_A = K_A C_A / (1+K_A C_A + K_B C_B)$,

Where Θ_A is the fraction of the available surface covered by species A at equilibrium, K_i is the adsorption equilibrium constant for species i and C_i is the gas phase concentration of species i. The dependence of K_i on temperature makes Θ_A temperature dependent. Θ_A also depends on the heat of adsorption of species A and B. In turn, the apparent reaction order with respect to such species involved in the reaction depends not only on the gas phase concentration but also on the reaction temperature. It is therefore necessary to measure the kinetic data over different catalysts at the same temperature for objective comparison of relative surface concentrations of reactive species. The reaction rate is directly proportional to the product of Θ_A and Θ_B, if the surface reaction is second order. An apparent reaction order of ~1 for a particular reactant implies that the relative surface concentration is near zero; whereas an apparent reaction order of -1 implies that the reactant is strongly bonded to the surface and its coverage is near 1. In the latter case, the reaction rate is dependent upon the number of sites left free by this strongly adsorbed reactant [31]. Therefore, any fractional orders measured in between these extremes can paint a quantitative picture of relative surface concentrations and heats of adsorption of different surface intermediates. In case of WGS, the proposed mechanisms can be classified in two categories, namely the red-ox mechanism and associative mechanism [32]. The red-ox mechanism involves dissociation of water to form adsorbed atomic oxygen, which reacts with adsorbed CO to form CO_2. The surface oxidation of CO has been suggested as the rate limiting step for Mo_2C surface [33,34]. The vacant site left

after the surface oxidation of CO is re-oxidized by water. In the associative mechanisms, the adsorbed CO reacts with the OH species formed after water disassociation to form a reaction intermediate, namely formate or carboxyl. The decomposition of the carboxyl intermediate to form CO_2 has been suggested as the rate limiting step [35]. In short, for any WGS mechanism, the suggested rate limiting step is a second order surface reaction. Hence, the aforementioned analysis can be invoked. The apparent CO and CO_2 orders can be used to gauge the relative size of the carbon pool while the apparent H_2O and H_2 orders yield similar information about the hydroxyl pool (generated due to adsorption and dissociation of water on the catalytic surface) [36]. Most importantly, since the measured reaction rate directly depends on the number of 'dominant' active sites on the catalyst surface, the apparent reaction orders are related to the relative surface concentrations over these dominant active sites. We do not disregard the contribution of metal-free Mo_2C towards the overall reaction rate for the catalysts with rate promoting metals. The term 'dominant' signifies that the inherent rate of the active sites formed by metal-Mo_2C contact is higher than the Mo_2C itself. Therefore, it is safe to assume that the change in the surface concentration of any species adsorbed on a site other than the dominant active sites will not be reflected in the change in the reaction rate. Additionally, the surface concentrations are also a function of heats of adsorption and binding strengths [35] of the surface species and these heats of adsorption depend on the chemical nature of the site of adsorption. Hence, any change in the apparent kinetic parameters observed, is due to modification in the chemical nature of the dominant active sites.

In the present scenario, addition Ag did not lead to a significant promotion and addition of Cu lead to a minor improvement (1.6 times higher) in the WGS reaction rates per unit area over Mo_2C, and there was no significant change observed in the apparent kinetic parameters over Mo_2C. This suggests that addition of these metals did not modify the nature of the dominant active sites. On the contrary, upon the addition of the rate promoting metals (Ni, Pd, Au and Pt) the kinetic parameters changed significantly, marking the change in the chemical nature of such sites.

The near zero apparent reaction order with respect to H_2O for Mo_2C, Cu/Mo_2C and Ag/Mo_2C suggests that hydroxyl species (O, OH and H_2O) are the most abundant surface species on the dominant active sites. Consequently, the apparent CO orders over these catalysts are higher than the H_2O orders, implying that relative surface concentration of adsorbed CO is lower than that of the water-generated species. The near zero H_2O order for Mo_2C also suggests that hydroxyl species are bonded more strongly to the Mo_2C surface, meaning that this surface has high reactivity towards activation of water (adsorption and dissociation). This interpretation is in coherence with the DFT calculations made by Liu et al [33], where dissociation of water is shown to be spontaneous over the clean Mo_2C (001) surface. The elementary steps $* + H_2O^* \rightarrow H^* + OH^*$ and $* + OH^* \rightarrow O^* + H^*$ were shown to be exothermic for the Mo-terminated and C-terminated Mo_2C surfaces, implying that water dissociation occurs spontaneously (* denotes the adsorbed species). It was also proposed in the same work that the oxygen generated due to dissociation of water, binds to the Mo_2C surface

strongly, thereby decreasing the number of sites available for the adsorption of other adsorbents. However, they did not allow the surface oxygen formed due to water dissociation to take part in the catalytic cycle. Nonetheless, it is plausible that CO and H_2O will compete for the same sites over the Mo_2C surface. As a consequence, the CO binding strength decreases with increasing oxygen coverage, resulting in lower coverage (higher apparent order) for CO. However, as shown in Figure 2.2, the promotion in the WGS reaction rate is accompanied by a decrease in the apparent CO order. This implies that as the relative concentration of the adsorbed CO on the dominant active sites is increased, the WGS reaction rate per unit surface area of catalyst increases. In other words, with an abundance of water-generated species on the surface of Mo_2C, when there isn't enough adsorbed CO to react with those species, the rate promoting metals provide an alternative site for CO activation. This should decrease the severity of competitive adsorption between CO and H_2O over the catalyst surface and enhance the rate.

As mentioned, apparent reaction orders are dependent on both surface concentrations and adsorption enthalpies. Thus, it appears that the rate promoting metals create sites that bind to CO more strongly compared to the Mo_2C surface under WGS. This observation is in accordance with Sabatier's principle, which says that the optimal value of the adsorption strength of the reactive intermediate over a catalyst surface maximizes the reaction rate. Similar analysis of a volcano-shaped curve has been performed by Grenoble et al [37] for WGS over various metals supported on Al_2O_3. In summary, CO is adsorbed too weakly on the oxygen covered Mo_2C surface to be as reactive as the CO adsorbed on the supported rate promoting metal particles. Therefore, relative CO

adsorption strength can be potentially used as a descriptor to predict the extent of promotion in the WGS reaction rate by different metals over the Mo_2C surface.

It was observed that with a decrease in the CO order, the apparent H_2O order increased from ~0 to more than 0.6 for the catalysts with rate promoting metals. This entails lower coverage of hydroxyl intermediates on the dominant active sites. However, as said before, the water activation is spontaneous over the Mo_2C surface, which is evident from the near zero reaction order with respect to H_2O for unsupported Mo_2C. There are additional experimental evidences for spontaneous water dissociation provided by Hwu et al [38] with single crystal studies over C/Mo (110) to show that water readily dissociates over the carbide surface even at 75°C to produce H_2.Tominaga et al have shown with their DFT calculations that water readily dissociates over Mo_2C (001) surface [34]. Besides, it has been shown that for supported WGS catalysts, metal-support interface is the preferred site for water dissociation as compared to the metal (111) surfaces [39–41]. This suggests that the Metal/Mo_2C catalysts are bi-functional for WGS, wherein the CO is activated by the supported metal particles and water dissociation is carried out by Mo_2C support. To explain the increase in the apparent reaction order with respect to water for the catalysts with rate-promoting admetals, we envision that WGS rate is now controlled by the probability of the combination CO adsorbed on the admetal with a hydroxyl group from the support surface in the vicinity. In other words, the WGS rate is now limited by the supply of the hydroxyl from the support to the CO adsorbed over the admetal. The hydroxyl species would migrate towards the metal particles to react with CO. Such bi-

functional nature of the supported catalysts for WGS is well-documented in the literature [42]. It is believed that the underlying support plays a direct role in activating water molecules. Therefore, we believe that the kinetically relevant steps i.e. the rate determining steps in the WGS mechanism occur either on the admetal surface or on the admetal-Mo_2C interface. This claim is consistent with the observation by Schweitzer et al [23], stating that the WGS reaction rate per total moles of Pt over Pt/Mo_2C was proportional to the number of perimeter sites of the supported Pt particles.

In order to substantiate the claims related to the modification of the adsorption energetics of CO with addition of different admetals, we performed diffuse reflectance infrared spectroscopy (DRIFTS) over the 1.5% Pt/Mo_2C catalyst. The idea was to relate the modification in the CO binding strength with the vibrational frequency of the adsorbed CO molecules and also quantify the CO coverage under reaction conditions. However, since all the Metal/Mo_2C catalysts are black in color, essentially all of the IR radiation was absorbed and no peaks related to the adsorbed CO molecules could be observed even at dilution ratios of 80:1 with diamond dust (see Appendix A for details).

However, the CO TPD experiment does show subtle differences in the desorption spectra with addition of metals. The evolution of CO_2 during CO TPD over supported catalysts has been reported in the literature before [43,44]. The possible causes for CO_2 formation have been suggested to be CO oxidation, water-gas shift reaction or CO disproportionation. Assuming that CO_2 is formed due to one of these surface reactions, it

is plausible that the activation barriers for these reactions are likely to get affected by the adsorption strength of CO. Thus, variation of the adsorption strength of CO with different admetals can reflect in the CO_2 evolution temperature. Therefore, CO_2 peak positions can be used as a means of comparison of the relative adsorption strength of the fraction of CO that reacts to form CO_2 [45] . The CO desorption spectra show that the Cu/Mo_2C and Ag/Mo_2C did not lead to any noticeable modification of the CO adsorption sites over Mo_2C. This claim is supported by the CO_2 evolution plots from Ag/Mo_2C and Cu/Mo_2C, which match with those from Mo_2C in terms of shapes and peak positions. Ni/Mo_2C exhibits a more pronounced peak at ~170°C compared to the Mo_2C catalyst, suggesting that Ni creates additional sites with CO binding affinity similar to the sites over Mo_2C associated with the 170°C desorption peak. For Pd, Au and Pt the relative intensity of this peak at 170°C appeared diminished compared to Mo_2C, which suggests that these metals partially block the adsorption sites over Mo_2C associated with the peak at 170°C. However, significant differences are observed between CO_2 evolution from noble metals supported over Mo_2C and the Mo_2C support. Ni, Pd, Pt and Au exhibit shoulders at higher temperatures in the CO_2 evolution spectra as compared to Mo_2C, which suggests that these metals create adsorption sites for CO with a higher binding affinity. In summary, the CO TPD data shows that the rate-promoting metals lead to subtle but noticeable modifications in the CO adsorption sites over Mo_2C. This supports our theory formulated from the correlation between WGS rates per unit surface area and the apparent CO order for Metal/Mo_2C catalysts, based on which, the CO adsorption strength over the sites created by admetals can be potentially used as a descriptor.

2.4.2 Interactions of admetals with Mo_2C

Au nanoparticles supported on oxide supports such as iron oxide, titanium dioxide and alumina are known to sinter upon their exposure to high temperature [46]. In fact, this tendency of sintering was utilized to vary the average particle size of supported Au clusters over Au/TiO_2 and Au/Al_2O_3 to study the effect of Au particle size on the WGS reaction rate [47]. The particle size of the supported Au clusters has been shown to play an important role in the activity of such catalysts for reactions such as CO oxidation and WGS [47,48]. A driving force for sintering occurs when the cohesive interaction between Au atoms is stronger than the adhesive interaction between Au and the support. Additionally, at temperatures as high as 600 ºC, supported Au clusters can have sufficient mobility to assist sintering by particle-particle collision. Such behavior was expected for the Au clusters supported on passivated Mo_2C, i.e. during the carburization pretreatment at 600 ºC, and the average Au particle size over Au/Mo_2C was expected to increase. However, as mentioned above, a significant decrease in the average Au particle size (from ~9 nm to 3 nm) was observed during carburization, based on the EXAFS results. The purpose of the carburization pretreatment is to remove oxygen from the surface of passivated Mo_2C support to bring it back in its native form. As the temperature is increased, i.e. as more oxygen is removed, the Au nanoparticles get smaller. This suggests that the adhesive interaction between the relatively oxygen-free Mo_2C surface and the supported Au nanoparticles is stronger than the cohesive interaction between the Au atoms. The decrease in the average particle size of Au clusters was confirmed with the HAADF-STEM (Figure 2.8). The observed change in the average particle size of Au clusters explains the difference in the XRD patterns for fresh and used (carburized)

Au/Mo_2C. The Au (111) peak at 38.2º was observed for the fresh Au/Mo_2C catalyst, for which the average Au particle size was ~ 9 nm (estimated from EXAFS). Although this peak at 38.2º overlaps with other peaks assigned to the Mo_2C support, it is absent from the pattern for the used catalyst that had undergone carburization. The absence of the peak related to Au metal confirms the decrease in the average particle size of Au crystallites. Similarly, for Ag/Mo_2C the average particle size for the Ag crystallites also decreases after carburization, since the Ag (111) peak at 38.3º, observed in the XRD pattern for the fresh Ag/Mo_2C, is absent after carburization.

For the Pt particles, the observed coordination geometry (bond distances and the average coordination numbers) can be satisfied by various morphologies. As argued by Schweitzer et al. [23], the Pt should form flat raft-like particles, which are only a few layers thick. The EXAFS data of such relatively flat particles (compared to the cubo-octahedral geometry) is expected to show Pt-Mo coordination. The authors have claimed that since the maximum Pt-Mo CN observed was 1.5, Pt-Mo alloy particles were not formed. However, in our case, the observed Pt-Mo CN was ~4, suggesting that a higher number of Pt atoms are bound to Mo than can be accommodated in a flat raft-like Pt particle. If the metal particles observed are the intermixed alloys of Pt and Mo, one would expect to observe the Pt-Mo bonds. Our HAADF-STEM micrographs with EELS scan through the metal particles shown in Figure 2.11, (at the edge of the support crystallite) show that there is Pt as well as Mo present in some of the particles. This suggests that all the Pt particles on Pt/Mo_2C are not necessarily flat and it is possible that Pt-Mo bimetallic

particles are formed. These differences in structure in the two examples may be explained by the fact that our preparation method for Pt/Mo_2C has some differences with the method used by Schweitzer et al.

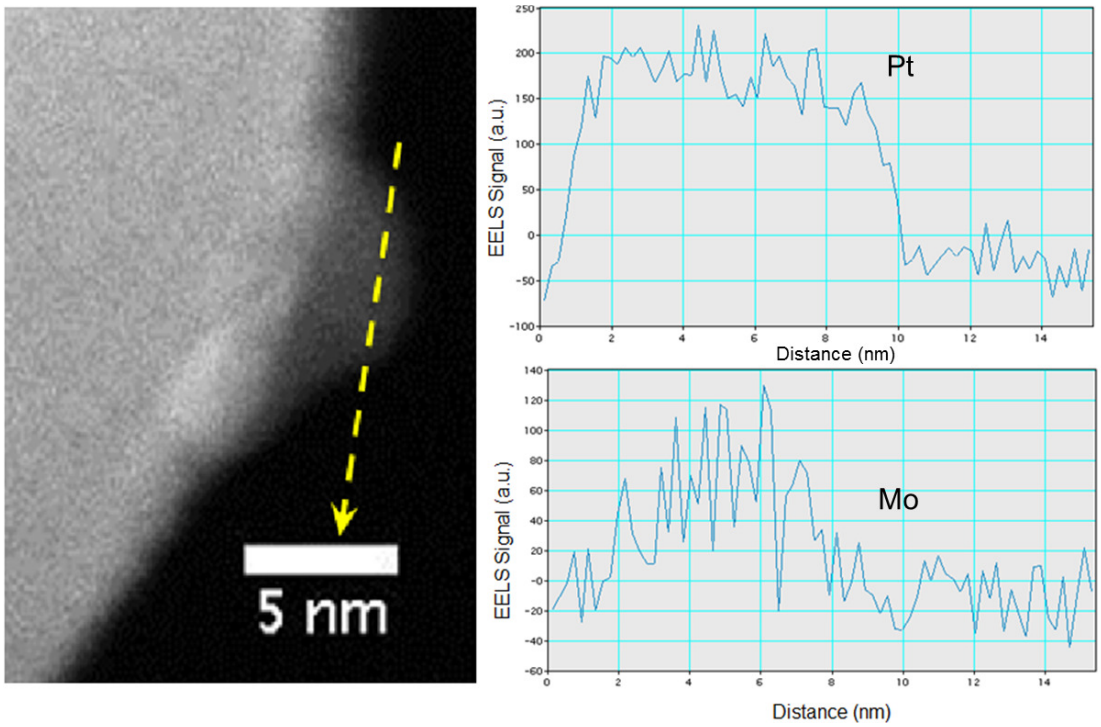

Figure 2.11 (Left) Representative HAADF-STEM micrograph of the 'used' 1.5% Pt/Mo2C catalyst used to assess the compostion of the observed particles The yellow line represnts the locus of the points at which the EELS scans were collected through the particle. (Right) The EELS signal vs. intensity plots at Pt and Mo edge

In our method, the passivated Mo_2C support was used for Pt deposition, whereas the Pt precursor solution was directly contacted with the unpassivated native Mo_2C surface in the method used by Schweitzer et al.

In summary, it was observed that the Au and Pt particles interact strongly with the native Mo_2C surface, and the particles do not appear to sinter at temperatures as high as 600 ºC. This would make Mo_2C an ideal support for making thermally robust supported metal catalysts. The ability of the Mo_2C support to stabilize the metal particles of Au and Pt could be particularly interesting from the standpoint of electronic effects induced in the metal particles. Rodriguez and Illas [49] have predicted, using density functional calculations, that the carbide surface causes significant electronic perturbations in admetals like Au. The electron density transferred to the admetals was predicted to facilitate their bonding with electron-acceptor molecules like CO. This could serve as the explanation for the admetals such as Au, which normally show weak CO bonding, being the preferred sites for CO activation during WGS.

2.5 Conclusions

A series of catalysts with Pt, Au, Pd, Ni, Cu and Ag deposited on Mo_2C was prepared. Deposition of Ag did not lead to any improvement, Cu showed a minor promotion in the WGS rate per unit surface area over Mo_2C measured at 120 ºC in presence of 6.8% CO, 21.9% H_2O, 8.5% CO_2, 37.4% H_2, whereas Pt, Pd, Au and Ni were identified as the rate promoting metals. The WGS rates per unit surface area of catalyst over Pt/Mo_2C, Au/Mo_2C, Ni/Mo_2C and Pd/Mo_2C were higher than that of the commercial $Cu/ZnO/Al_2O_3$ catalyst. The promotion in the WGS rate per unit surface area of catalyst was accompanied by an increase in the apparent H_2O order, a decrease in the apparent

CO order, and a decrease in apparent activation energy. The enhancement in the rate and the kinetic parameters depend on type of admetal. Hence, it was predicted that the

location of the dominant active site was modified from the Mo_2C support to the admetal surface or admetal-Mo_2C interface. The Metal/Mo_2C catalysts are suggested to be bi-functional in nature for WGS reaction. The adsorption strength of CO, which increases as the CO reaction order decreases, was identified as a potential descriptor for promotion by an admetal towards WGS reaction over these catalysts. Even though difficulties were faced in observing the changes in adsorption energetics with addition of admetals to Mo_2C using vibrational spectroscopy, we have demonstrated the use of the apparent kinetic parameters to elucidate the role of admetals. The CO TPD experiments also showed that the rate-promoting admetals lead to subtle but noticeable modifications in the CO adsorption properties of Mo_2C. Systematic DFT calculations and microkinetic models will be needed to further corroborate our hypotheses related to this property-activity relationship. The *In Situ* XAS and High Resolution STEM-EELS results indicated a strong interaction between supported Au and Pt nanoparticles and the Mo_2C support surface and suggest that Mo_2C would be an ideal support for making thermally robust supported metal catalysts.

CHAPTER 3. PROBING THE ACTIVE SITES FOR WATER-GAS SHIFT OVER PLATINUM/ MOLYBDENUM CABIDE USING CARBON NANOTUBES

3.1 Introduction

Metal-modified transition metal carbides have been a topic of interest in the field of heterogeneous catalysis, owing to the intriguing catalytic properties displayed by these materials [50]. Previous studies have shown that admetals such as Pt and Ni [51–53]. The ability of molybdenum carbide surfaces to stabilize the small admetal nanoparticles gives an added advantage.

In Chapter 2, it has been demonstrated that the transition metal-modified molybdenum carbide catalysts exhibit the water gas shift (WGS) reaction rates that are 4 to 8 times higher than the commercial catalyst when normalized by the surface area of the catalyst. We have also shown that the admetals modify the CO adsorption properties of the bulk Mo_2C and promote the WGS reaction rate over Mo_2C. As the apparent reaction parameters for WGS over metal/Mo_2C changed with the admetal, we concluded that the kinetically important steps occur in the vicinity of the sites created by the admetal particles. However, unlike the oxide supports, Mo_2C exhibits its own WGS activity; hence the WGS rates measured over metal/Mo_2C are a combination of the rates due to Mo_2C support sites and the rate due to the sites created by the admetal. Additionally, as

Mo_2C adsorbs probe molecules (such as CO and H_2), the metal/Mo_2C catalysts pose a problem of improper normalization of WGS reaction rates as the exposed surface area of the admetal particles cannot be selectively measured [23]. Also, the bulk Mo_2C is a high-Z type of material, which offers a poor contrast between admetal particles and the Mo_2C support in electron microscopy. Summarizing, from the point of view of catalyst characterization for determination of the active sites, bulk Mo_2C is not an ideal material. In order to overcome the aforementioned limitations, in the present work, we have utilized Multi-Walled Carbon Nanotubes (MWCNT) as support, for the synthesis of Pt/Mo_2C, using which we have de-convoluted the importance of Pt or Pt-Mo_2C contact sites towards the WGS reaction rates from the contribution of Mo_2C. We have performed *in situ* X-ray absorption spectroscopy to observe the working state of the catalysts during the carburization pretreatment and WGS reaction. The high angle annular dark field-scanning transmission electron microscopy (HAADF-STEM) combined with Electron Energy Loss Spectroscopy (EELS) was used to understand the morphology and qualitatively determine the elemental composition of the supported metal particles over Mo_2C.

3.2 Experimental methods

3.2.1 Catalyst synthesis

The catalysts prepared for this work were a series of Pt/Mo_2C/MWCNT samples with varying Pt and Mo weight loadings. The low-Z MWCNTs have been shown to be a good support for catalyst characterization using electron microscopy and x-ray absorption techniques [54]. The MWCNT support was purchased from Cheap Tubes Inc. The as

purchased support was treated with 69 wt. % HNO_3 for 4 h at 120°C, followed by washing with deionized water. After drying the support overnight, the metals were added by sequential wetness impregnations. The aqueous solution of ammonium paramolybdate ($(NH4)_6Mo_7O_{24}\cdot 4H_2O$, Alfa Aesar) was used as the Mo precursor. After the impregnation of Mo, the material was dried overnight in a static oven at 150 ºC. The dried material was subjected to temperature programmed reduction in presence of pure hydrogen (ramp rate 3 ºC/min, final temp. 600 ºC) and was maintained at final temperature for 4 hours. During this reduction process, the carbon from the support reacts with the Mo to form Mo_2C domains [55]. This material was passivated at RT with 1% O_2/Ar mixture, before Pt was impregnated using the aqueous solution of tetrammineplatinum nitrate (Sigma Aldrich). Two sets of catalysts were prepared: (1) varying the Mo loading (to vary the amount of Mo_2C formed) while keeping the Pt loading fixed and (2) varying the Pt loading (to increase the number of Pt/Mo_2C contact sites) at a fixed Mo loading. For the first series, the Pt loading was kept fixed at 1.5 wt. %, while the Mo loading was varied as 2%, 3%, 10% and 20%. For the other series, the Mo loading was fixed at 10%, while the Pt loading was varied as 0.5%, 1.5%, 3% and 5%. A Mo free sample 4% Pt/MWCNT was also synthesized and tested for WGS.

3.2.2 WGS Kinetic Measurements

The WGS reaction rates and apparent kinetic parameters were measured using a four fixed bed reactor system described elsewhere [24] . Appropriate amounts of each catalyst were loaded. The catalysts were reduced in pure H_2 (75 sccm) at 600°C (3 °C/min) for 4 h, in order to remove the oxygen introduced during passivation from the surface of Mo_2C.

Following the reduction pretreatment, the catalysts were cooled to 120°C under Ar. The WGS reaction mixture comprising of 6.8% CO, 21.9% H_2O, 8.5% CO2, 37.4% H_2 and balance Ar was introduced as feed to the reactors. Prior to the measurement of apparent kinetic parameters, the catalysts were maintained under the aforementioned WGS conditions for 20 h. In order to achieve differential conditions, the conversion of CO was kept below 10%. For the measurement of apparent reaction orders, one gas concentration was varied at a time (4–21% CO, 5–25% CO_2, 11–34% H_2O, and 14–55% H_2). The apparent activation energies were measured by varying the temperature over a range of 30°C, while keeping the gas concentrations fixed at standard conditions. After the measurement of apparent kinetic parameters, the catalysts were passivated at room temperature.

3.2.3 Catalyst Characterization

The CO uptake was measured over each catalyst at 35°C using the Micromeritics ASAP 2020 analyzer. Prior to the chemisorption measurement, the passivated catalysts were reduced in H_2 at 600°C. The CO uptake measurements are used as a measure of the total number of active sites (Mo_2C sites and the sites created by the addition of Pt).

The *in situ* x-ray absorption (XAS) experiments were carried out at the Pt L_{III} edge and the Mo K edge were carried out at the MRCAT 10 BM (bending magnet) beam line at the Advance Photon Source at Argonne National Laboratory. Due to the low-Z CNTs, all the XAS experiments could be carried out in the transmission mode. The XAS experiments were conducted in 1 in OD quartz tubes connected to Ultra-Torr fittings with welded ball valves (for gas inlet/outlet and sealing) and Kapton windows. The catalyst samples were

pressed into a 6 well sample holder as self-supporting wafers. The catalysts were reduced at 600°C in pure H_2. The scans at Pt L_{III} edge and Mo K edge were collected at RT in presence of Helium. The x-ray absorption was also measured for the catalysts with varying Pt loading under WGS conditions at 160°C, following the reduction at 600°C. The catalysts were exposed to a mixture of 6.8% CO, 8.5% CO_2, 22% H_2O, 37.4% H_2 and balance Helium.

The XAS data was analyzed using WINXAS 3.1 software. The x-ray absorption near edge structure (XANES) data was energy-calibrated by computing the first derivative of the first peak of the spectra for Pt and Mo metal foil standards and comparing them to the known edge position. The edge energies for the Pt and Mo edge data for various catalyst samples were computed from the first derivative of the XANES spectra. The extended x-ray absorption fine structure (EXAFS) data was fit using experimental standards and references computed using the FEFF6 code. Phase shifts and amplitudes for Pt-Pt and Mo-Mo scatters were obtained from the foil standards of the respective elements. The phase and amplitude for the Pt-Mo bimetallic alloy was obtained using the FEFF6. From the least square fits for the first shell, average coordination numbers, bond distances and the Debye-Waller factors were obtained for all the tested catalysts.

STEM and EELS analyses were carried out using the dedicated aberration-corrected STEM Hitachi HD-2700C at 200 kV equipped with a modified Gatan Enfina ER spectrometer hosted at the Center for Functional Nanomaterials, Brookhaven National Laboratory. The convergence angle and the ADF collection angles were 28 mrad and 64-

341 mrad, respectively. The Enfina spectrometer entrance aperture was set to 3 mm resulting in EELS collection angle of 26.7 mrad and an energy resolution of 0.35 eV as measured from the full width at half maximum (FWHM) of the zero-loss peak. The EELS spectra for Mo, and Pt were collected at the $M_{4,5}$ edges. The EELS dwell time was varied between 0.1–0.3 seconds to avoid beam induced structural changes. The step size for line-scans and mapping was varied between 1-3 Å. The core-loss intensities were extracted by extrapolating the background using a power-law model and subtracting it from the acquired signal. Data processing was carried out using Gatan Digital Micrograph.

The area of the MWCNT support covered by the Mo_2C domains as well as the Pt containing particles was computed using ImageJ software. The average particle size of the Pt containing particles over the catalysts used for WGS was measured using the Adobe Photoshop software.

3.3 Results

3.3.1 Interpretation of WGS kinetics

The method of preparation of Mo_2C/MWCNT was adapted from the published literature [8]. As mentioned before, two sets of Pt/Mo_2C/MWCNT catalysts were prepared: (1) varying the Mo loading (to vary the amount of Mo_2C formed) while keeping the Pt loading fixed (1.5%) and (2) varying the Pt loading (to increase the number of Pt-Mo_2C contact sites) at a fixed Mo loading (10%). The detailed WGS kinetic data over these

catalysts is presented in Table 3.1. Except for the 10% Mo/MWCNT (Pt free) catalyst and the 4% Pt/MWCNT (Mo free) catalyst, all the other catalysts in these two sets were tested at 120ºC, so that the WGS kinetic parameters can be objectively compared. As shown in Table 3.1 and Figure 3.1, the apparent WGS reaction orders over Pt/Mo_2C/MWCNT catalysts are independent of Pt loading as well Mo loading. The apparent orders observed are $H_2O \sim 0.75$, $CO \sim 0$, $CO_2 \sim 0$ and $H_2 \sim -0.25$. This suggests that the chemical nature of the active sites over these catalysts is similar across the two sets of samples tested for WGS. More importantly, the apparent reaction orders over Pt/Mo_2C/MWCNT catalysts are similar to the apparent reaction orders measured over Pt/bulk Mo_2C (Appendix A). Additionally, the apparent activation energies of these catalysts (49-56 kJ/mol) are similar to the apparent activation energy for Pt/bulk Mo_2C. Thus, these catalysts are used as 'surrogates' for the characterization of Pt/Mo_2C systems, as they possess the active sites of similar chemical nature.

Table 3.1WGS Kinetics data over Pt/Mo_2C/MWCNT at 120°C

Catalyst	0.5% Pt 10% Mo	1.5% Pt 10% Mo	3 % Pt 10% Mo	5% Pt 10% Mo	1.5% Pt 2% Mo	1.5% Pt 3% Mo	1.5% Pt 20% Mo	10% Mo
Rate/10^{-2} mol H_2 (mol Pt)$^{-1}$ s^{-1}	1.6	1.7	1.4	1.2	0.9	1.3	1.7	1.9
Rate/10^{-6} mol H_2 (g.cat.)$^{-1}$ s^{-1}	0.4	1.3	2.1	3.1	0.7	1	1.3	1.5
Ea /kJ(mol)$^{-1}$(±3)	58	55	52	48	49	51	55	55
H_2O (±0.04)	0.75	0.7	0.79	0.75	0.78	0.8	0.7	0.72
CO (±0.04)	-0.01	-0.04	-0.02	0	0.01	-0.01	-0.04	-0.03
CO_2 (±0.04)	-0.04	-0.01	-0.09	-0.11	-0.13	-0.03	-0.01	-0.05
H_2 (±0.04)	-0.19	-0.24	-0.25	-0.3	-0.3	-0.24	-0.24	-0.32

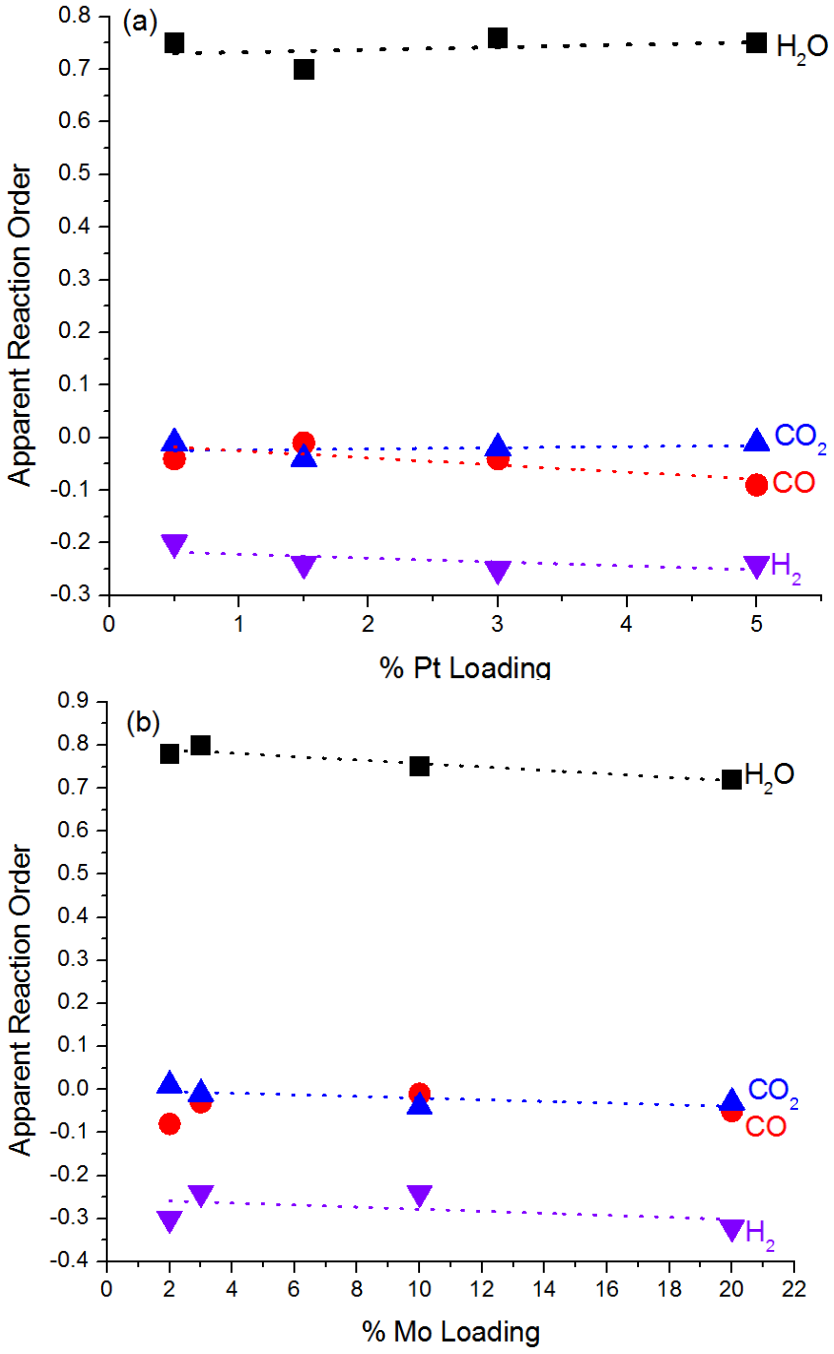

Figure 3.1 Dependence of apparent WGS reaction orders measured at 120°C on (a) Pt loading at 10% Mo loading (b) Mo loading at 1.5% Pt loading

The central idea is to de-convolute the importance of Pt sites (Pt-Mo_2C contact sites) from the Mo_2C sites, towards the WGS reaction, as Mo_2C has significant reactivity for WGS at 120 ºC. As all the catalysts in the two sets possess the active sites of similar nature, the difference in the WGS rates (normalized by the amount of catalyst) is caused only by the difference in the absolute number of active sites over these catalysts.

As shown in Figure 3.2, for a constant amount of Pt (1.5%), the WGS rate per gram of catalyst at 120 ºC increases by a factor of 2.1,with a change in Mo weight loading from 2% to 20%.

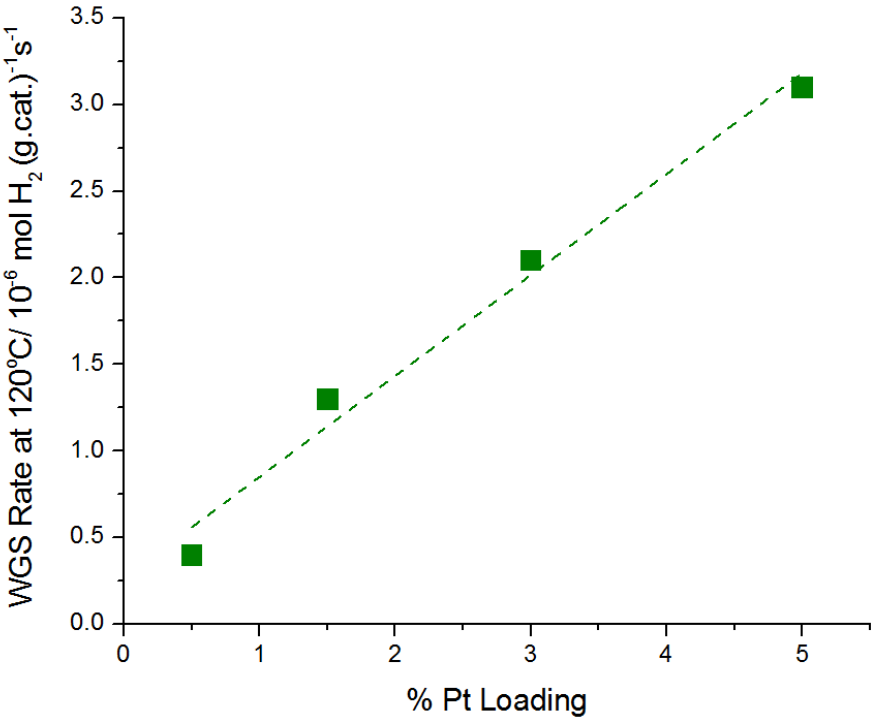

Figure 3.2 WGS rate per gram at 120°C versus % Pt loading at a fixed (10%) Mo loading

On the other hand, for a constant amount of Mo (10%), the WGS rate per gram increases by a factor of 8.2 with a change in the Pt weight loading from 0.5% to 5% (Figure 3). The shape of the curve for varying Mo loading suggests that the WGS rate per gram of catalyst at 120 ºC levels off after a certain amount of Mo. However, there is a sharp linear increase in the WGS rate per gram when Pt loading is increased, while the Mo loading is fixed.

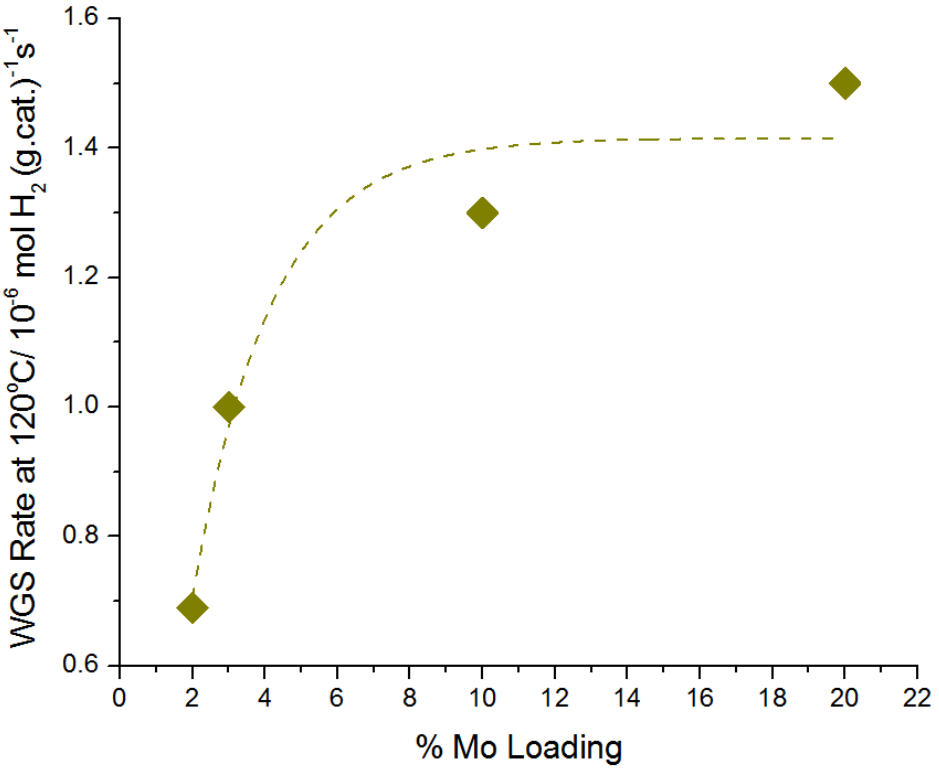

Figure 3.3 WGS rate per gram at 120°C versus % Mo loading at a fixed (1.5%) Pt loading

3.3.2 Catalyst Characterization

CO uptake experiments were performed to count the total number of active sites on the surface of each catalyst. The catalysts were reduced at 600 ºC (to mimic the pretreatment performed before the WGS kinetic measurement) prior to the CO adsorption at 35 ºC. As shown in Figure 3.4, the moles of CO adsorbed per gram of catalyst increases linearly with the Mo loading, suggesting the creation of more Mo_2C sites with increasing amount of Mo. However, for the set of catalysts with increasing Pt loading, the amount of CO adsorbed remained constant with the amount of Pt, implying that the presence of Pt had a negligible effect on the CO chemisorptions properties of these catalysts. In Figure 3.5, the nominal turnover rate (TOR) i.e. the WGS rate per gram normalized by the moles of CO chemisorbed per gram of catalyst is plotted against the Mo and Pt loadings. For the increasing Mo series, the nominal TOR at 120ºC decreases with the increasing Mo loading, while for the increasing Pt series, the nominal TOR increases linearly with the Pt loading.

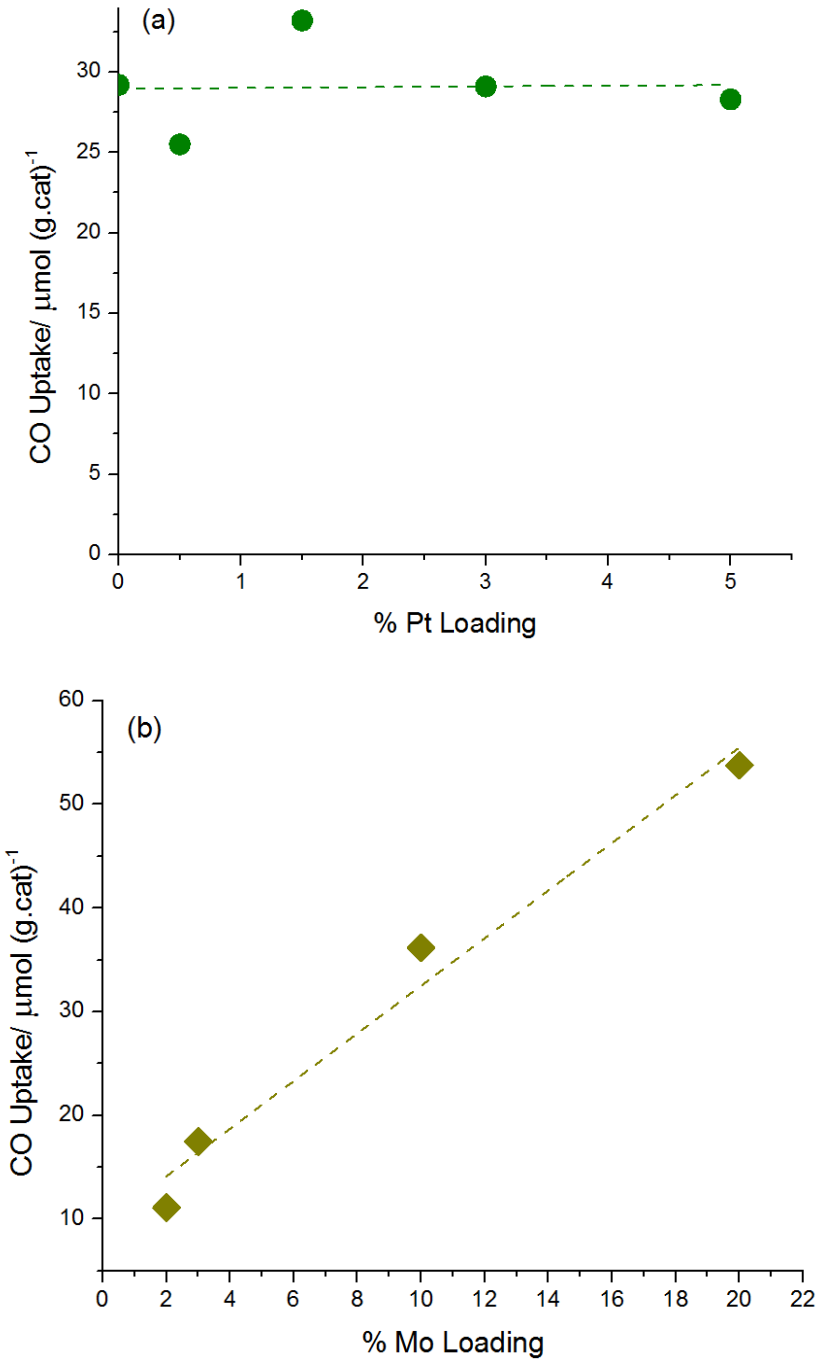

Figure 3.4 WGS rate per gram at 120°C versus (a) % Pt loading at a fixed (10%) Mo loading (b) % Mo loading at a fixed (1.5%) Pt loading

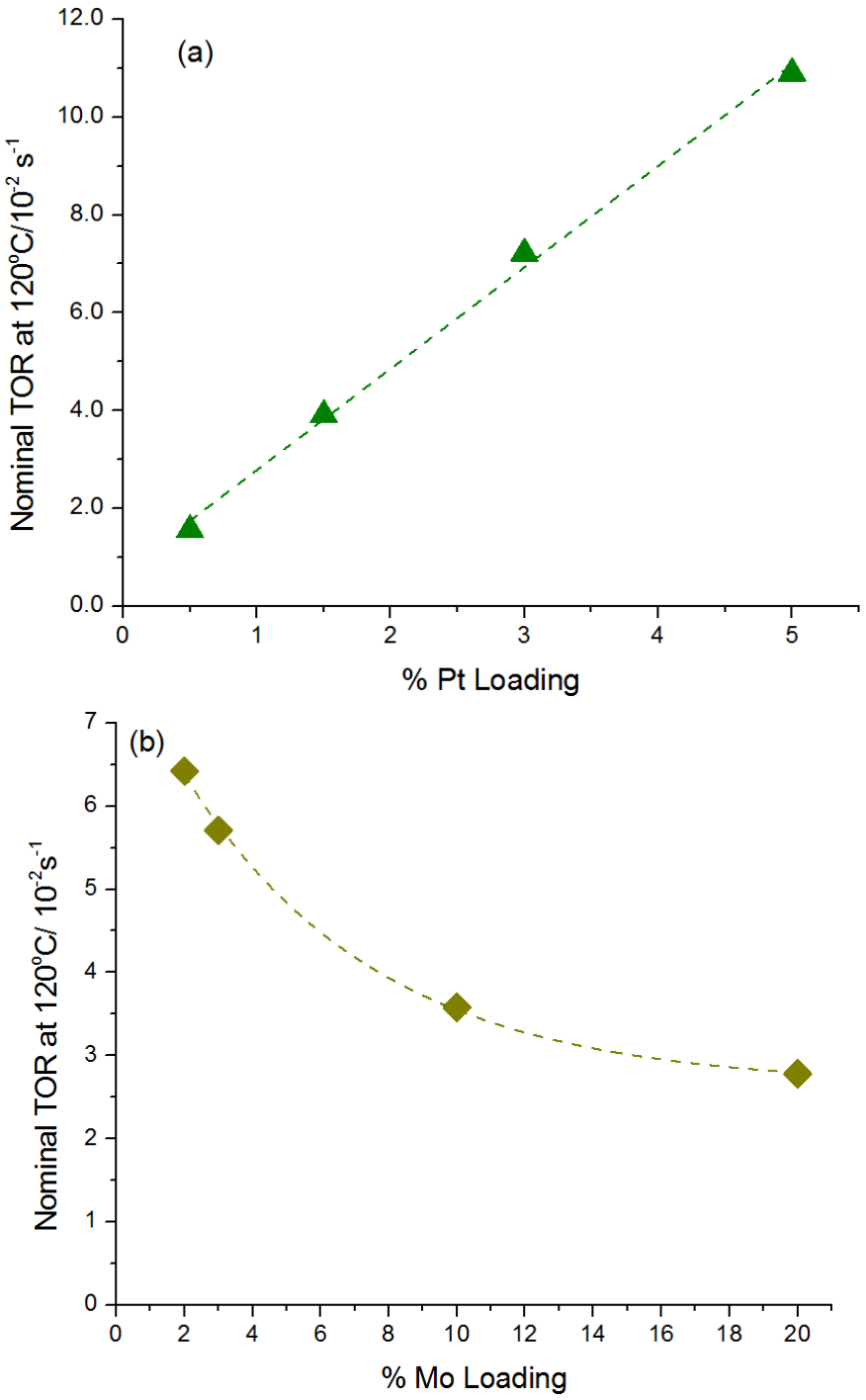

Figure 3.5 (a) Nominal WGS TOR at 120 ºC vs. % Pt loading (b) Nominal WGS TOR at 120 ºC vs. % Mo loading for the Pt/Mo_2C/MWCNT catalysts.

In situ X-ray absorption was performed over all the Pt/Mo_2C/MWCNT catalysts to study the morphology and oxidation state of Pt clusters after the 600 ºC reduction treatment. Figure 3.6 (a) depicts the representative Pt L_{III} XANES spectrum measured under Helium atmosphere for 1.5% Pt/ 2% Mo/ MWCNT after the reduction at 600 ºC. As compared to the Pt foil, there are observable differences exhibited. There is a shift in the leading edge towards higher energy. However, the edge energies (obtained from the energy of the first inflection point) is similar (rather, the shift is not enough to account for the presence of oxidized Pt) for the Pt foil (11.5640 keV) and the catalyst (11.5652 keV), suggesting that Pt is fully reduced. The observed differences are attributed to the formation of Pt-Mo bimetallic nanoparticles [26]. The Fourier transforms of Pt L_{III} edge EXAFS spectra is shown in Figure 3.6 (b). Differences in the magnitude between the foil and the catalyst indicate scattering from elements other than Pt. The fit parameters (Table B.1) show the Pt-Pt contribution with coordination number 4.1 (after the reduction) with inter-atomic distance of 2.74 Å. The peak at 2.73 Å is attributed to Pt-Mo bond, with the inter-atomic distance consistent with metallic Mo atoms directly bonded to Pt. Thus, Pt L_{III} EXAFS also indicates the formation of Pt-Mo bimetallic particles. Table B.1 shows that before reduction, the Pt is oxidized (evident from Pt-O coordination) at all Mo loadings. After reduction, the Pt-Pt coordination numbers (~ 4) and Pt-Mo coordination numbers (~ 4.6) are similar for all the catalysts and are independent of the Mo loading.

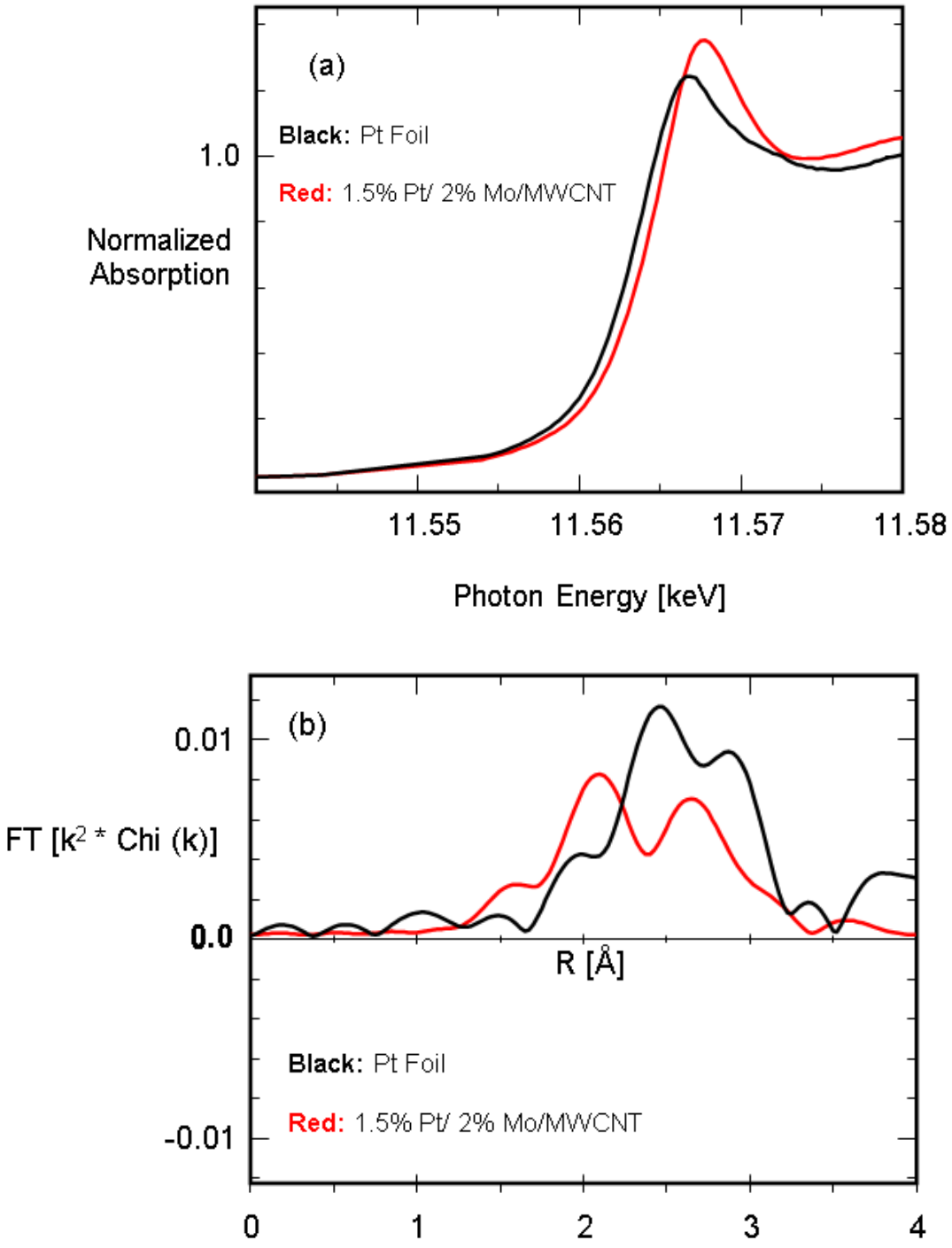

Figure 3.6 (a) *In situ* Pt L_{III} edge XANES spectrum for the 1.5%Pt/ 2% Mo/MWCNT catalyst after the 600 ºC reduction (b) *In situ* Pt L_{III} edge FT EXAFS spectrum for the 1.5%Pt/ 2% Mo/MWCNT catalyst after the 600 ºC reduction.

The Mo K edge XANES spectrum for the 1.5% Pt/ 20% Mo/ MWCNT, recorded after 600 ºC reduction, is shown in Figure 3.7 (a). This spectrum is identical to the bulk Mo_2C standard that was treated in 15% H_2/CH_4, which confirms the formation of Mo_2C domains on the MWCNT support. Figure 3.7 (b) shows the Mo K edge XANES after 600 ºC reduction, for the catalysts with varying Mo loading. While there are systematic changes observed in the post-edge features, the pre-edge features remain unchanged with the Mo loading. Additionally, the Mo edge energies are also the same for the catalysts with increasing Mo loading. Figure 3.8 (a) shows the FT magnitude of the Mo K edge EXAFS spectra for the Mo_2C standard and the 1.5% Pt/ 20% Mo/ MWCNT after the pretreatment. The shapes and the positions of the peaks (assigned to Mo-C and Mo-Mo) for the 1.5% Pt/ 20% Mo/ MWCNT catalyst match with the peaks for Mo_2C. The smaller intensity of the peaks for the 1.5% Pt/ 20% Mo/MWCNT catalyst indicates the formation of Mo_2C domains that are smaller in size as compared to the bulk carbide. As shown in Figure 3.8 (b) (the Mo Kedge EXAFS for catalysts with increasing Mo loading), the intensity of the Mo-Mo peak increases with increasing Mo loading, suggesting that addition of more Mo leads to the formation of larger Mo_2C domains. No evidence for Mo-Pt bonds was obtained at the Mo K edge EXAFS, probably due to the excess amount of Mo as compared to Pt.

.

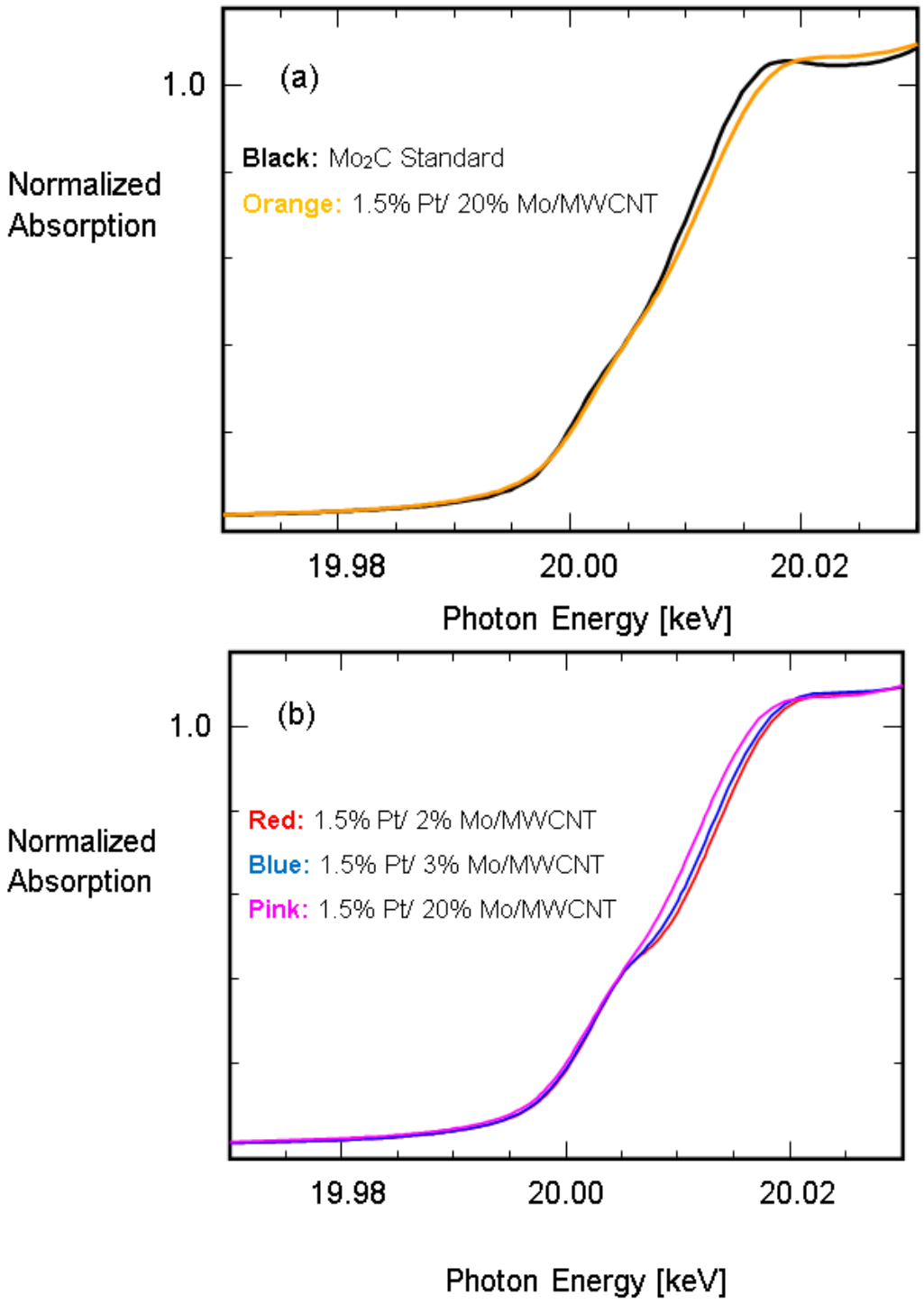

Figure 3.7 (a) *In situ* Mo K edge XANES spectrum for the 1.5%Pt/ 20% Mo/MWCNT catalyst after the 600 ºC reduction (b) *In situ* Mo K edge XANES spectra for the Pt/Mo_2C/MWCNT catalysts with varying Mo loading after the 600 ºC reduction.

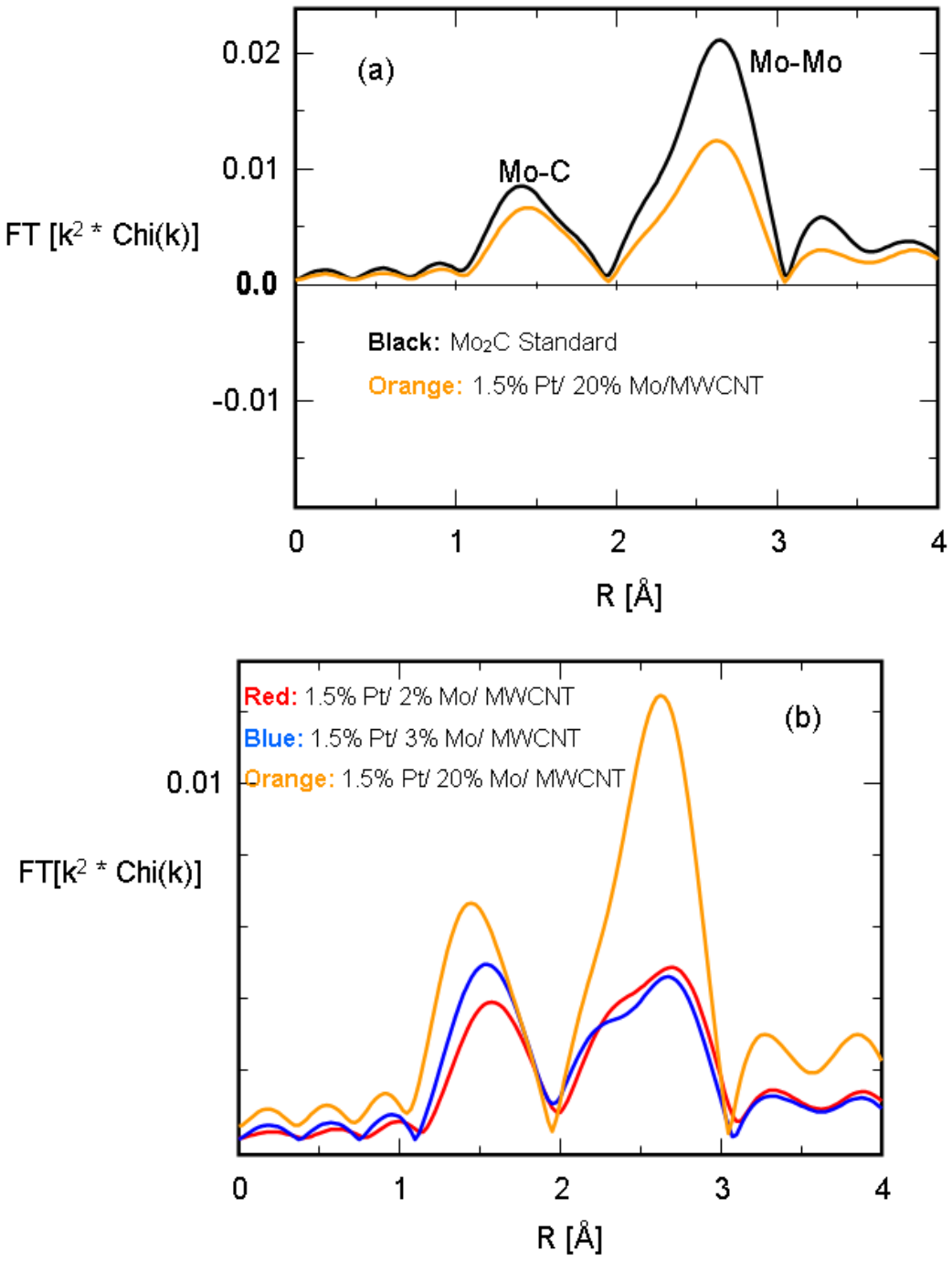

Figure 3.8 (a) *In situ* Mo K edge FT EXAFS spectrum for the 1.5%Pt/ 20% Mo/MWCNT catalyst after the 600 ºC reduction (b) *In situ* Mo K edge FT EXAFS spectra for the Pt/Mo_2C/MWCNT catalysts with varying Mo loading after the 600 ºC reduction.

Table B.2 shows the details of the EXAFS fits for the Pt/Mo_2C/MWCNT catalysts with varying Pt loading at a fixed Mo loading. The X-ray absorption over these catalysts was performed at two different stages, viz. at room temperature after the 600 ºC reduction and during the course of WGS reaction at 160ºC. The average Pt-Pt and Pt-Mo coordination numbers and the Pt L_{III} edge energies are similar for all the catalysts in this set. These parameters obtained after the 600ºC reduction are in turn similar to the parameters obtained for 1.5% Pt/ 2% Mo/ MWCNT (from the varying Mo series), suggesting that Pt was in a similar chemical state and similar coordination environment. Thus, after the 600 ºC reduction, all the catalysts with varying Pt loading possess Pt-Mo bimetallic particles, where Pt is in fully reduced state. The Mo K edge FT EXAFS spectra confirm the formation of Mo_2C (even in absence of Pt) as shown in Figure 3.9. The first shell (Mo-C) is same for all the catalysts with varying Pt loadings. However, the intensity of the Mo-Mo peak at the second shell changes significantly with the addition of Pt. With higher amount of Pt, the intensity of Mo-Mo peak becomes smaller, marking a decrease in the size of Mo_2C domains.

The edge energies at both the edges (Mo K edge and Pt L_{III} edge) and the average coordination numbers (Pt-Pt, Pt-Mo, Mo-C and Mo-Mo) do not change significantly when the catalysts are exposed to the WGS reaction mixture at 160 ºC. This suggests that Pt stays in fully reduced state, alloyed with Mo during WGS reaction. No evidence of the Mo_2C surface getting oxidized under WGS was obtained from the Mo K edge spectra. In summary, the *in situ* XAS data indicate that the Pt-Mo bimetallic particles are formed

over all the Pt/Mo_2C/MWCNT catalysts. The coordination environment of Pt (the average coordination number) does not depend either on the Pt loading or the Mo loading.

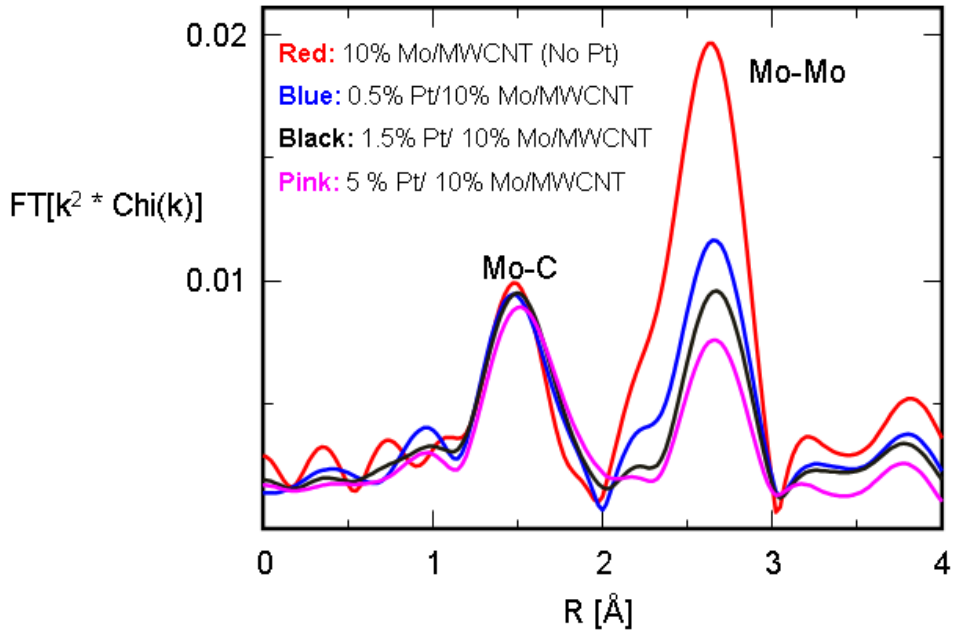

Figure 3.9 *In situ* Mo K edge FT EXAFS spectrum for the Pt/ Mo_2C/MWCNT catalysts with varying Pt loading (at fixed Mo loading) after the 600 ºC reduction.

Figure 3.10 (a) shows a HAADF-STEM image of the 5 % Pt/10 % Mo/MWCNT catalysts. A magnified image of carbon nanotube region exhibits features of two different contrast levels (Figure 3.10 (b)). The contrast on HAADF-STEM images stems from differences in mass-thickness, where the intensity scales roughly with the atomic number squared ($\approx Z^2$). Thus based on the contrast difference, the bright features are assigned as Pt particles, whereas regions of lower contrast are designated as patches of Mo_2C in Figure 3.10 (c). The chemistry of the observed particles was investigated with the EELS

at both Pt and Mo edges and the particles are confirmed to contain both Pt and Mo, as shown in Figure 3.11. The particles are pre-dominantly found to be well-mixed Pt-Mo alloys. Using the HAADF-STEM images, the surface area of the Pt-Mo bimetallic particles was quantified and normalized by the surface area of the observed MWCNT surface, as shown in Figure 3.10 (c).

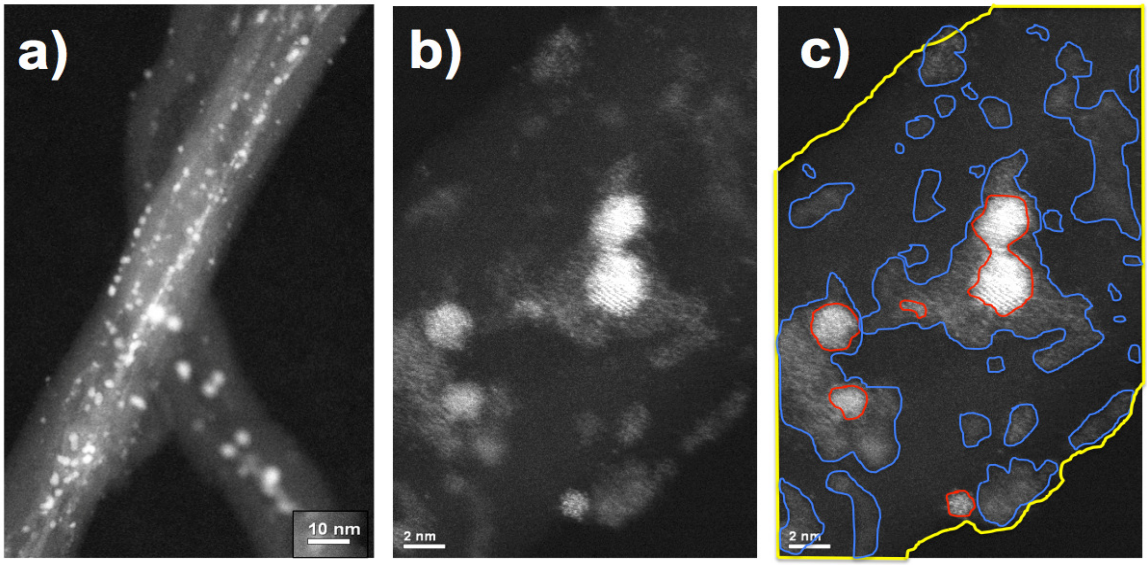

Figure 3.10 Representative HAADF-STEM micrographs obtained for the used 5% Pt/ 10 Mo/MWCNT catalyst. The brightest domains are the Pt-Mo bimetallic particles surrounded by the Mo_2C domains with a relatively lower brightness against the carbon nanotube surface.

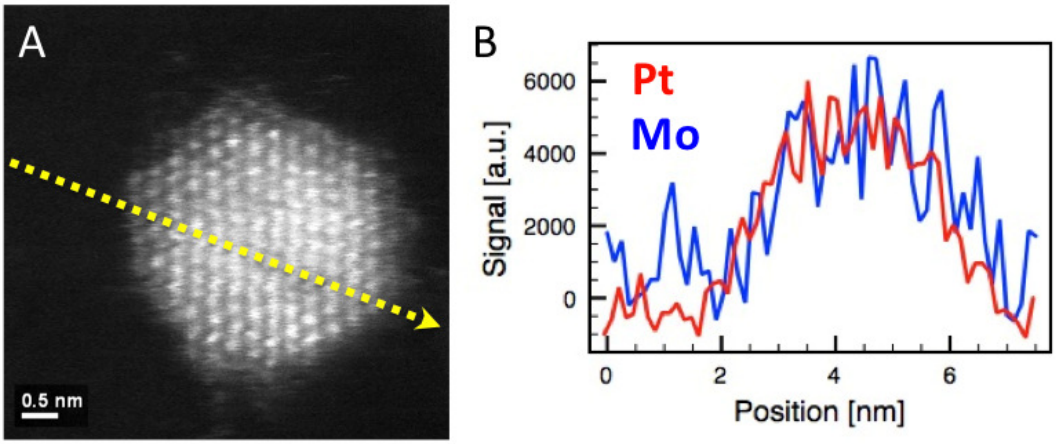

Figure 3.11 Typical high resolution HAADF-STEM micrograph of the used 5% Pt/ 10% Mo/MWCNT catalyst used to assess the composition of the observed particles. The EELS signal profile (intensity vs. distance) along the dotted line through the particle shows the presence well-mixed Pt-Mo alloy.

The fractions of the surface area covered by the Pt-Mo bimetallic particles for various catalysts are listed in Table 3.2. The particle size distribution of these catalysts measured after the reaction is also listed in Table 3.2.

Table 3.2 Estimation of the fraction of the support surface area covered by the Pt-Mo bimetallic particles for the Pt/Mo_2C/MWCNT catalysts with varying Pt loading.

Catalyst	MWCNT area scanned (nm^2)	Number of Pt-Mo objects counted	Pt-Mo area measured (nm^2)	% Area covered by Pt-Mo	Average particle size (nm)
0.5% Pt/ 10% Mo	6425	24	33.4	0.5	2.1 ± 0.8
3% Pt/ 10% Mo	5673	66	100.1	1.8	2.2 ± 0.8
5% Pt/ 10% Mo	3272	33	123.6	3.8	2.5 ± 1.0

3.4 Discussion

Preparation of Pt/Mo_2C catalysts using MWCNT support offers multiple advantages from the standpoint of establishing structure-activity relationships. The MWCNTs provide an ease of characterization. For example, the X-ray absorption spectroscopy for the bulk Mo_2C catalysts was carried out in the fluorescence mode, as the bulk Mo_2C phase absorbs all the incident X-rays. The MWCNT supports are practically transparent to the incident X-rays as carbon is a low-Z material. This enabled us to perform the *in situ* XAS experiments in transmission mode and with a greater throughput, as 6 samples could be tested simultaneously. Also, bulk Mo_2C offers a poor contrast between admetal particles and the support for electron microscopy. On the other hand, due to the high transparency and low density of the carbon, STEM micrographs with clear contrast between the

admetal and the Mo_2C domains could be obtained for Mo_2C/MWCNT supported catalysts. Most importantly, the importance of Pt-Mo_2C contact sites towards the WGS reaction rates could be de-convoluted from the contribution of Mo_2C sites using the Pt/Mo_2C/MWCNT systems. To our advantage, the similarity of apparent kinetic parameters for Pt/bulk Mo_2C and Pt/Mo_2C/MWCNT ensures that the active sites are similar in chemical nature. The ease of characterization and the chemical similarity have enabled us to use these catalysts to probe the active sites of Pt/bulk Mo_2C catalyst.

As described before, the apparent kinetic parameters measured at 120 ºC for the Pt/Mo_2C/MWCNT systems were independent of the Pt or Mo loading. This implies that all the Pt/Mo_2C/MWCNT catalysts tested for WGS have active sites of similar chemical nature. Thus, the differences in the WGS reaction rate per gram, observed over these catalysts were purely due to the difference in the absolute number of dominant active sites. The more prominent increase in the WGS reaction rate per gram at 120 ºC, with creation of more Pt-Mo_2C sites, as compared to the increase in the rates with increasing Mo_2C sites suggests that the dominant active sites are formed by the contact sites of Pt and Mo_2C domains. The monotonic decrease in the nominal TOR (defined by normalizing the WGS rate per gram by the total number of active sites i.e. total number of CO chemisorbed) with increasing Mo loading suggests that the inherently 'less active' sites are created with increasing amount of Mo_2C. However, the linear increase in the nominal TOR at 120 ºC, with increasing Pt loading, suggests that inherently 'more active' sites are created with increase in the number of Pt-Mo_2C contact sites. Based on this

observation, we conclude that the dominant active sites for WGS at 120 ºC are formed by the contact between Pt and Mo_2C domains.

It should be noted that the maximum Mo loading for the Pt/Mo_2C/MWCNT systems tested here was 20%. Theoretically, even at 20% Mo loading, only 36% of the MWCNT surface can be covered (BET surface area: 240 m^2/g) with Mo_2C domains. Thus, during Pt impregnation on Mo_2C/MWCNT, most of the Pt is likely to get deposited on the MWCNT surface, as opposed to the Mo_2C domains. The possibility of Pt contacting MWCNT surface increases with decreasing Mo loading.

All the implications drawn from the WGS kinetic data are based on the assumption that Pt is preferentially bound to the Mo_2C domains and not the MWCNT surface during the reaction. The location of Pt is critical for the kinetic data and its implications, as there is significant difference in the WGS rates for the Pt supported on the MWCNT surface and the Pt deposited on the Mo_2C domains. To illustrate the difference, the WGS rate per total moles of Pt for the 4% Pt/MWCNT (no Mo or Mo_2C) is compared with the 1.5% Pt/ 3% Mo/MWCNT (with Mo in the carbide form) catalyst at 120 ºC. As shown in Table 3, the WGS rate per total moles of Pt for the catalyst with 3% Mo in the carbide form is three orders of magnitude higher than the Pt/MWCNT catalyst. In fact, the Pt/MWCNT catalyst was tested at 270 ºC and the rate was extrapolated to 120 ºC using the Arrhenius dependence, as there would be no measurable rate obtained over this catalyst at 120 ºC, owing to its inherent low activity. Based on this observation, it can be assumed that for

the $Pt/Mo_2C/MWCNT$ catalysts, the Pt that is in contact with the MWCNT surface is inactive for WGS at 120 ºC. Thus, the location of Pt is critically important before any quantitative implications are drawn from the WGS kinetic data.

Table 3.3 Comparison of WGS reaction rates normalized by total moles of Pt at 120 ºC between the Pt/MWCNT catalyst (no Mo_2C) and the Pt/3% Mo/MWCNT catalyst with Mo in carburized form.

Catalyst	Pretreatment	Test Temp. / $^{\circ}C$	WGS Rate at 120 $^{\circ}C$ /10^{-5} mol H_2 (total mol Pt)$^{-1}$ s^{-1}
1.5% Pt/3% Mo/MWCNT	Reduction in pure H_2 at 600 ºC	120	1300
4% Pt/MWCNT	Reduction in 25% H_2/Ar at 300 ºC	270	1.1

To determine the fraction of Pt in contact with the Mo_2C domains, we have used the *in situ* XAS data obtained over these systems. As it was shown before, after the 600 ºC reduction, the Pt-Pt and Pt-Mo average coordination numbers obtained at the Pt L_3 edge for these catalysts were independent of the Mo and Pt loading. This suggests that the coordination environment of Pt was independent of the amount of Mo over these catalysts. If it is assumed that at fixed Pt loading, the amount of Pt in contact with the Mo_2C domain increases with the Mo loading, the average Pt-Mo coordination number

should have increased with the Mo loading, as XAS takes an average over the entire sample. Since, no such trend was observed, the obtained EXAFS data is interpreted to claim that a significant fraction of Pt is in intimate contact with Mo_2C i.e. Pt preferentially binds to the Mo_2C domains. Additional quantitative evidence for this claim was obtained from the *in situ* XANES spectra. It was shown from the *in situ* XANES data at the Pt L_{III} edge for the Pt/bulk Mo_2C, that there is an observable shift in the leading edge towards higher energy, which is attributed to the effect of alloying with Mo [6]. Thus, by modeling the *in situ* XANES spectra for the Pt/Mo_2C/MWCNT systems as the linear combinations of the XANES spectra of Pt/bulk Mo_2C and the Pt/MWCNT (no Mo), we have quantified the fraction of Pt in contact with the Mo_2C domains. As shown in Figure 3.12, every catalyst has close to 100% Pt in contact with Mo_2C, except for the sample with 2% and 3% Mo loadings, which had 27% and 18% Pt in contact with the MWCNT respectively (Table B.3). The WGS rates at 120°C normalized by the fraction of the Pt in contact with Mo_2C (active Pt) for all the Pt/Mo/MWCNT catalysts are of the order of ~ 1 x 10^{-2} mol H_2 (mol Pt)$^{-1}$ s^{-1} and are within a factor of 1.6.

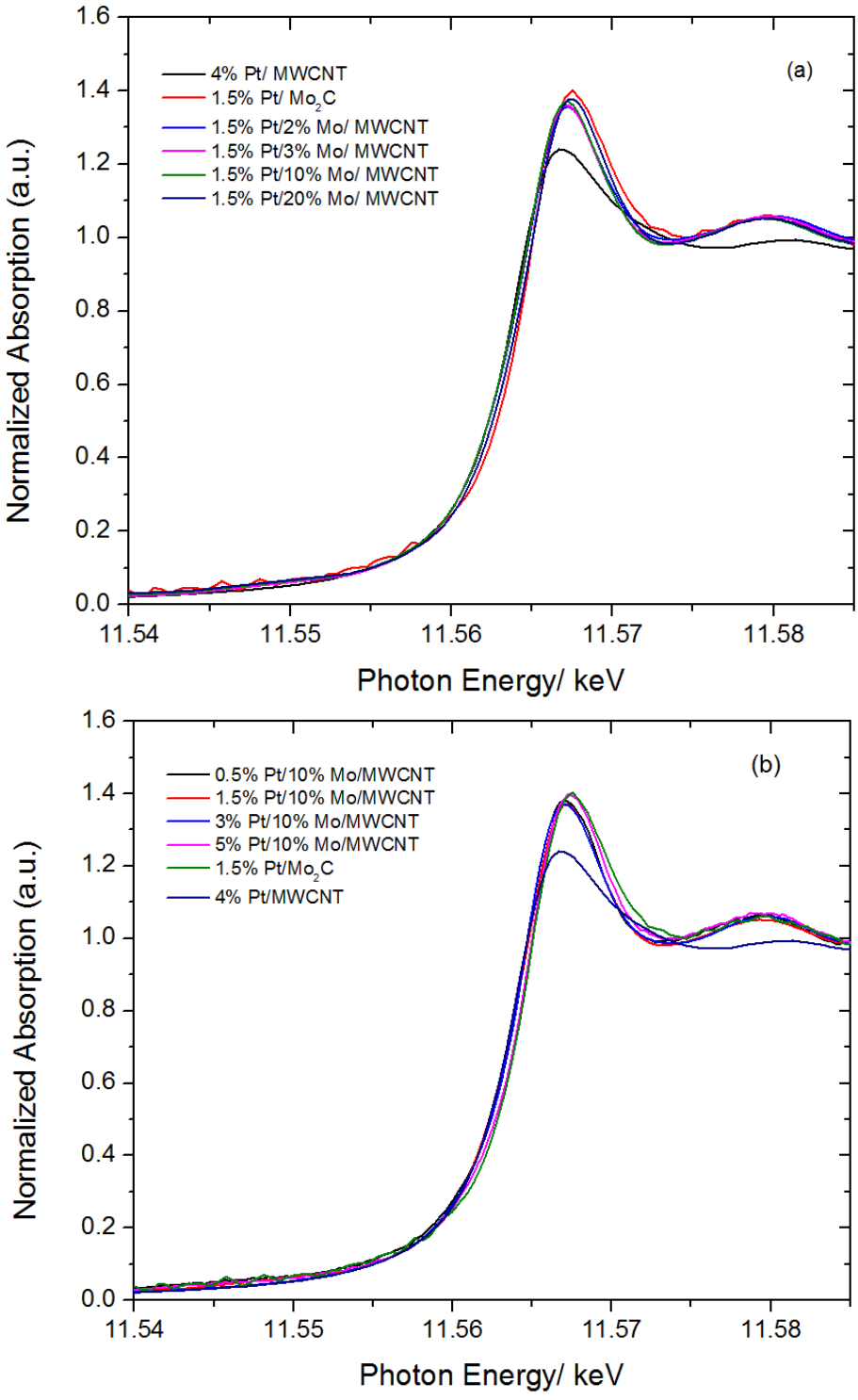

Figure 3.12 Pt L_{III} XANES spectra for (a) catalysts with varying Mo loading (b) catalysts with varying Pt loading plotted with the XANES spectra for the 1.5% Pt/Mo_2C and the 4 Pt/MWCNT catalysts used for linear combination XANES analysis.

A visual evidence for the claim that most of the Pt is in contact with Mo_2C, was obtained from the HAADF-STEM images. It was observed that all the noticeable Pt-Mo bimetallic particles had Mo_2C around them in the vicinity, confirming the preferential binding of Pt to the Mo_2C (Figure B.1). Such preferential binding of Pt to Mo_2C domains has been reported before for Pt supported over Mo_2C/Al_2O_3 [56]. Our speculation is that even though some Pt gets deposited in the MWCNT surface during synthesis, it migrates to the Mo_2C domains during the 600 ºC reduction pretreatment. At 600 ºC, Pt particles can have enough mobility to move around on the support surface. These Pt particles form an alloy with the reduced Mo phase and are surrounded by the Mo_2C domains. The alloy formation is possibly achieved by the incorporation of Mo inside the Pt particles, which is evident from the decrease in the intensity of second shell (Mo-Mo peak) of the Mo K edge EXAFS spectra, with increase in the Pt loading (Figure 3.9). The preferential binding of Pt to the Mo_2C domains highlights the strong adhesive interaction between the admetal particles and the carbide surface.

To ascertain that the active sites are formed by the contact of Pt-Mo bimetallic particles and the Mo_2C domains, we have used HAADF-STEM images to quantify the fraction of the support surface area covered by the observable Pt-Mo bimetallic particles (listed in Table 3.2). As shown in Figure 3.13, there is a liner correlation between the WGS rate per gram at 120 ºC and the fraction of the surface area of the support occupied by the Pt-Mo bimetallic particles. Based on this correlation, we conclude that the dominant active sites for WGS on the $Pt/Mo_2C/MWCNT$ systems are located either on the Pt-Mo bimetallic particles or the interface between Pt-Mo particles and the Mo_2C domains.

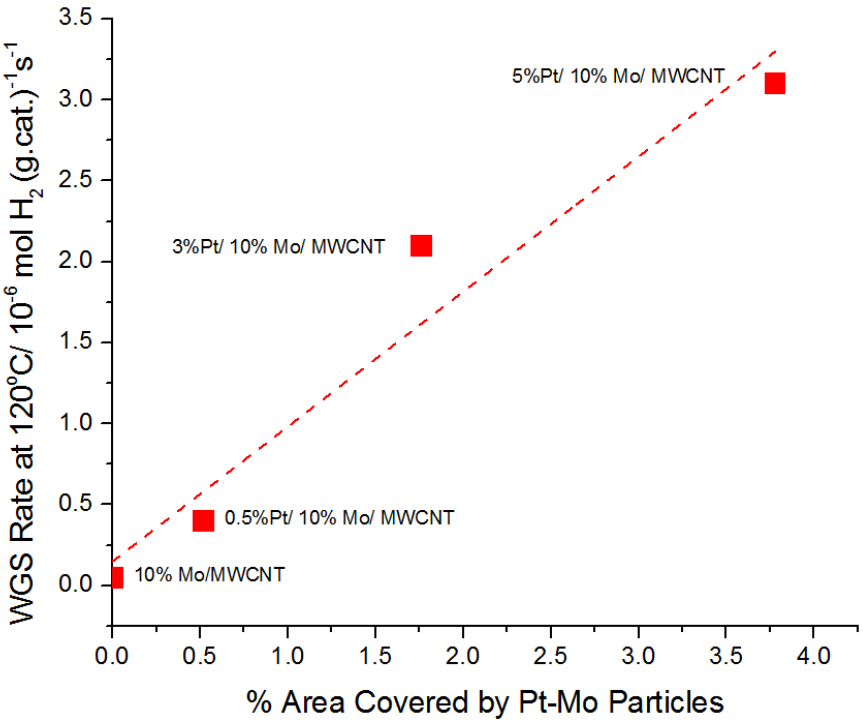

Figure 3.13 WGS rate per gram of catalyst at 120 ºC for the Pt/Mo_2C/MWCNT catalysts, plotted against the fraction of the support surface area covered by the Pt-Mo bimetallic nanoparticles for the catalysts with varying Pt loading.

Regardless of the Pt loading, the catalysts with fixed Mo loading have similar particle sizes. The average particle sizes were 2.2 ± 0.8 nm, 2.2 ± 0.8 nm, and 2.5 ± 1.0 nm for the used catalysts with 0.5%, 3% and 5% Pt with fixed (10%) Mo loading. This suggests that even when the amount of Pt was increased by a factor of 10 (from 0.5% to 5%); there were sufficient nucleation centers available on the Mo_2C domains for the formation of new Pt containing particles. The WGS rates normalized by the dispersion (1/average particle size in nm) of the Pt-Mo particles for these catalysts are plotted in Figure 3.14. These normalized rates are independent of the amount of Pt on each catalyst and are of the order of ~ 3 x 10^{-2} mol H_2 (mol exposed metal in Pt-Mo particles)$^{-1}$ s^{-1} at 120°C. Thus, this rate can be termed as the apparent WGS turnover rate.

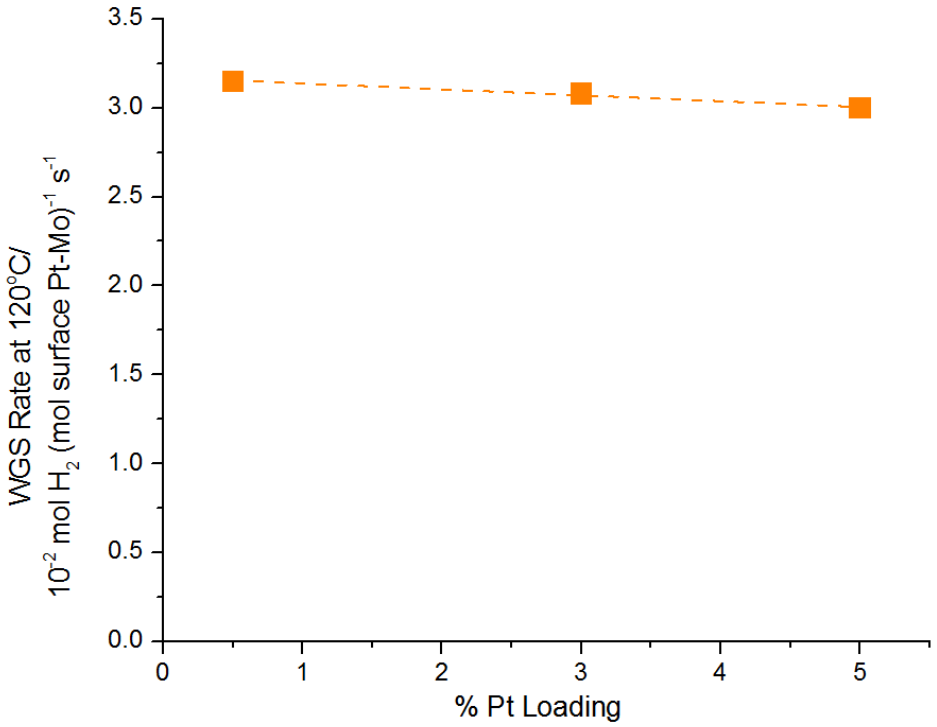

Figure 3.14 WGS rates at 120°C normalized by the moles of exposed metal in the Pt-Mo particles (computed using the STEM images) plotted against % Pt loading at a fixed Mo loading.

3.5 Conclusions

Two different series of catalysts with varying amounts of Mo (at fixed amount of Pt) and varying amount of Pt (at fixed amount of Mo) were prepared. The number of Mo_2C sites and the number of admetal-Mo_2C contact sites were individually varied. The more prominent increase in the WGS reaction rate per gram at 120ºC, with creation of more Pt-Mo_2C sites, as compared to the increase in the rates with increasing Mo_2C sites suggests that the dominant active sites are formed by the contact sites of Pt and Mo_2C domain. This observation was ascertained with normalization the WGS rates per gram by the number of moles of CO chemisorbed on each Pt/Mo_2C/MWCNT catalyst (CO titrates Mo_2C as well as the admetal sites). A linear increase in the nominal TOR was observed

with increasing Pt loading while the Mo loading was fixed, whereas a progressive decrease in the nominal TOR was observed with increasing Mo loading while the amount of Pt was fixed. Characterizations of these catalysts performed using *in situ* XAS and the HAADF-STEM micrographs, indicate that the Pt preferentially binds to the Mo_2C domains after the 600ºC reduction and during the course of WGS reaction and forms Pt-Mo bimetallic particles. This highlights the strong adhesive interaction between the admetal and the Mo_2C domains. The chemical similarity between Pt/bulk Mo_2C and Pt/Mo_2C/MWCNT enabled us to use the latter to probe the active sites for WGS over Pt supported on Mo_2C.

A linear correlation between WGS reaction rate per gram at 120 ºC and the fraction of the surface area covered by the Pt-Mo particles was obtained. The possible locations of active sites were determined to be either the Pt-Mo particle surface or the interface between the Pt-Mo particles and the Mo_2C domains.

CHAPTER 4. LOW TEMPERATURE ACTIVATION OF PLATINUM-MODIFIED BULK MOLYBDENUM CARBIDE FOR WATER-GAS SHIFT

4.1 Introduction

Molybdenum carbide is certainly an attractive catalyst as an alternative to the $Cu/Zn/Al_2O_3$, as learnt from the previous chapters and the published literature [22,57]. The high activity and possible affordability are the key advantages which can promote commercialization of the metal carbide catalysts [58]. However, the high temperature required during the activation procedure of the Mo_2C or metal/Mo_2C catalysts could be a potential issue. Operating at temperatures as high as 600°C could be impractical for automotive applications, or even for industrial WGS reactors. To say the least, a lower pretreatment temperature could lead to a lower capital cost for the equipment as well as lower operating cost.

In previous chapters, it was learnt that the admetals are deposited on the passivated surface of molybdenum carbide. It was suggested that to bring back the carbide surface in its native form i.e. to remove oxygen from the layer of passivation over the Mo_2C surface, the catalysts are re-carburized at 600°C after metal deposition prior to WGS rate measurements. This procedure of activation was adopted from Schweitzer et al. [23]. It was shown that the pretreatment with H_2 at 450°C over the bulk Mo_2C catalyst leads to relatively lower WGS rates per gram compared to a pretreatment with 15% CH_4/H_2 at 590°C [59].

In this study, the effect of a milder pretreatment (reduction in 25 % H_2/Ar) over the WGS activity of Mo_2C and Pt/Mo_2C was investigated. Difference in the pretreatment temperatures should lead to a difference in the residual oxygen content of the carbide surface. This residual oxygen content was measured using temperature programmed reduction experiments performed post WGS reaction. The coordination environment of Pt was studied using *in situ* Pt L_{III} EXAFS experiments.

4.2 Experimental Methods

4.2.1 Catalyst Preparation

The unsupported Mo_2C was synthesized by temperature programmed carburization of ammonium heptamolybdate precursor [$(NH4)_6Mo_7O_{24}\cdot 4H_2O$; 81-83% as MoO_3] from Alfa Aesar in a fixed bed reactor system with 0.5 grams of the precursor loaded in a quartz reactor tube over a quartz plug. The precursor was exposed to pure H_2 (75 sccm) and the temperature was ramped to 350-370 ºC at 4 ºC/min and was soaked at this temperature for 10 h. The temperature was further ramped to 600 ºC at 3 ºC/min while the gas was switched to 15% CH_4/H_2 (75 sccm) mixture. The reactor was maintained at this temperature for 3.5 to 4 h. It was then cooled to RT under the flow of Ar and then passivated in a flow of 1% O_2/Ar. The oxygen concentration in the passivation mixture was progressively increased to 20% and the Mo_2C support was ultimately exposed to air. Passivation was performed in order to avoid the spontaneous combustion of the freshly synthesized Mo_2C upon exposure to the ambient air. The passivated Mo_2C was used as a support for the synthesis of 1.5% Pt/Mo_2C catalyst using incipient wetness impregnation.

8 wt. % solution of chloroplatinic acid (Sigma Aldrich) was used. After the deposition of Pt, the catalyst was dried overnight in vacuum at RT. It was then reduced in pure H_2 in a tubular reactor at 450°C for 4 h, followed by passivation at RT in 1% O_2/He.

4.2.2 Kinetic Measurements

The details of the kinetic measurements have been given in Chapter 2. The key idea of this study was to study the effect of pretreatment over Mo_2C and Pt/Mo_2C on their respective activities towards WGS. Following sequence of experiments was performed in the kinetic measurement apparatus:

(i) Appropriate amounts of passivated as prepared Mo_2C and Pt/Mo_2C were loaded in the reactors. These catalysts were carburized at 600°C in presence of 15% CH_4/H_2 (75 sccm) for 4 hours, cooled to 120°C under Ar and WGS rates were measured under standard conditions.

(ii) After the measurement of WGS kinetic parameters, these catalysts were passivated using the method described above..

(iii) The passivated catalysts were now reduced at 300°C in presence of 25% H_2/Ar (50 sccm) for 2 hours, without physically removing them from the reactors.. The catalysts were then exposed to the WGS reaction mixture and the temperatures were adjusted so that a measurable CO conversion (~ 10%) could be achieved. The WGS rates and kinetic parameters were measured at these temperatures.

4.2.3 Catalyst Characterization

To assess whether the Pt supported over passivated Mo_2C causes H_2 to spill over the carbide, hydrogen-oxygen titration experiments were performed over Mo_2C and Pt/Mo_2C using the Micromeritics ASAP 2020 instrument. The as prepared catalysts were loaded in a U-shaped quartz cell and were pretreated in 15% CH_4/H_2 at 600°C for 4 hours. This was followed by an oxygen uptake experiment at 35°C, which leads to the passivation of these catalysts. The oxygen uptake experiment was followed by hydrogen titration at 35°C.

The *in situ* Pt L_{III} edge EXAFS spectroscopy was used to monitor the changes in the coordination environment of Pt with different pretreatments. The experiments were performed at the insertion device beam line of the Materials Research Collaborative Access Team (MRCAT) at the Advanced Photon Source, Argonne National Laboratory. Scans at the Pt L_{III} edge (11.564 keV) were performed in fluorescence mode. In situ experiments were performed in 1 in OD quartz tubes connected to Ultra-Torr fittings with welded ball valves (for gas inlet/outlet and sealing) and Kapton windows. The catalyst mass was calculated to give an absorbance (μx) of approximately 2.0, with an edge step ($\Delta\mu x$) between 0.4 and 1.5. The sample was pressed into a wafer which was kept at a 45º angle with the X-ray beam inside the in situ reactor, and the fluorescence detector was kept perpendicular to the length of the reactor tube. The catalysts was subjected to the aforementioned high temperature carburization pretreatment in presence of 15% CH_4/H_2 at 600 ºC and then cooled to RT. The scans were performed at RT in order to eliminate

the contribution of thermal vibrations to the EXAFS data. This was followed by passivation of the catalyst at RT. The passivated catalyst was then reduced at 300°C in presence of 25% H_2/Ar for 2 h. Following the reduction pretreatment, the scans at Pt edge were taken at RT, to assess the effect of the series of pretreatment. The EXAFS spectra were analyzed using WINXAS 3.1 software, as described in Chapters 2 and 3.

Temperature programmed reduction (TPR) experiments were performed using Micromeritics Autochem II 2920 instrument, coupled with an Agilent 5975C mass selective detector (MSD). Typically, a sample was heated from RT to 900°C at 10°C/min. The oxygen content was estimated by measuring the amounts of H_2O, CO and CO_2 evolved during the TPR experiments. Calibrations for CO, CO_2 and CH_4 for the MSD were developed by injecting known quantities of these gases. Calibration for water was developed by a TPR experiment over a bulk silver oxide (Ag_2O) sample from Micromeritics, for which, the amount of hydrogen consumed was known. A known quantity of Argon was injected into the MSD using the loop in the Autochem after every experiment, which was used as an internal standard for quantification. The TPR experiments were performed after different pretreatments viz. carburization, passivation, carburization followed WGS for 20 hours and carburization followed by passivation followed by 300°C reduction in 25% H_2/Ar followed by WGS for 20 hours. Catalyst loaded in the Autochem cell could be exposed to the WGS reaction mixture by passing the dry (water free) WGS mixture through water vapor generator in the Autochem and flowing the gas over the catalyst.

4.3 Results

4.3.1 Kinetic measurements

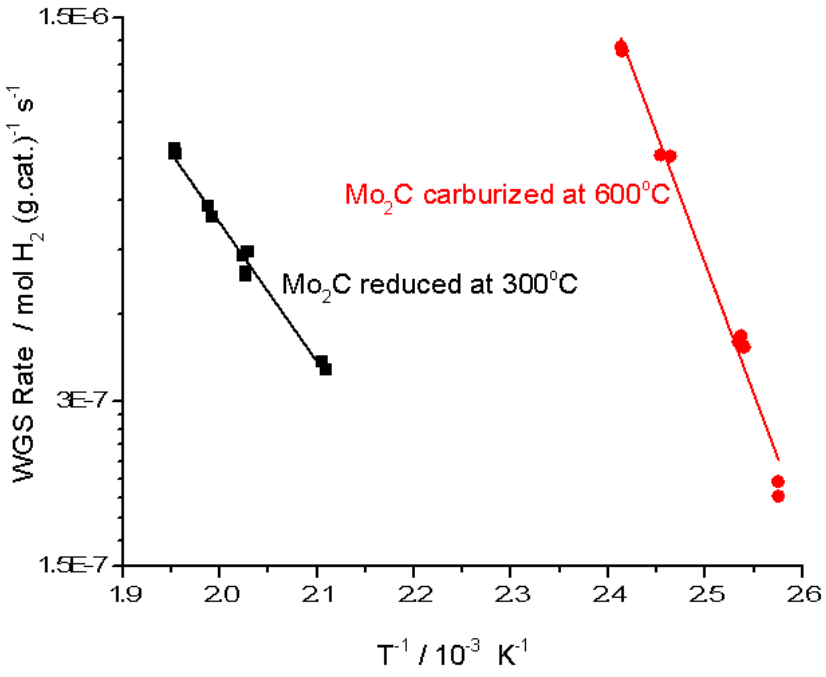

Figure 4.1Arrhenius plots for WGS over bulk Mo_2C after different pretreatments

Figure 4.1 shows the Arrhenius plots for WGS over the bulk Mo_2C catalyst produced after different reduction pretreatments. After the 600°C carburization, the kinetics could be measured at 130°C. Following this measurement, the catalyst was passivated at RT and reduced at 300°C in 25% H_2/Ar. After the reduction at 300°C the kinetics had to be measured at 220°C, owing to the non-measurable CO conversions below this temperature. Using the measured apparent activation energy, the WGS rate for the catalyst reduced at 300°C was extrapolated to 130°C. At 130°C, the WGS rate per unit surface area of the Mo_2C after the 600°C carburization was 3.7 $\times 10^{-9}$ mol H_2 m^{-2} s^{-1}, which was ~9 times higher than the Mo_2C catalyst that had been reduced at 300°C after passivation

(4.1×10^{-10} mol H_2 m^{-2} s^{-1}). The kinetic parameters could not be directly compared for these catalysts, as there is a vast difference in the measurement temperatures.

Figure 4.2 shows Arrhenius plots for WGS over 1.5% Pt/Mo_2C catalyst produced after different reduction pretreatments. After the 600°C carburization, the kinetics could be measured at 120°C. Following this measurement, the catalyst was passivated at RT and reduced at 300°C in 25% H_2/Ar. After the reduction at 300°C, unlike the bulk Mo_2C catalyst, the kinetics for the Pt/Mo_2C could be measured at 120°C.

At 120°C, the WGS rate per unit surface area of the Pt/Mo_2C after the 600°C carburization was 2.6×10^{-8} mol H_2 m^{-2} s^{-1}, which was only ~2 times higher than the Pt/Mo_2C catalyst that had been reduced at 300°C after passivation (1.4×10^{-8} mol H_2 m^{-2} s^{-1}).

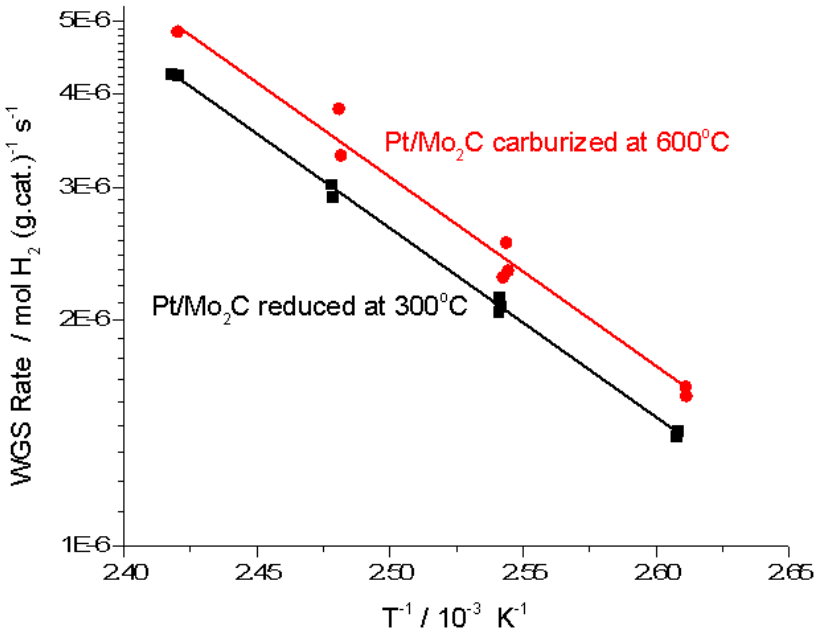

Figure 4.2 Arrhenius plots for WGS over bulk 1.5% Pt/Mo_2C after different pretreatments

The kinetic parameters could be compared for the Pt/Mo_2C catalyst after the different pretreatments, as the test temperatures were similar. Table 4.1 shows that the kinetic parameters for the Pt/Mo_2C catalyst after the 600°C carburization and after activating the catalyst with 300°C reduction. The apparent activation energies and the apparent reaction orders of the Pt/Mo_2C after these two different pretreatments are similar within errors.

Table 4.1 Apparent WGS kinetic parameters over Mo_2C and Pt/Mo_2C after different pretreatments

Sample	Pretreatment	Test Temp. /°C	E_a /kJ(mol)$^{-1}$ (±3)	H_2O (±0.04)	CO_2 (±0.04)	CO (±0.04)	H_2 (±0.04)
1.5% Pt/Mo_2C	600°C carburization	120	45	0.72	-0.02	0.05	-0.33
1.5% Pt/Mo_2C	300°C reduction	120	48	0.82	0.03	0.04	-0.34
Mo_2C	600°C carburization	130	88	-0.04	-0.07	0.52	-0.25
Mo_2C	300°C reduction	220	48	0.10	-0.08	0.73	-0.22

4.3.2 Catalyst Characterization

Table 4.2 shows the results for the Oxygen uptake-H_2 titration experiments over Mo_2C and 1.5% Pt/Mo_2C catalyst after 600°C carburization. The oxygen uptake values were similar for both the catalysts, suggesting that presence of Pt does not affect the oxygen adsorption capacity of the carbide surface significantly. However, the H_2 titration/uptake experiment performed immediately after oxygen uptake shows very different results for these catalysts. The amount of H_2 used up in titration was ~85 times higher for the Pt/Mo_2C catalyst at 35°C.

Table 4.2 Amounts of O_2 and H_2 uptakes over Mo_2C and 1.5% Pt/Mo_2C after 600°C carburization (O_2 uptake experiments performed before H_2 uptake measurements)

Catalyst	Oxygen Uptake at 35°C after 600°C Carburization/ mmol g^{-1}	H_2 Titration at 35°C after O2 Uptake/ mmol g^{-1}
Mo_2C	0.98	0.006
1.5% Pt/Mo_2C	0.94	0.51

Temperature programmed reduction (TPR) experiments were performed over Mo_2C and 1.5% Pt/Mo_2C after various pretreatments to quantify the residual oxygen in the catalyst. The TPR plots are normalized by the quantification sensitivity for each molecule in the MSD, so that the area in the plot is directly proportional to the amount detected, independent on the molecule considered [60]. Figure 4.3 shows the TPR profiles for passivated forms of Mo_2C and Pt/Mo_2C. The monolayers of oxygen computed form the H_2O. CO and CO_2 amounts were 1.52 and 1.46 ML for Mo_2C and Pt/Mo_2C respectively.

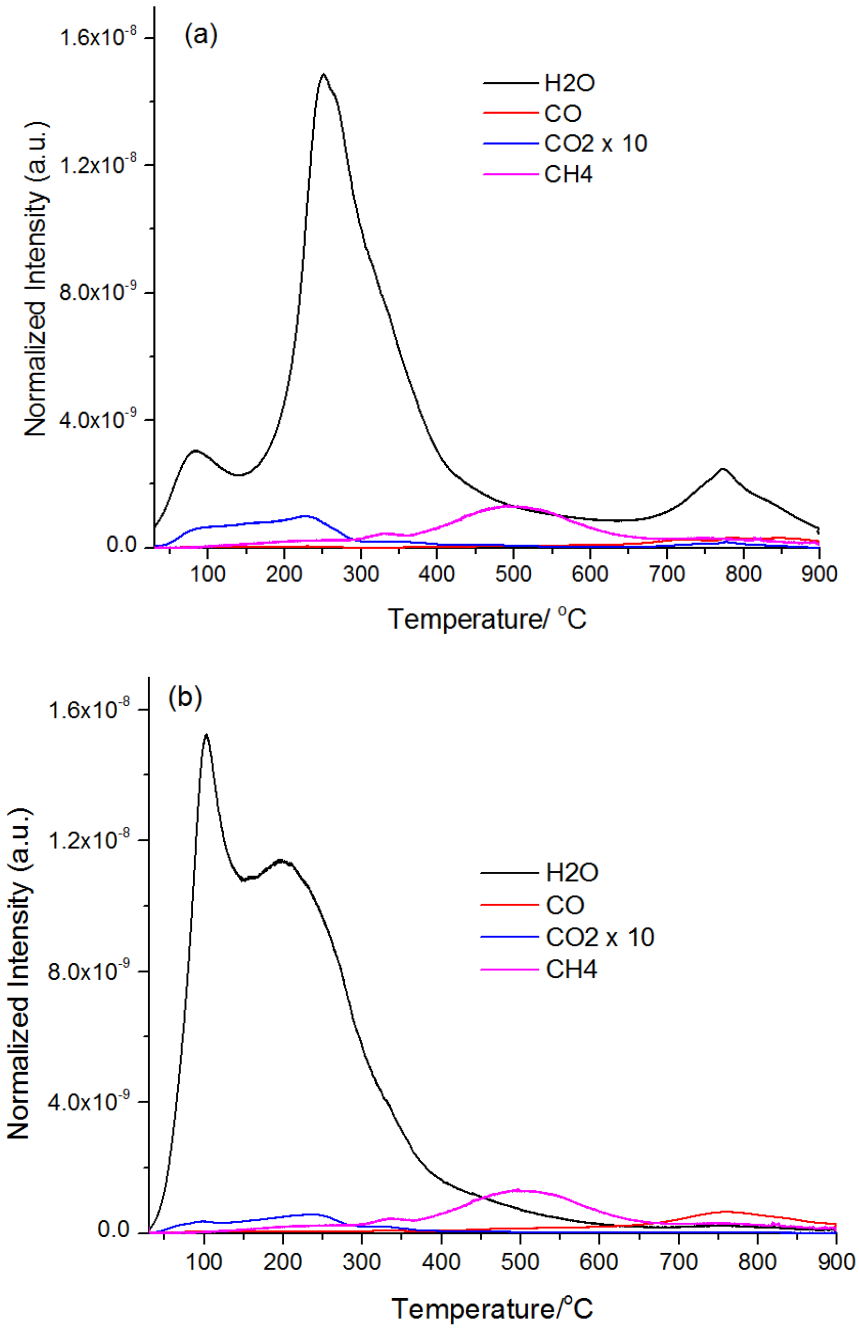

Figure 4.3 TPR profiles for (a) passivated Mo_2C (H_2O, CO, CO_2 and CH_4 amounts were 1510, 69, 13 and 136 µmol g^{-1} respectively) (b) passivated 1.5% Pt/Mo_2C (H_2O, CO, CO_2 and CH_4 amounts were 1370, 42, 6 and 156 µmol g^{-1} respectively).

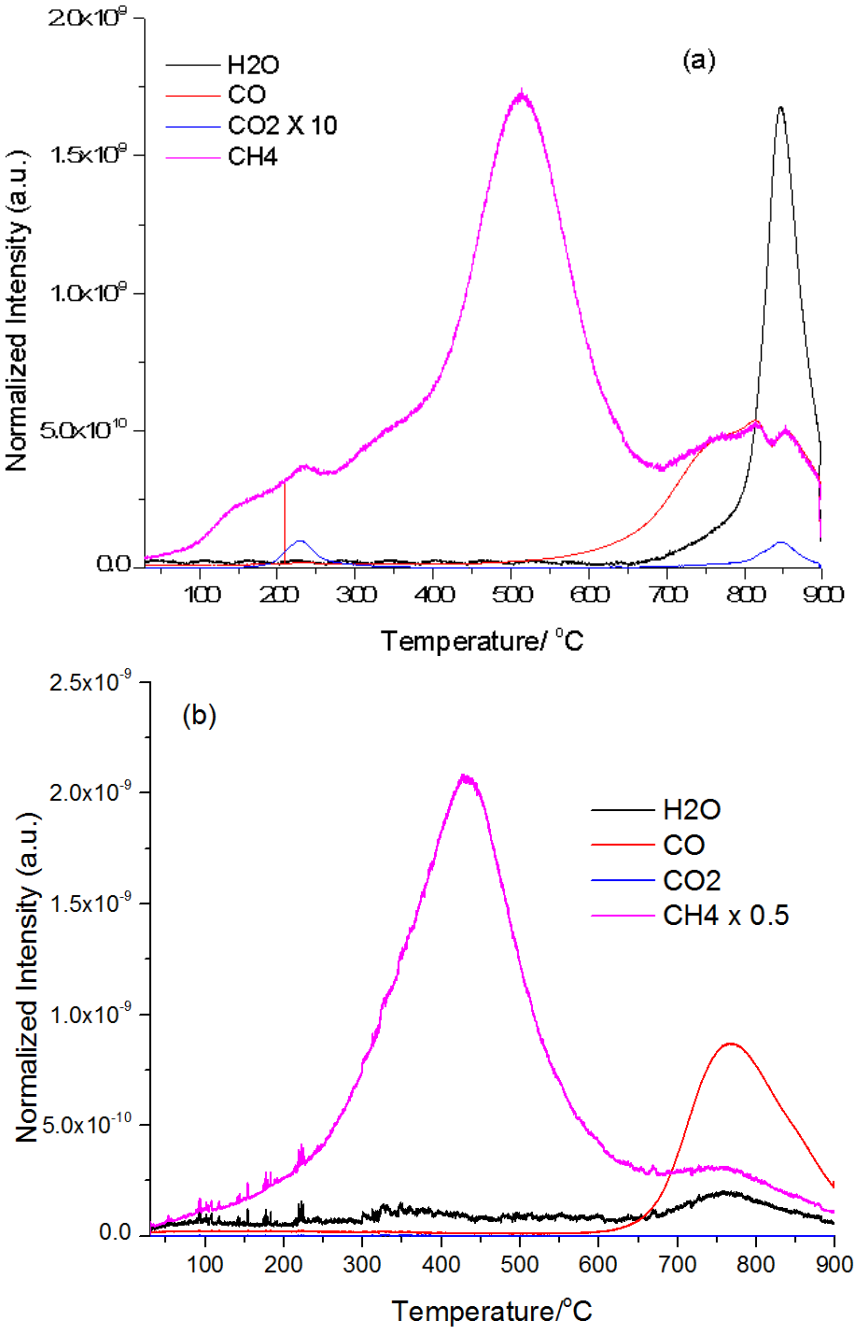

Figure 4.4 TPR profiles for 600°C carburized (a) Mo_2C (H_2O, CO, CO_2 and CH_4 amounts were 65, 68, 1.1 and 280 µmol g^{-1} respectively) (b) 1.5% Pt/Mo_2C (H_2O, CO and CH_4 amounts were 6, 47 and 344 µmol g^{-1} respectively).

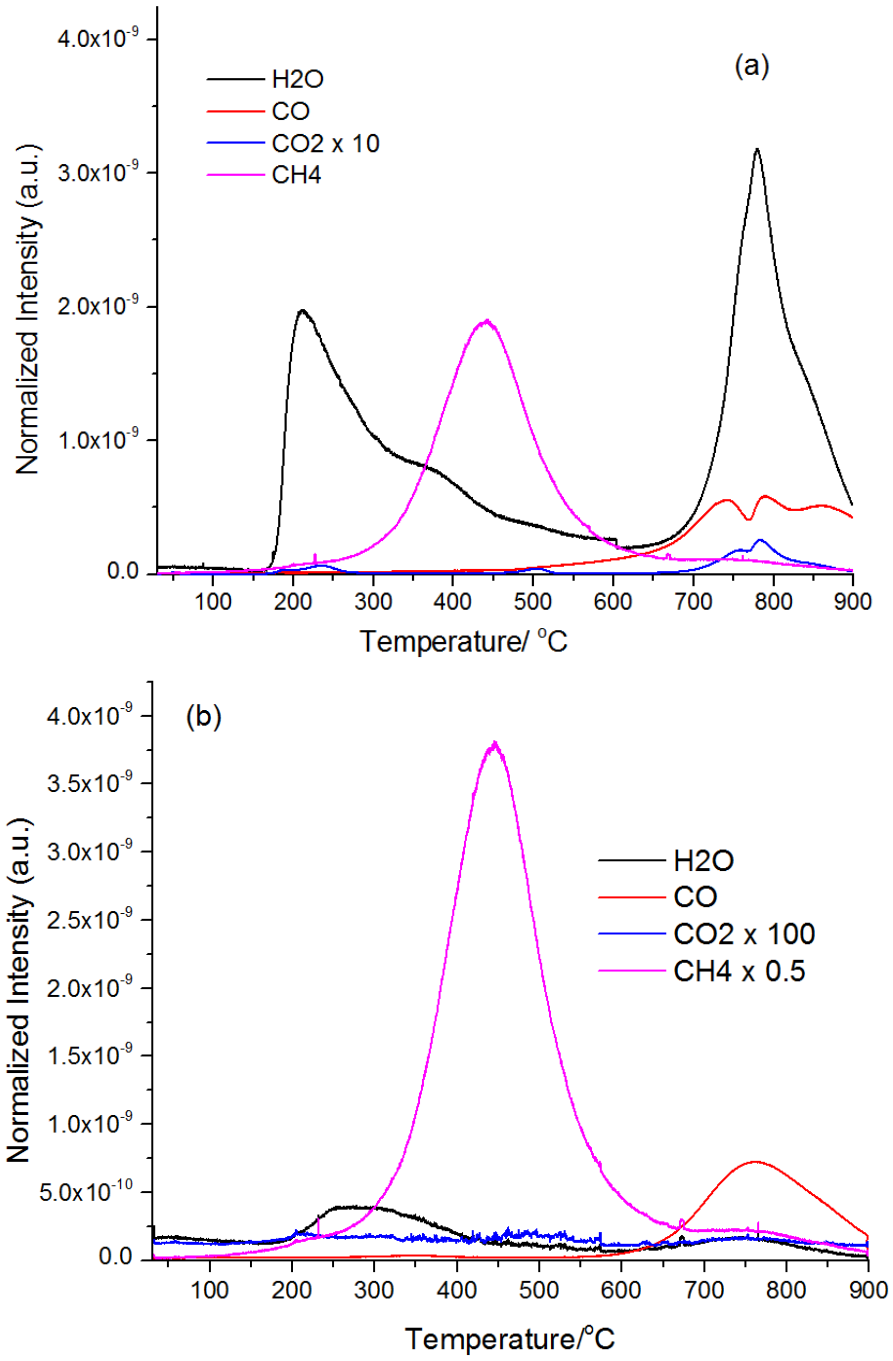

Figure 4.5 TPR profiles for 600°C carburized catalyst after 20 hours under WGS (a) Mo_2C (H_2O, CO, CO_2 and CH_4 amounts were 486, 79, 1.8 and 210 µmol g^{-1} respectively) (b) 1.5% Pt/Mo_2C (H_2O, CO, CO_2 and CH_4 amounts were 115, 47, 0.54 and 357 µmol g^{-1} respectively).

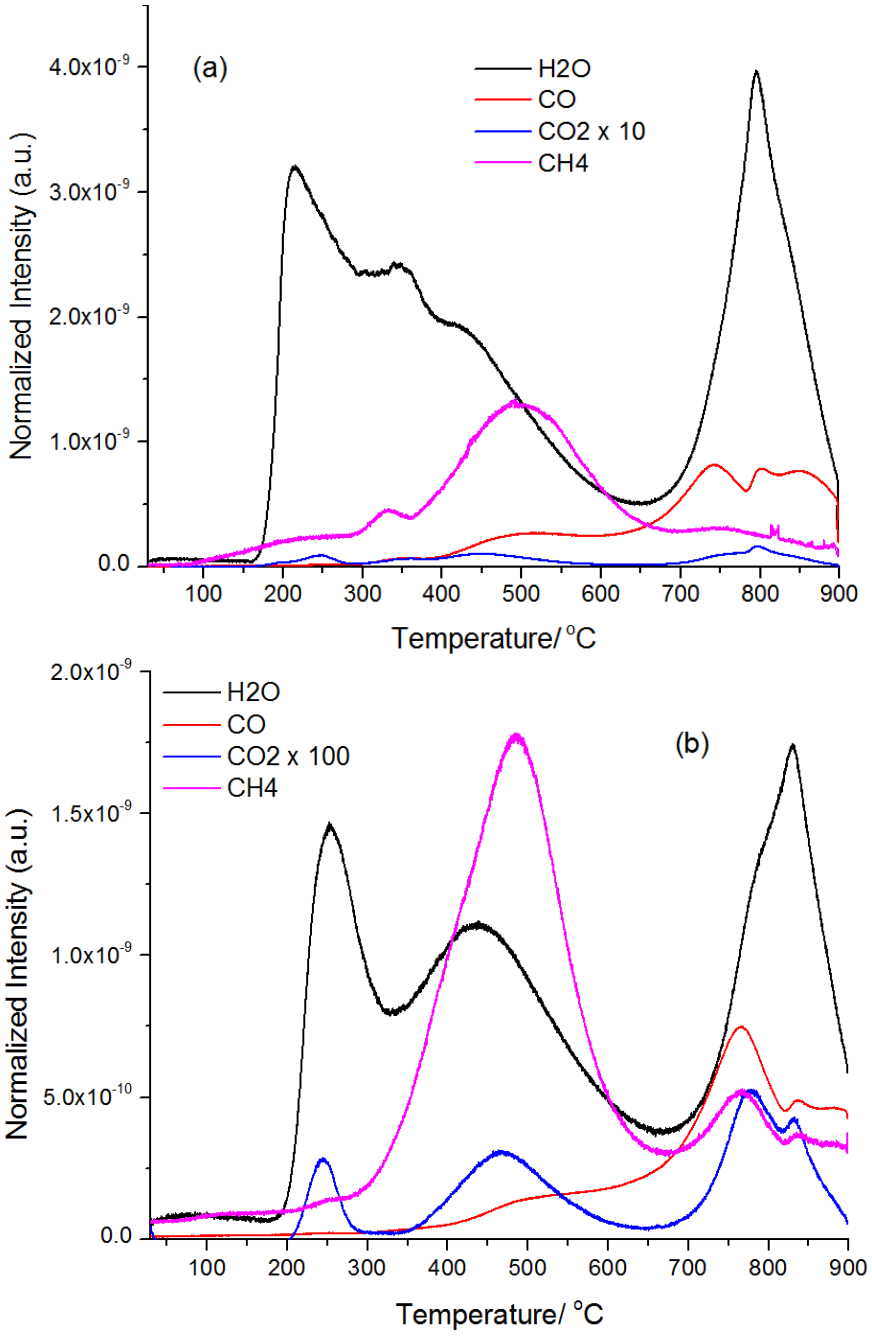

Figure 4.6 TPR profiles for 600°C carburized-passivated-300°C reduced catalyst after 20 hours under WGS (a) Mo_2C (H_2O, CO, CO_2 and CH_4 amounts were 756,132, 2.5 and 175 µmol g^{-1} respectively) (b) 1.5% Pt/Mo_2C (H_2O, CO, CO_2 and CH_4 amounts were 379, 97, 1.1 and 205 µmol g^{-1} respectively).

The oxygen surface coverage estimated from TPR and the BET surface area of ~65 m^2/g (assuming 1 monolayer = 10^{19} sites i.e. 10^{19} sites/m^2) for the passivated samples was significantly more than 1 monolayer, if all the oxygen detected in TPR is assumed to be residing at the surface [60]. The amount of residual oxygen decreases significantly after the 600°C carburization pretreatment for both Mo_2C and Pt/Mo_2C to 0.12 and 0.05 monolayers respectively. After keeping the catalysts at 120°C under standard WGS conditions (7% CO, 8.5% CO_2, 21.9% H_2O, 37.4% H_2 and balance Ar), there was an increase in the residual oxygen content. For Mo_2C, the residual O-content increased from 0.12 to 0.52 monolayers. For Pt/Mo_2C, this amount increased from 0.05 to 0.15 monolayers. When the catalysts were carburized, passivated, reduced at 300°C and exposed to standard WGS for 20 hours, the oxygen contents were higher than the carburization-WGS sequence. For this case, Mo_2C was found to have 0.83 monolayers, whereas 0.44 monolayers of Oxygen were detected from the TPR of Pt/Mo_2C. For the carburized catalysts directly subjected to TPR, the water peaks were observed only above 600°C, which could be the oxygen not removed during the carburization. For the catalysts exposed to WGS mixture immediately after carburization, there are peaks for water observed below carburization temperatures, suggesting that water dissociation leads to surface oxidation of the Mo_2C support. For the catalysts which were carburized, passivated, rduced and then exposed to WGS, the intensity of the water peaks below 600°C is higher compared to the carburization-WGS sequence, suggesting that 300°C reduction has a lower extent of oxygen removal. Nonetheless, it is important to note that overall, the oxygen content of the Pt-free Mo_2C was relatively higher compared to the Pt/Mo_2C catalyst.

A methane peak between 450 and 470°C is ubiquitous in all the TPR experiments. Methane formation in this temperature range has been reported before for bulk unsupported Mo_2C [61]. The amounts of methane were maximum in the TPR directly after carburization and minimum in the TPR after passivation.

For all the TPR experiments, significant CO peaks were observed only above 600°C i.e. above the carburization temperature. This observation is in accordance with the previously reported H_2-TPR results [62].

Table 4.3 shows the Pt L_{III} EXAFS data for the 1.5% Pt/Mo_2C catalyst after different pretreatments. It has been established before in Chapters 2 and 3 that Pt forms an alloy with Mo after 600°C carburization. Hence, a Pt-Mo scatter along with a Pt-Pt scatter was observed after carburization. This catalyst was then passivated at RT and reduced at 300°C in 25% H_2/Ar. The EXAFS scans collected at RT after this sequence of pretreatments were both qualitatively and quantitatively similar to the catalyst that was only carburized at 600°C i.e. both Pt-Pt and Pt-Mo coordination numbers were unchanged after the passivation-reduction of the carburized catalyst. The edge energies computed from the second derivative of the near edge regions were similar after both pretreatments and were similar to the metallic foil (11.5640 keV). This suggests that Pt was in a reduced state after both the pretreatments.

Table 4.3 *In situ* Pt L_{III} edge EXAFS data over 1.5% Pt/Mo_2C after different pretreatments.

Pretreatment	Edge Energy/keV	Scatter	Coordination Number	R/ Å	Eo/eV
600°C Carburization	11.5638	Pt-Pt Pt-Mo	5.6 3.5	2.74 2.73	-5.6 3.7
600°C Carburization-Passivation at RT-Reduction at 300°C	11.5638	Pt-Pt Pt-Mo	5.8 3.2	2.74 2.73	-5.6 5.4

4.4 Discussion

Under the WGS reaction conditions, it has been shown through experimental and theoretical studies that a buildup of oxygen on the Mo-terminated Mo_2C surface is detrimental to its activity towards WGS [33,57]. Liu et al suggested that the oxygen binds too strongly to the surface Mo atoms, making the surface inert for binding of other adsorbates [33]. Moon et al showed using the XPS experiments over the Mo_2C subjected to WGS that Mo on the surface transformed from $Mo^{+\delta}$ to Mo^{+4} and Mo^{+6}, leading to a loss of initial activity. These reports suggest that removal of oxygen generated due to water dissociation is necessary activate Mo_2C for WGS. Also, as evident from the pyrophoric nature of the Mo_2C, it has a high affinity towards oxygen. Temperatures as high as 600°C are required to remove oxygen from the surface of Mo_2C.

Our kinetic results show that the Mo_2C carburized at 600°C could be tested at 120°C and has a rate per unit surface area that is comparable to the commercial low temperature

WGS catalyst $Cu/ZnO/Al_2O_3$. However, if this catalyst is passivated and then subjected to a milder reduction at 300°C in 25% H_2/Ar, the WGS rate per unit surface area is lower by 9 times compared to the carburized version. This implies that to avail the high activity of Mo_2C, the passivated catalyst always has to be carburized at 600°C. On the contrary, the carburized version of 1.5% Pt/Mo_2C exhibits WGS rates per unit surface area that are ~6 times higher compared to Mo_2C. When this carburized Pt/Mo_2C catalyst is passivated and subjected to a milder reduction at 300°C, the WGS rate per unit surface area is only ~2 times lower compared to the Pt/Mo_2C after carburization. Unlike Mo_2C, this catalyst after 300°C could still be tested at 120°C, suggesting that it had a measurable rate even at 120°C.

The TPR experiments were performed to observe the dependence of the WGS rates on the residual oxygen content of these catalysts. The carburized Mo_2C and Pt/Mo_2C catalysts have 0.12 and 0.05 monolayers of oxygen, suggesting that 600°C carburization is able to remove a majority of the oxygen content form the passivated catalysts, which had more than 1 monolayers of oxygen. However, after subjecting the catalysts to WGS for 20 hours, there is a buildup of oxygen. The oxygen content of Mo_2C increased 4 times (0.12 to 0.52 monolayers). However, the oxygen content of the Pt/Mo_2C increased only to 0.15 monolayers. This suggests that Pt is able to keep Mo_2C surface in a relatively reduced form, possibly by hydrogen spillover. The spillover of H_2 by Pt over the oxide [63] , oxy-carbide [62] and carbide [64] is well-documented in the literature. Under WGS, another possible avenue for enhanced oxygen removal by Pt could be the promoted WGS

rates. If surface oxidation of CO is assumed to be the rate limiting step [34], increase in the WGS reaction rate entails higher rate of oxygen removal.

Thus, it is likely that the ability of Pt particles to spill over H_2 and at least keep the Mo_2C around their periphery free of oxygen, plays a role towards low temperature activation of passivated Pt/Mo_2C. From the TPR experiments, it is clear that the extent of oxygen removal by 300°C reduction after passivation is significantly higher for Pt/Mo_2C as compared to Mo_2C. The residual oxygen content of Pt/Mo_2C after such pretreatment followed by WGS was 0.44 monolayers, whereas for Mo_2C, it was 0.83 monolayers. As suggested in Chapter 2, Mo_2C has high activity towards activation of water; whereas, Pt acts a reservoir of CO, thereby promoting the WGS reaction rate. Thus, if the reaction occurs at the interface sites, it is plausible that the adsorbed CO on Pt needs only a few oxygen free Mo_2C sites for the supply of hydroxyl groups, the catalyst can be activated after passivation even by reduction at 300°C, as such oxygen free Mo_2C sites could be created due to hydrogen spillover. In absence of Pt, when CO and H_2O are likely to compete for the same sites over Mo_2C, the number of such active sites created by the 300°C reduction after passivation would have been much lower compared to the carburized Mo_2C. This must manifest into about 9 times lower WGS rate and the kinetics could have been measured at 220°C with a detectable CO conversions. Moreover, for the Pt/Mo_2C catalyst activated by 300°C reduction, the apparent kinetic parameters measured at 120°C are similar within error to the Pt/Mo_2C catalyst that was carburized at 600°C before measuring the kinetics at 120°C (Table 4.1). This suggests that active sites of similar chemical nature are created over Pt/Mo_2C irrespective of the pretreatment history.

The *in situ* Pt L_{III} edge EXAFS results indicate that there was no change in the average coordination environment of Pt with different pretreatments. Pt was found to have formed an alloy with Mo after the 600°C carburization. Passivation is on oxidation process. Because oxides usually have lower surface energy, if Mo inside the Pt gets oxidized during passivation, it may migrate to the surface of Pt particles [65]. Since, the reduction temperature (300°C) after passivation is significantly lower than the carburization temperature, such migration of Mo during passivation would have reflected in lowering of Pt-Mo coordination number measured using EXAFS. However, since the Pt-Mo coordination is not affected, we conclude that the series of different pretreatments has no effect on the mixing of two metals.

The experiment of O_2 uptake-H_2 titration offers a qualitative evidence for hydrogen spillover by Pt. The uptake of hydrogen after passivation of the carburized catalyst was ~85 times higher for Pt/Mo_2C catalyst as compared to Mo_2C. Assuming a 1:0.667 stoichiometry factor for H_2 titration over oxidized Pt [66], if Pt was 100% dispersed, it would account for only 0.12 mmol/g of H_2. Since the H_2 uptake for Pt/Mo_2C is significantly higher than what is needed for a hypothetically 100% dispersed Pt, the rest of the H_2 must have been spilled over to Mo_2C, so that Mo_2C sites adsorb hydrogen. It should be noted that the numbers in the O_2 uptake-H_2 titration experiments reported here should strictly be used in a relative sense. These numbers would not have any merit towards actual counting of the active sites as the extents of reduction will be different at different temperatures. Nonetheless, by comparing the H_2 uptake measured under the exact same conditions for Mo_2C and Pt/Mo_2C, this experiment qualitatively suggests that

Pt leads to H_2 spillover on passivated Mo_2C, thereby creating oxygen free Mo_2C sites. Thus, H_2 spillover leading to an enhanced oxygen removal from passivated Mo_2C is suggested as a mechanism for a 300°C activation of the Pt/Mo_2C catalyst. The absence of Pt does not lead to activation of Mo_2C at 300°C.

The results presented here have a great impact in terms of having a WGS catalyst that offers 4-5 times higher WGS rate on per gram basis measured at 120°C under the presence of 7% CO, 8.5% CO_2, 21.9% H_2O, 37.4% H_2 and balance inert and activating that catalyst with a relatively milder process, as opposed to what has been suggested before [23,56]. Based on previous reports, even though the higher activity of Pt/Mo_2C in comparison to the commercial catalysts seems attractive, the 600°C temperature required for the activation of this catalyst would have been a deterrent even for existing industrial WGS reactors.

4.5 Conclusions

The present study has demonstrated that unsupported Mo_2C modified by supported Pt metal offers WGS rates per gram of catalyst that were 4-5 times higher compared to the commercial Cu based catalyst at 120°C. After the deposition of Pt, a milder reduction treatment at 300°C in presence of H_2/Ar is sufficient for the activation of this catalyst at 120°C. It was also shown that in absence of Pt, the bulk unsupported Mo_2C could not be activated at 120°C. The H_2-TPR experiments performed after various pretreatments

indicate that Pt leads to a relatively greater extent of oxygen removal from the passivated Mo_2C, as compared to the Pt-free Mo_2C. The possible reason for enhancement in oxygen removal and low temperature activation is suggested to be the H_2 spillover caused by Pt. The O_2 uptake-H_2 titration experiments qualitatively prove the existence of a spillover mechanism.

CHAPTER 5. EFFECT OF COBALT ADDITION ON PLATINUM SUPPORTED OVER MULTI-WALLED CARBON NANOTEBS FOR WATER-GAS SHIFT

5.1 Introduction

Supported noble metal catalysts such as Pt and Au are of a vast interest for the water-gas shift (WGS) reaction. These catalysts do not suffer from the disadvantages of the commercial Cu based catalysts such as pyrophoric nature, high sensitivity to moisture and requirement of the controlled reduction process [32]. The supported Pt catalysts have been shown to have a promotion in the WGS rates with addition of various secondary metal promoters [65,67–70]. The exact role of secondary metals such as Re, Mo or Co has been a topic of debate in the literature. It is still unclear if a secondary metal alters the electronic properties of the Pt by forming an alloy, or it merely helps in promoting the activation of water during WGS [70]. Dietrich et al., showed with the use of a series of Pt-Co bimetallic catalysts with varying ratios of promoter to the Pt, that the rate of H_2 production in the aqueous phase reforming of glycerol increases with increasing amount of Co [54,71]. It was shown that the turnover rate of WGS over a series of Pt-Co samples correlates with the reforming rate of glycerol. However, the role of Co towards promoting the WGS rates is still not well understood. In this study, a series of Pt-Co bimetallic catalysts with increasing Co:Pt ratio were studied for WGS reaction. Pt and Co were observed to form an alloy after the reduction, with some Co remaining isolated.

A selective leaching of the isolated (unalloyed) Co from the catalysts was performed, in such a way that the alloy structure preserved. The effect of leaching on the WGS rates was studied in order to de-convolute the importance of Pt-Co alloy from the presence of partially oxidized Co species. In-situ X-ray absorption (XAS) studies were performed to study the structure of the Pt-Co alloy.

5.2 Experimental Methods

5.2.1 Catalyst Synthesis

Monometallic Pt and Pt-Co bimetallic catalysts supported on the Multi-walled Carbon Nanotubes (MWCNT) were synthesized using sequential incipient wetness impregnation method. The MWCNT support was purchased from Cheap Tubes Inc. The Pt weight loading was kept constant at 5 wt.%, while the Co loading was varied from 1.6 wt.% to 11.9 wt.% i.e. a series of catalysts with varying Pt:Co molar ratio (1:1, 1:2, 1:3, 1:5 and 1:8) were prepared. Aqueous solution of tetrammine platinum nitrate (Sigma Aldrich) was used as a Pt precursor. After Pt impregnation, the samples were dried overnight at 150°C in a static oven. Cobalt was impregnated using the aqueous solution of cobalt nitrate hydrate (Alfa Aesar).

Selective leaching of isolated Co was performed with a 5% acetic acid solution in a quartz tube plug flow reactor. The same reactor system was used by Dietrich et al. [54] for performing aqueous phase reforming of glycerol, the detailed description of it could be found in the said reference. Catalysts with Pt:Co ratios of 1:3, 1:5 and 1:8 were subjected to this leaching process. A monometallic Pt was also subjected to the same

leaching process, in order to see the effect of acetic acid on Pt. For leaching, an as prepared catalyst sample was loaded in a quartz tube reactor in between two quartz wool plugs. The catalyst was reduced at 450°C (5°C/min) for 2 hours in presence of 5% H_2/Ar mixture. Following the reduction, the catalyst was cooled to 25°C under Ar. It was then exposed to an upward flow of the liquid 5% acetic acid solution which was colorless. Liquid samples of the effluent solution were collected at a fixed time interval and were analyzed qualitatively for presence of Co with atomic absorption spectroscopy (AAS) using the Perkin Elmer AAnalyst 300 instrument.

Pt_3Co/MWCNT catalyst was prepared by deposition of the Pt_3Co alloy nanoparticles on to the MWCNT support. These Pt_3Co nanoparticles which were spherical in shape were prepared by an organic solvothermal method, details of which can be found elsewhere [72]. A desired amount of as synthesized Pt_3Co particles were kept in 10 ml toluene. Required amount of the MWCNT support was added to the solution and the mixture was sonicated in an ultrasound bath for 1 hour. The solvent was removed by heating the vial at 50°C. The relatively dried mass of the catalyst was kept in air inside a static oven at 185°C.

5.2.2 Kinetic Measurements

The details of the plug flow reactor system used for WGS kinetic measurements can be found in the published literature [24]. 0.2-0.25 g of each catalyst was loaded in the plug flow reactor on top of a quartz wool plug. A thermocouple protected by an SS sheath was inserted in the catalyst bed. As a pretreatment, all the catalysts were reduced in 25% H_2/Ar at 450°C (5°C/min). For the Pt_3Co/MWCNT catalyst prepared using the organic

solvothermal method, there were organic ligands such as $Pt(acac)_2$ retained from the synthesis [72]. In order to burn off these ligands prior to the reduction pretreatment, this catalyst was annealed in presence of 50 sccm of air flow inside the reactor at 300°C. Following the pretreatment, the catalysts were exposed to a standard WGS reaction mixture (7% CO, 8.5% CO_2, 21.9% H_2O, 37.4% H_2 and balance Ar). The reaction temperatures were adjusted such that CO conversion below 10% could be achieved, in order to maintain differential conditions. The catalysts were stabilized at these temperatures for 20 hours, before the apparent reaction orders and the apparent activation energies were measured. The details of the measurements have been described before in Chapters 2 and 3.

5.2.3 Catalyst Characterization

CO chemisorption was used as a probe molecule in order to measure the moles of exposed metal on the catalyst used for kinetic measurements. The CO uptake experiments were performed using the Micromeritics ASAP 2020 instrument. Prior to CO adsorption, the aforementioned reduction pretreatment at 450°C was performed.

X-ray diffraction (XRD) was performed on the used catalysts using a Rigaku Smartlab X-Ray Diffractometer. The scans were performed between $2\Theta = 30°$ and $2\Theta = 60°$, at the scan speed of 0.1°/min with a step size of 0.05°.

Ex-situ XAS experiments at the Pt L_{III} edge and the Co K edge were carried out at the MRCAT 10 ID (insertion device) beam line at the Advance Photon Source at Argonne

National Laboratory. Due to the low-Z CNTs, all the XAS experiments could be carried out in the transmission mode. The XAS experiments were conducted in 1 in OD quartz tubes connected to Ultra-Torr fittings with welded ball valves (for gas inlet/outlet and sealing) and Kapton windows. The catalyst samples were pressed into a 6 well sample holder as self-supporting wafers. The catalysts were reduced at 450°C in pure 5% H_2/Ar. The scans at Pt L_{III} edge and Co K edge were collected at RT in presence of Helium. The XAS data was analyzed using WINXAS 3.1 software. The x-ray absorption near edge structure (XANES) data was energy-calibrated by computing the first derivative of the first peak of the spectra for Pt and Co metal foil standards and comparing them to the known edge position. The edge energies for the Pt and Mo edge data for various catalyst samples were computed from the first derivative of the XANES spectra. The extended x-ray absorption fine structure (EXAFS) data was fit using experimental standards and references computed using the FEFF6 code. Phase shifts and amplitudes for Pt-Pt and Co-Co scatters were obtained from the foil standards of the respective elements. The phase and amplitude for the Pt-Co bimetallic alloy was obtained using the FEFF6. From the least square fits for the first shell, average coordination numbers, bond distances and the Debye-Waller factors were obtained for all the tested catalysts.

5.3 Results

5.3.1 WGS Kinetics

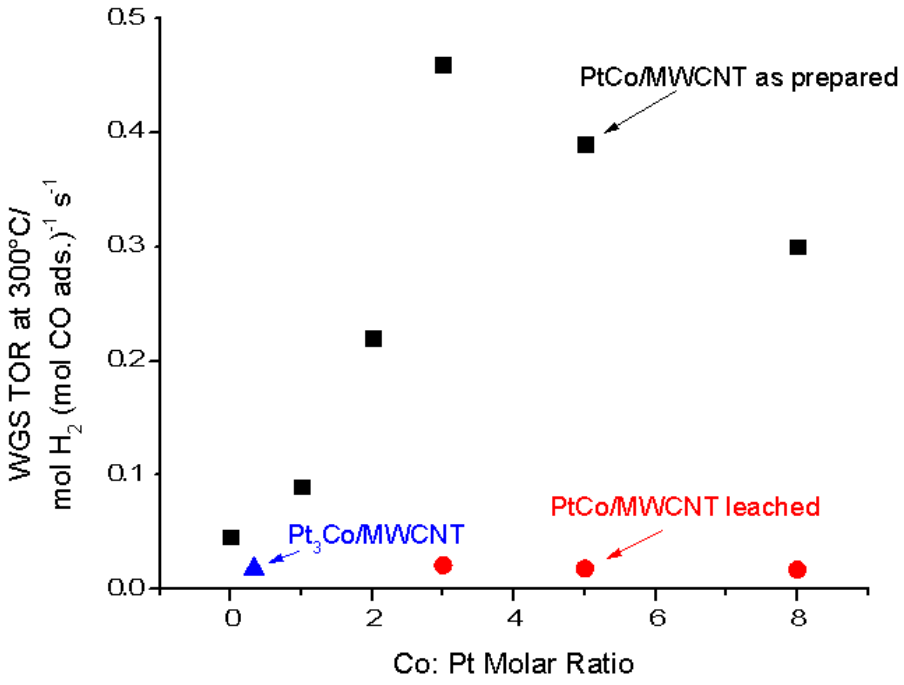

Figure 5.1 Variation of WGS TOR at 300°C vs. Co:Pt molar ratio for the as prepared, leached and the Pt3Co/MWCNT catalysts.

Figure 3.1 shows the WGS TOR (normalized by the moles of CO adsorbed during chemisorption) plotted against the Co:Pt molar ratio. Although the amount of cobalt will be different from the as prepared samples after leaching, the graph is plotted this way for the ease of comparison. For the as prepared samples, the TOR increased from 5.1×10^{-2} mol H_2 (mol CO ads.)$^{-1}$ s^{-1} for the monometallic Pt sample, to 4.6×10^{-2} mol H_2 (mol CO

ads.)$^{-1}$ s^{-1} for the PtCo 1:3 sample. The increase in the TOR was almost of an order of magnitude.

For the PtCo 1:5 and 1:8 catalyst, there was a decrease in the TOR with respect to the PtCo 1:3. The 1:3, 1:5 and 1:8 leached catalysts have TORs of 2.1×10^{-2} , 1.8×10^{-2} and 1.7×10^{-2} mol H_2 (mol CO ads.)$^{-1}$ s^{-1}. These were 17 to 21 times lower than there as prepared counterparts. The Pt_3Co/MWCNT catalyst had TOR of 1.8×10^{-2} mol H_2 (mol CO ads.)$^{-1}$ s^{-1}, which was similar to the leached PtCo catalysts prepared by sequential impregnation of Pt and Co.

Table C.1 shows detailed kinetic parameters for all the PtCo catalysts tested. The PtCo 1:3, 1:5 and 1:8 catalysts were tested at the same temperature (250°C) and hence, the kinetic parameters can be directly compared. The apparent reaction orders and the apparent activation energies (~136 kJ/mol) were similar for these catalysts within error. For the acetic acid leached counterparts of the 1:3, 1:5 and 1:8 catalysts, the kinetic parameters were also similar when these leached catalysts were tested at 310°C. The Pt_3Co/MWCNT catalyst that was tested at the 330°C, also exhibited similar reaction orders and the apparent activation energy as the leached catalysts.

Table 5.1 shows the comparison of the kinetic parameters of as prepared monometallic Pt/MWCNT and the Pt/MWCNT that had undergone the same 5% acetic acid treatment as the PtCo bimetallic catalyst. The WGS TOR at 300°C and the kinetic parameters (measured at 290 and 300°C) were similar for these catalysts within experimental errors.

Table 5.1Comparison of WGS kinetic parameters for the as prepared and the acetic acid treated Pt/MWCNT monometallic catalysts.

Catalyst	WGS TOR at 300°C/ mol H_2 (mol CO)$^{-1}$ s^{-1}	E_{app}/ kJ (mol)$^{-1}$	H_2O (±0.04)	CO (±0.04)	CO_2 (±0.04)	H_2 (±0.04)
Pt/MWCNT As prepared	4.6×10^{-2}	86	0.83	0.10	-0.08	-0.38
Pt/MWCNT 5% acetic acid treated	4.2×10^{-2}	90	0.77	0.08	-0.06	-0.34

5.3.2 Catalyst Characterization

Figure 5.2 shows the XRD patterns for the Pt, PtCo as prepared and the Pt Co leached catalysts post WGS reaction. The peaks at 39.8° and 46.4° are present for all the catalysts. Using the JCPDS database, these peaks are assigned to Pt. The as prepared PtCo 1:3, 1:5 and 1:8 catalysts have a peak at 44.4°. This peak was assigned to a metallic cobalt phase. This peak is absent from the patterns for the samples that were subjected to the acetic acid leaching process. The leached samples show a broad peak at 43.1°, which using the database, was assigned to an alloy of Pt and Co.

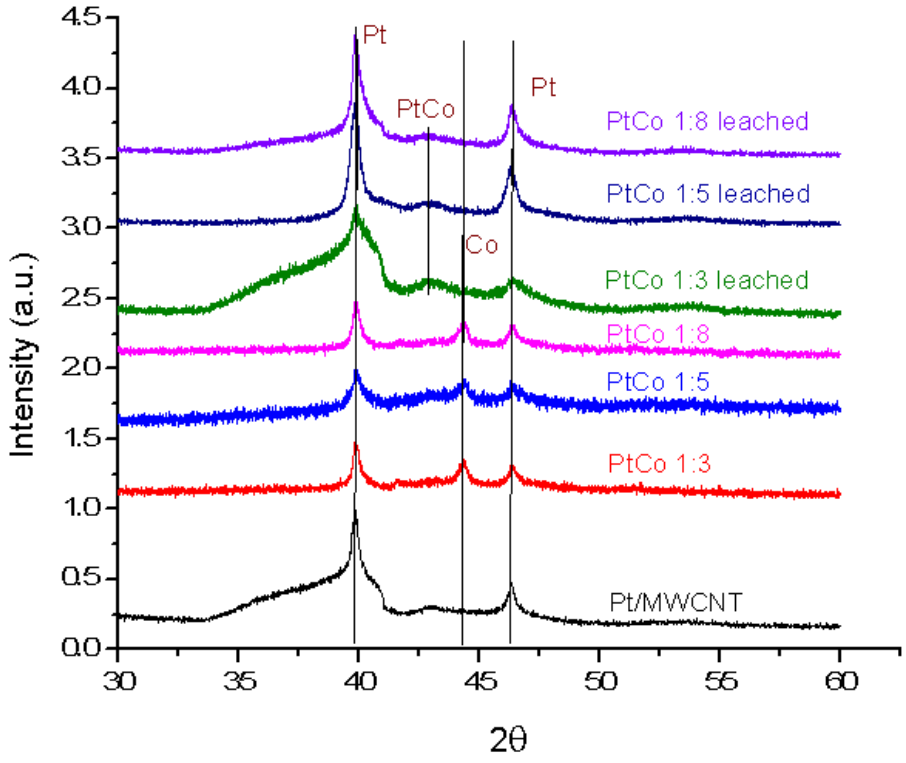

Figure 5.2 XRD patterns for Pt, PtCo as prepared and PtCo leached catalysts supported on MWCNT.

The *ex situ* XAS experiments at Pt L_{III} and Co K edge were performed to characterize the catalysts for the effect of the reduction pretreatment at 450°C. The Co K edge XANES spectra for these catalysts are shown in Figure 5.3. Spectra for Co foil and the CoO standard are also shown. The XANES spectra qualitatively show that the Co is predominantly reduced. However, the quantifications were made using the linear combination XANES tool available in the WINXAS 3.1 software to estimate the fraction of Co that stays oxidized after the 450°C reduction pretreatment (Table C.3).

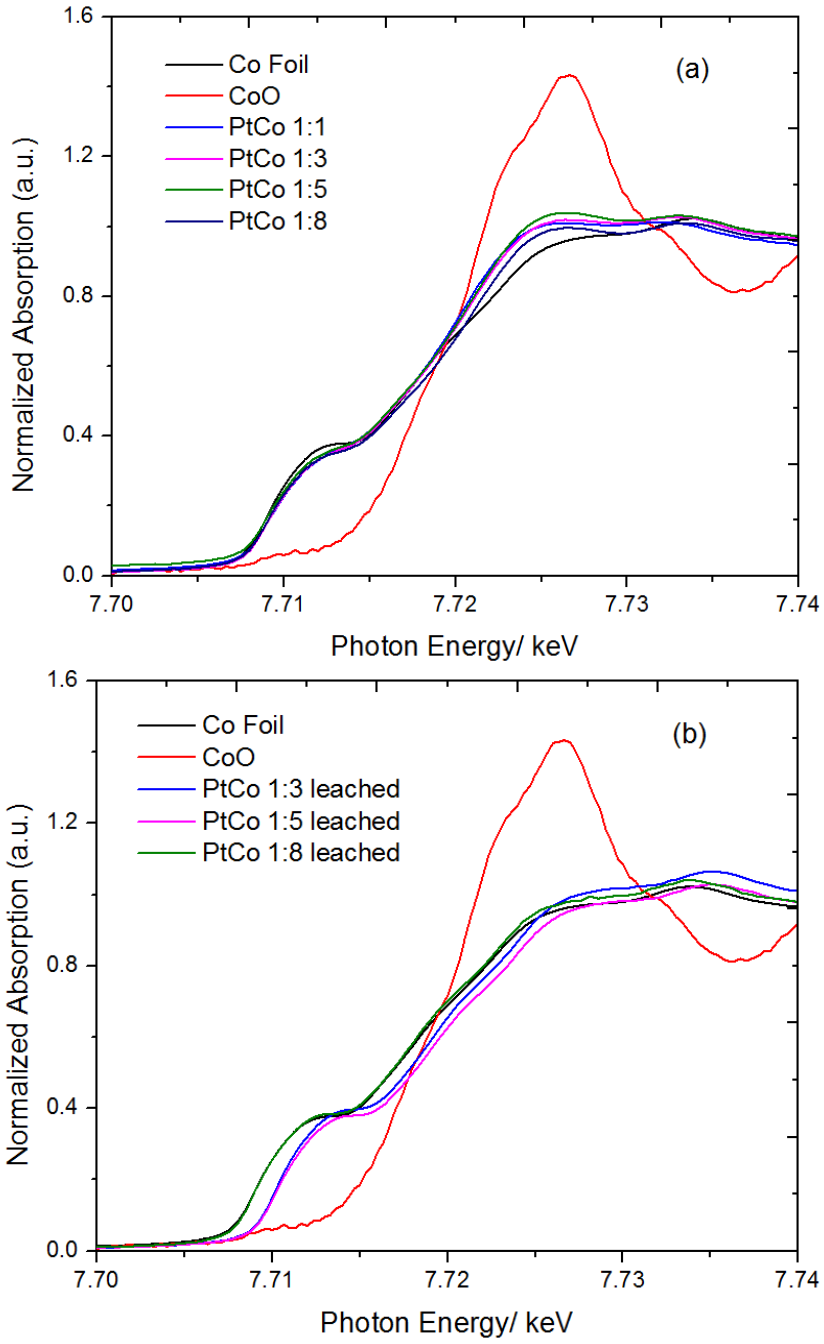

Figure 5.3 Co K edge XANES spectra at RT after the 450°C reduction for (a) as prepared and (b) leached PtCo catalysts

The as prepared PtCo 1:1, 1:2, 1:3, 1:5 and 1:8 catalysts have about 9%, 11%, 13%, 14% and 20% cobalt in the oxidized state respectively. This result is coherent with the observation made by Dietrich et al. [54] on similar catalytic systems. On the other hand, for the catalysts subjected to the acetic acid leaching process, the amount of oxidized cobalt was below the detection limit of the XANES i.e. 100% cobalt remained in the metallic state after the reduction pretreatment.

Figure 5.4 shows the Pt L_{III} edge EXAFS spectra for the as prepared and the leached PtCo/MWCNT catalysts. For the as prepared catalysts, the spectra exhibit differences from the metallic Pt foil in terms of the peak shapes and the peak positions. These changes are assigned to a presence of a second scatter apart from Pt-Pt i.e. Pt-Co [54,71]. The Pt-Pt and the Pt-co contributions can bees seen at 2.9 and 2.3 Å respectively. The average coordination numbers (CN) determined from the EXAFS fit parameters are listed in Table C.4. The Pt-Pt CN does not change significantly with increasing Co:Pt ratio and remains between 5 and 6. Similarly, the Pt-Co CN stays between 2 and 3 for the as prepared catalysts with various Co;Pt molar ratios. For the catalysts subjected to the acetic acid leaching process, the features assigned to Pt-Pt and Pt-Co at 2.9 and 2.3 Å are still retained. There is ~10% increase in the Pt-Pt CN for the catalysts to around 6.6. The Pt-Co CN decreases in comparison to the as prepared counterparts (3.5 to 2.5 for 1:3, 2.9 to 1.4 for 1:5 and 2.5 to 1.7 for 1:8 catalysts). Nonetheless, the Pt-Co bonds are still retained after the leaching process. The Pt_3Co/MWCNT catalyst also exhibits the features in the EXFAS spectrum that are similar to the catalysts prepared using sequential

impregnation method. The Pt-Pt and Pt-Co CNs for this catalyst were 6.2 and 3.4 respectively.

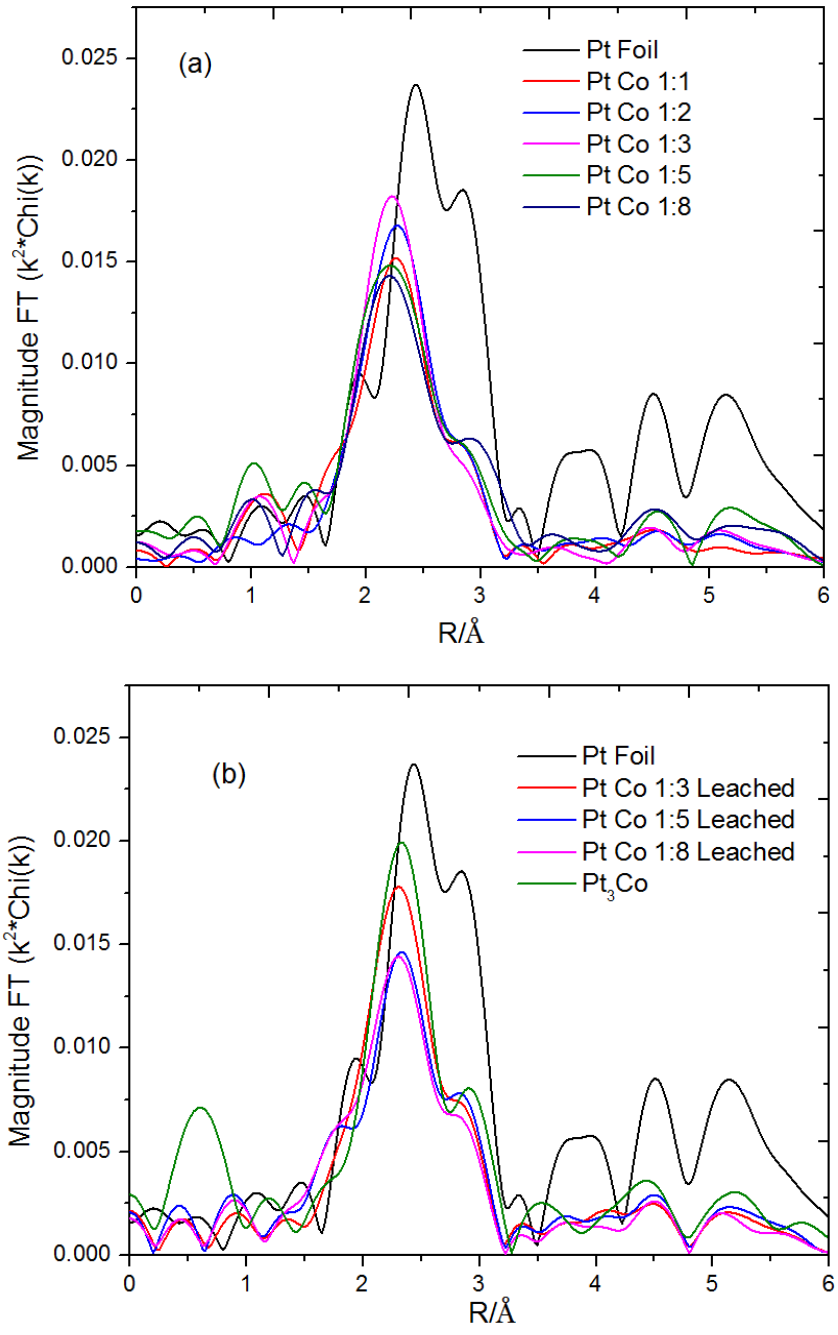

Figure 5.4 Pt L_{III} edge EXAFS spectra collected at RT after 450°C reduction of PtCo/MWCNT catalysts (a) as prepared (b) leached and Pt_3Co/MWCNT

5.4 Discussion

The PtCo/MWCNT catalysts synthesized with a similar method have been used for the aqueous phase reforming of glycerol [54]. It was suggested by Dietrich et al. that the Co from the catalysts were leached out into the product stream. The leaching was attributed to the presence of organic acids formed as a product of reforming. Based on their observation, the leaching method in the present work was devised.

As shown in Figure 5.1, the WGS TOR increased by a factor of 9 with addition of Co up to Co:Pt=1:3.The promotion in the WGS rate lead to lower test temperatures with increasing amounts of Co. The 1:3, 1:5 and the 1:8 catalysts exhibit similar kinetic parameters compared at the same test temperature of 250°C. The apparent activation energies and reaction orders of these catalysts, although cannot be directly compared, are significantly different from the monometallic Pt.

The apparent activation energies for the 1:1 sample (96 kJ/mol) and the 1:2 sample (116 kJ/mol) are in between the values for the monometallic Pt (86 kJ/mol) and the fully promoted PtCo 1:3 sample (137 kJ/mol). Similar trends are observed for the apparent reaction orders over these catalysts. This suggests that as the Co amount is increased, the population of an active site for WGS which is chemically different compared to the monometallic Pt increases. A further increase in the Co:Pt ratio after 1:3 does not lead to any noticeable changes in the apparent kinetic parameters, alluding to the numerical dominance of this new type of active site over the monometallic Pt sites.

After the leaching process, all the leached catalysts have similar kinetic parameters measured at 310°C, which are in turn similar to the Pt_3Co/MWCNT catalyst, which predominantly has all the cobalt in the alloyed form [72]. The kinetic parameters for the leached catalysts and the Pt_3Co/MWCNT catalyst are significantly different compared to the monometallic Pt. For example, these catalysts exhibit higher apparent activation energies (~116 kJ/mol) compared to the monometallic Pt (86 kJ/mol). This result implies that even though the WGS TOR over the leached catalysts is lower compared to the monometallic Pt, the chemical nature of the active site is discernably different compared to the monometallic Pt. The modification to the chemical nature could have been caused by the presence of Co inside the particles, which will be discussed later.

The leaching process also caused a decrease in the number of exposed metal sites measured by CO chemisorption as indicated in Table C.2. This also reflected in the total coordination number at the Pt L_{III} edge EXAFS data. The total coordination number increased after leaching (Table C.3), suggesting that the particles sintered during the process.

There was no significant change in the apparent kinetic parameters when the monometallic Pt was subjected to the leaching process. Although no Pt was physically leached, this experiment was performed to verify that the acetic acid treatment does not chemically alter the monometallic Pt active sites. However, similar to PtCo catalysts that were leached, there was a sintering of Pt particles observed for the monometallic catalyst, which is marked by a lower CO chemisorption value. Nonetheless, the TOR i.e. the WGS

rate normalized by CO chemisorption is similar to the as prepared Pt/MWCNT, suggesting that the active sites were not chemically modified.

Based on the XRD patterns, it is clear that with addition of Co, there is an isolated phase of metallic cobalt that is created on these catalysts. There was no observable peak for cobalt oxide; however, the absence of the cobalt oxide peaks could have been due to the smaller size of the cobalt oxide clusters, which may fall below the detection limit of the XRD. For the leached catalysts, the absence of the Co peak suggests that the metallic Co was leached to a level below detection limit of the XRD.The PtCo alloy peak shown for the leached sample hints at the alloy being preserved after leaching, which is confirmed with the EXFAS results.

The Co K edge linear combination XANES data indicated that there was a marginal increase in the fraction of cobalt that remained oxidized with the increase in the Co:Pt molar ratio (Table C.3). Thus, the presence of CoO phase that was not detected in the XRD was confirmed with XANES. The absence of the CoO phase for the leached samples suggests that all the Co is in metallic state (possibly, due to alloying).

Based on the Pt L_{III} edge EXAFS data, it was observed that the Pt-Pt and Pt-Co coordination numbers are relatively independent of the Co:Pt molar ratio for the as prepared catalyst. This implies that the PtCo alloy of similar composition is formed at all the Co weight loadings. The excess of Co that is not alloyed with Pt would probably manifest into the isolated metallic Co phase (observed in XRD) and the CoO phase

(observed with XANES). From the Pt edge EXAFS data, leached catalysts, still have the alloy structure of PtCo preserved i.e. the cobalt from the alloy particles is not completely leached out (although, there is a decrease in the Pt-Co coordination numbers as compared to the as prepared counterparts). In short, combining the XRD, Co K edge XANES and the Pt L_{III} edge EXAFS data, it appears that the isolated cobalt phase and the CoO phases are selectively leached out during the acetic acid leaching, with the Pt-Co alloy still preserved. Thus, the leaching has enabled us in selectively removing one type of possible active site i.e. the interface between the PtCo alloy and the CoO_x (partially oxidized cobalt) phase.

Unlike the systematic change in WGS TOR and the kinetic parameters with increasing Co:Pt ratio from monometallic Pt to the 1:3 as prepared catalyst, the structure of the Pt-Co alloy particles was independent of the Co:Pt molar ratio. This indirectly implies that even though the alloy of the same structure was formed at the lowest Co loading (1:1), the WGS TOR was not fully promoted until the ratio increased to 1:3. However, there is a marginal but noticeable increase in the CoO fraction estimated with linear combination XANES, with an increase in the Co:Pt ratio from 0 to 3. Thus, the kinetics, XRD and XANES results indicate that the presence of isolated Co and CoO phases are required for promotion in the WGS reaction rate. Previous studies [69] on the other bimetallic catalysts such as Pt-Re have made similar claims about the alloy formation being just a consequence of having reduced metals in close proximity. The partially oxidized secondary metal phases promote the rate by providing sites for activation of water.

The Pt_3Co/MWCNT catalyst has helped us further our claims that leaching removes isolated Co and CoO phases from the bimetallic catalysts to an extent where the WGS rate is not promoted. The Pt_3Co nanoparticles synthesized by reported organic solvothermal method have been shown to be homogeneous in composition [73]. One might argue that the catalysts synthesized using the sequential impregnation of Pt and Co would be inhomogeneous in structure [54], wherein monometallic Pt could coexist with the alloy particles. However, for the acetic acid leached catalysts, the similarity of WGS TOR and apparent kinetic parameters at between 310°C and 330°C to the homogeneous Pt_3Co alloy particles supported on MWCNT suggests that the PtCo alloy particles must be statistically dominant over these catalysts after leaching. Furthermore, the Pt edge EXAFS data also shows that Pt is alloyed, confirming the retention of alloy after leaching. Thus, by benchmarking the kinetics and the EXAFS data over leached catalysts against the Pt_3Co/MWCNT catalyst, it can be proposed that the PtCo alloy formation is inconsequential towards promotion in the WGS TOR using Co as a promoter.

It therefore appears that the isolated Co and CoO phases are the reason of promotion in WGS TOR.

In order to rule out the dominance of one type of active site over the other for a given reaction on a given catalyst, it is convenient when the sites of one particular type are selectively removed and a significant effect is observed over the reaction rate. In the present case, the two candidates for the cause of promotion in the WGS rate were the Pt-Co alloy and the interface between the Pt/PtCo and the CoO_x phases. When the CoO_x phase was selectively removed, the WGS TOR decreased by ~20 times compared to a

fully promoted PtCo/MWCNT as prepared bimetallic catalyst. This suggests that alloy formation is a mere coincidence, which results from the juxtaposition of reduced Pt and reduced Co.

The present study highlights the importance and indispensability of the sites formed by the partially oxidized secondary metal promoter towards understanding the WGS mechanism. As suggested by Azzam et al. [70], the partially secondary metal (ReO_x) could directly take part in the reaction by activating water and the direct interaction of Pt and Re may be insignificant. The results in the present study suggest that a similar analogy could be drawn for Co-promoted Pt catalysts. However, the density functional theory studies reported in the literature for Pt-Metal bimetallic catalysts have focused on the electronic effects induced due to alloy formation, in order to understand the mechanism of promotion [74,75]. Thus, the present experimental study highlights the need to accommodate the oxide/alloy interface sites into the theoretical predictions for WGS catalysis.

5.5 Conclusions

A series of PtCo bimetallic catalysts were studied for WGS. Cobalt has been shown to promote the WGS TOR over Pt supported on MWCNT at 300°C by a factor of 9 at a Co:Pt ratio of 1:3, measured under 7% CO, 8.5% CO_2, 21.9% H_2O, 37.4% H_2 and balance Ar. A fraction of Co was shown to be in isolated CoO_x phase (metallic Co and CoO). This CoO_x phase was selectively removed by leaching with 5% acetic acid, while the Pt-Co alloy was preserved. The leaching lead to a decrease in the WGS TOR at

300°C by 20 times. The WGS kinetics of the leached catalysts were similar to the Pt_3Co/MWCNT catalyst with homogeneous PtCo alloy. The results suggest that the formation of PtCo alloy is inconsequential towards promoting the WGS rate with Co. Based on the present results, the interface between PtCo particles and the CoO_x phase is suggested to be the locus of the active sites for WGS.

LIST OF REFERENCES

LIST OF REFERENCES

[1] R.J. Farrauto, Introduction to solid polymer membrane fuel cells and reforming natural gas for production of hydrogen, Appl. Catal. B Environ. 56 (2005) 3–7. doi:10.1016/j.apcatb.2004.08.011.

[2] R. Farrauto, S. Hwang, L. Shore, W. Ruettinger, J. Lampert, T. Giroux, et al., New Material Needs For Hydrocarbon Fuel Processing: Generating Hydrogen for the PEM Fuel Cell, Annu. Rev. Mater. Res. 33 (2003) 1–27. doi:10.1146/annurev.matsci.33.022802.091348.

[3] D.S. Newsome, The Water-Gas Shift Reaction, Catal. Rev. 21 (1980) 275–318. doi:10.1080/03602458008067535.

[4] Q. Fu, H. Saltsburg, M. Flytzani-Stephanopoulos, Active Nonmetallic Au and Pt Species on Ceria-Based Water-Gas Shift Catalysts, Science. 301 (2003) 935–938. doi:10.1126/science.1085721.

[5] J. Xu, G.F. Froment, Methane steam reforming, methanation and water-gas shift: I. Intrinsic kinetics, AIChE J. 35 (1989) 88–96. doi:10.1002/aic.690350109.

[6] T. Bunluesin, R.J. Gorte, G.W. Graham, Studies of the water-gas-shift reaction on ceria-supported Pt, Pd, and Rh: Implications for oxygen-storage properties, Appl. Catal. B Environ. 15 (1998) 107–114. doi:10.1016/S0926-3373(97)00040-4.

[7] Y. Li, Q. Fu, M. Flytzani-Stephanopoulos, Low-temperature water-gas shift reaction over Cu- and Ni-loaded cerium oxide catalysts, Appl. Catal. B Environ. 27 (2000) 179–191. doi:10.1016/S0926-3373(00)00147-8.

[8] F. Boccuzzi, A. Chiorino, M. Manzoli, D. Andreeva, T. Tabakova, FTIR Study of the Low-Temperature Water–Gas Shift Reaction on Au/Fe2O3 and Au/TiO2 Catalysts, J. Catal. 188 (1999) 176–185. doi:10.1006/jcat.1999.2636.

[9] S. Hilaire, X. Wang, T. Luo, R.J. Gorte, J. Wagner, A comparative study of water-gas-shift reaction over ceria supported metallic catalysts, Appl. Catal. Gen. 215 (2001) 271–278. doi:10.1016/S0926-860X(01)00535-X.

[10] C. Rhodes, G.J. Hutchings, A.M. Ward, Water-gas shift reaction: finding the mechanistic boundary, Catal. Today. 23 (1995) 43–58. doi:10.1016/0920-5861(94)00135-O.

[11] J.R. Ladebeck, J.P. Wagner, Catalyst development for water–gas shift, in: Handb. Fuel Cells, John Wiley & Sons, Ltd, 2010. http://onlinelibrary.wiley.com/doi/10.1002/9780470974001.f302017/abstract (accessed November 10, 2014).

[12] B. Coq, F. Figueras, Structure–activity relationships in catalysis by metals: some aspects of particle size, bimetallic and supports effects, Coord. Chem. Rev. 178–180, Part 2 (1998) 1753–1783. doi:10.1016/S0010-8545(98)00058-7.

[13] S.D. Stamatis, Bayesian microkinetic modeling of epoxy resin curing and water gas shift catalysis, Theses Diss. Available ProQuest. (2011) 1–224.

[14] H.H. Hwu, J.G. Chen, Surface Chemistry of Transition Metal Carbides, Chem. Rev. 105 (2005) 185–212. doi:10.1021/cr0204606.

[15] J.H. Sinfelt, D.J.C. Yates, Effect of Carbiding on the Hydrogenolysis Activity of Molybdenum, Nature. 229 (1971) 27–28. doi:10.1038/10.1038/physci229027b0.

[16] R.B. Levy, M. Boudart, Platinum-Like Behavior of Tungsten Carbide in Surface Catalysis, Science. 181 (1973) 547–549. doi:10.1126/science.181.4099.547.

[17] M. Boudart, A.W. Aldag, L.D. Ptak, J.E. Benson, On the selectivity of platinum catalysts, J. Catal. 11 (1968) 35–45. doi:10.1016/0021-9517(68)90007-9.

[18] R. Kojima, K. Aika, Molybdenum nitride and carbide catalysts for ammonia synthesis, Appl. Catal. Gen. 219 (2001) 141–147. doi:10.1016/S0926-860X(01)00676-7.

[19] H.-G. Kim, K.H. Lee, J.S. Lee, Carbon monoxide hydrogenation over molybdenum carbide catalysts, Res. Chem. Intermed. 26 (2000) 427–443. doi:10.1163/156856700X00435.

[20] J.B. Claridge, A.P.E. York, A.J. Brungs, C. Marquez-Alvarez, J. Sloan, S.C. Tsang, et al., New Catalysts for the Conversion of Methane to Synthesis Gas: Molybdenum and Tungsten Carbide, J. Catal. 180 (1998) 85–100. doi:10.1006/jcat.1998.2260.

[21] B. Dhandapani, T. St. Clair, S.T. Oyama, Simultaneous hydrodesulfurization, hydrodeoxygenation, and hydrogenation with molybdenum carbide, Appl. Catal. Gen. 168 (1998) 219–228. doi:10.1016/S0926-860X(97)00342-6.

[22] J. Patt, D.J. Moon, C. Phillips, L. Thompson, Molybdenum carbide catalysts for water–gas shift, Catal. Lett. 65 (2000) 193–195. doi:10.1023/A:1019098112056.

[23] N.M. Schweitzer, J.A. Schaidle, O.K. Ezekoye, X. Pan, S. Linic, L.T. Thompson, High Activity Carbide Supported Catalysts for Water Gas Shift, J. Am. Chem. Soc. 133 (2011) 2378–2381. doi:10.1021/ja110705a.

[24] L. Bollmann, J.L. Ratts, A.M. Joshi, W.D. Williams, J. Pazmino, Y.V. Joshi, et al., Effect of Zn addition on the water–gas shift reaction over supported palladium catalysts, J. Catal. 257 (2008) 43–54. doi:10.1016/j.jcat.2008.04.005.

[25] N.A. Koryabkina, A.A. Phatak, W.F. Ruettinger, R.J. Farrauto, F.H. Ribeiro, Determination of kinetic parameters for the water–gas shift reaction on copper catalysts under realistic conditions for fuel cell applications, J. Catal. 217 (2003) 233–239. doi:10.1016/S0021-9517(03)00050-2.

[26] P.J. Dietrich, R.J. Lobo-Lapidus, T. Wu, A. Sumer, M.C. Akatay, B.R. Fingland, et al., Aqueous Phase Glycerol Reforming by PtMo Bimetallic Nano-Particle Catalyst: Product Selectivity and Structural Characterization, Top. Catal. 55 (2012) 53–69. doi:10.1007/s11244-012-9775-5.

[27] J.T. Miller, A.J. Kropf, Y. Zha, J.R. Regalbuto, L. Delannoy, C. Louis, et al., The effect of gold particle size on AuAu bond length and reactivity toward oxygen in supported catalysts, J. Catal. 240 (2006) 222–234. doi:10.1016/j.jcat.2006.04.004.

[28] B. Shelimov, J.-F. Lambert, M. Che, B. Didillon, Initial Steps of the Alumina-Supported Platinum Catalyst Preparation: A Molecular Study by 195Pt NMR, UV–Visible, EXAFS, and Raman Spectroscopy, J. Catal. 185 (1999) 462–478. doi:10.1006/jcat.1999.2527.

[29] G.C. Bond, M.A. Keane, H. Kral, J.A. Lercher, Compensation Phenomena in Heterogeneous Catalysis: General Principles and a Possible Explanation, Catal. Rev. 42 (2000) 323–383. doi:10.1081/CR-100100264.

[30] I. Chorkendorff, J.W. Niemantsverdriet, Concepts of Modern Catalysis and Kinetics, John Wiley & Sons, 2006.

[31] G.C. Bond, The Use of Kinetics in Evaluating Mechanisms in Heterogeneous Catalysis, Catal. Rev. 50 (2008) 532–567. doi:10.1080/01614940802480338.

[32] C. Ratnasamy, J.P. Wagner, Water Gas Shift Catalysis, Catal. Rev. 51 (2009) 325–440. doi:10.1080/01614940903048661.

[33] P. Liu, J.A. Rodriguez, Water-Gas-Shift Reaction on Molybdenum Carbide Surfaces: Essential Role of the Oxycarbide, J. Phys. Chem. B. 110 (2006) 19418–19425. doi:10.1021/jp0621629.

[34] H. Tominaga, M. Nagai, Density Functional Theory of Water−Gas Shift Reaction on Molybdenum Carbide, J. Phys. Chem. B. 109 (2005) 20415–20423. doi:10.1021/jp053706u.

[35] L.C. Grabow, A.A. Gokhale, S.T. Evans, J.A. Dumesic, M. Mavrikakis, Mechanism of the Water Gas Shift Reaction on Pt: First Principles, Experiments, and Microkinetic Modeling, J. Phys. Chem. C. 112 (2008) 4608–4617. doi:10.1021/jp7099702.

[36] C.V. Ovesen, P. Stoltze, J.K. Nørskov, C.T. Campbell, A kinetic model of the water gas shift reaction, J. Catal. 134 (1992) 445–468. doi:10.1016/0021-9517(92)90334-E.

[37] D.C. Grenoble, M.M. Estadt, D.F. Ollis, The chemistry and catalysis of the water gas shift reaction: 1. The kinetics over supported metal catalysts, J. Catal. 67 (1981) 90–102. doi:10.1016/0021-9517(81)90263-3.

[38] H.H. Hwu, J.G. Chen, Reactions of methanol and water over carbide-modified Mo(1 1 0), Surf. Sci. 536 (2003) 75–87. doi:10.1016/S0039-6028(03)00607-1.

[39] A.B. Vidal, P. Liu, Density functional study of water-gas shift reaction on M3O3x/Cu(111), Phys. Chem. Chem. Phys. 14 (2012) 16626. doi:10.1039/c2cp42091k.

[40] J.A. Rodriguez, S. Ma, P. Liu, J. Hrbek, J. Evans, M. Pérez, Activity of CeOx and TiOx Nanoparticles Grown on Au(111) in the Water-Gas Shift Reaction, Science. 318 (2007) 1757–1760. doi:10.1126/science.1150038.

[41] S. Aranifard, S.C. Ammal, A. Heyden, On the importance of metal–oxide interface sites for the water–gas shift reaction over Pt/CeO2 catalysts, J. Catal. 309 (2014) 314–324. doi:10.1016/j.jcat.2013.10.012.

[42] K.G. Azzam, I.V. Babich, K. Seshan, L. Lefferts, Bifunctional catalysts for single-stage water–gas shift reaction in fuel cell applications.: Part 1. Effect of the support on the reaction sequence, J. Catal. 251 (2007) 153–162.
doi:10.1016/j.jcat.2007.07.010.

[43] J.L. Falconer, J.A. Schwarz, Temperature-Programmed Desorption and Reaction: Applications to Supported Catalysts, Catal. Rev. 25 (1983) 141–227. doi:10.1080/01614948308079666.

[44] J.S. Lee, K.H. Lee, J.Y. Lee, Selective chemisorption of carbon monoxide and hydrogen over supported molybdenum carbide catalysts, J. Phys. Chem. 96 (1992) 362–366. doi:10.1021/j100180a067.

[45] H. Miura, R.D. Gonzalez, Temperature-programmed desorption and temperature-programmed reaction studies of carbon monoxide over well-characterized silica-supported platinum-ruthenium bimetallic clusters, J. Phys. Chem. 86 (1982) 1577–1582. doi:10.1021/j100206a021.

[46] R. Zanella, C. Louis, Influence of the conditions of thermal treatments and of storage on the size of the gold particles in Au/TiO2 samples, Catal. Today. 107–108 (2005) 768–777. doi:10.1016/j.cattod.2005.07.008.

[47] M. Shekhar, J. Wang, W.-S. Lee, W.D. Williams, S.M. Kim, E.A. Stach, et al., Size and Support Effects for the Water–Gas Shift Catalysis over Gold Nanoparticles Supported on Model Al2O3 and TiO2, J. Am. Chem. Soc. 134 (2012) 4700–4708. doi:10.1021/ja210083d.

[48] N. Lopez, T.V.W. Janssens, B.S. Clausen, Y. Xu, M. Mavrikakis, T. Bligaard, et al., On the origin of the catalytic activity of gold nanoparticles for low-temperature CO oxidation, J. Catal. 223 (2004) 232–235. doi:10.1016/j.jcat.2004.01.001.

[49] J.A. Rodriguez, F. Illas, Activation of noble metals on metal-carbide surfaces: novel catalysts for CO oxidation, desulfurization and hydrogenation reactions, Phys. Chem. Chem. Phys. 14 (2012) 427. doi:10.1039/c1cp22738f.

[50] T.G. Kelly, J.G. Chen, Metal overlayer on metal carbide substrate: unique bimetallic properties for catalysis and electrocatalysis, Chem. Soc. Rev. 41 (2012) 8021. doi:10.1039/c2cs35165j.

[51] T.G. Kelly, J.G. Chen, Controlling C–O, C–C and C–H bond scission for deoxygenation, reforming, and dehydrogenation of ethanol using metal-modified molybdenum carbide surfaces, Green Chem. 16 (2014) 777. doi:10.1039/c3gc41259h.

[52] T.G. Kelly, K.X. Lee, J.G. Chen, Pt-modified molybdenum carbide for the hydrogen evolution reaction: From model surfaces to powder electrocatalysts, J. Power Sources. 271 (2014) 76–81. doi:10.1016/j.jpowsour.2014.07.179.

[53] Y. Ma, G. Guan, P. Phanthong, X. Hao, W. Huang, A. Tsutsumi, et al., Catalytic Activity and Stability of Nickel-Modified Molybdenum Carbide Catalysts for Steam Reforming of Methanol, J. Phys. Chem. C. 118 (2014) 9485–9496. doi:10.1021/jp501021t.

[54] P.J. Dietrich, M.C. Akatay, F.G. Sollberger, E.A. Stach, J.T. Miller, W.N. Delgass, et al., Effect of Co Loading on the Activity and Selectivity of PtCo Aqueous Phase Reforming Catalysts, ACS Catal. 4 (2014) 480–491. doi:10.1021/cs4008705.

[55] X. Li, D. Ma, L. Chen, X. Bao, Fabrication of molybdenum carbide catalysts over multi-walled carbon nanotubes by carbothermal hydrogen reduction, Catal. Lett. 116 (2007) 63–69. doi:10.1007/s10562-007-9093-x.

[56] G. Wang, J.A. Schaidle, M.B. Katz, Y. Li, X. Pan, L.T. Thompson, Alumina supported Pt–Mo2C catalysts for the water–gas shift reaction, J. Catal. 304 (2013) 92–99. doi:10.1016/j.jcat.2013.04.007.

[57] D.J. Moon, J.W. Ryu, Molybdenum Carbide Water–Gas Shift Catalyst for Fuel Cell-Powered Vehicles Applications, Catal. Lett. 92 (2004) 17–24. doi:10.1023/B:CATL.0000011079.20686.db.

[58] G.L. Semin, A.R. Dubrovskii, P.V. Snytnikov, S.A. Kuznetsov, V.A. Sobyanin, Using catalysts based on molybdenum and tungsten carbides in the water-gas shift reaction, Catal. Ind. 4 (2012) 59–66. doi:10.1134/S2070050412010102.

[59] L.T. Thompson, S.K. Bej, J.J. Patt, C.H. Kim, Carbide/nitride based fuel processing catalysts, US6897178 B1, 2005. http://google.com/patents/US6897178 (accessed November 1, 2014).

[60] F.H. Ribeiro, R.A. Dalla Betta, G.J. Guskey, M. Boudart, Preparation and surface composition of tungsten carbide powders with high specific surface area, Chem. Mater. 3 (1991) 805–812. doi:10.1021/cm00017a015.

[61] J.S. Lee, L. Volpe, F.H. Ribeiro, M. Boudart, Molybdenum carbide catalysts: II. Topotactic synthesis of unsupported powders, J. Catal. 112 (1988) 44–53. doi:10.1016/0021-9517(88)90119-4.

[62] P.A. Sermon, G.C. Bond, Hydrogen Spillover, Catal. Rev. 8 (1974) 211–239. doi:10.1080/01614947408071861.

[63] M. Lewandowski, A. Szymańska-Kolasa, P. Da Costa, C. Sayag, Catalytic performances of platinum doped molybdenum carbide for simultaneous hydrodenitrogenation and hydrodesulfurization, Catal. Today. 119 (2007) 31–34. doi:10.1016/j.cattod.2006.08.062.

[64] W.D. Williams, L. Bollmann, J.T. Miller, W.N. Delgass, F.H. Ribeiro, Effect of molybdenum addition on supported platinum catalysts for the water–gas shift reaction, Appl. Catal. B Environ. 125 (2012) 206–214. doi:10.1016/j.apcatb.2012.05.037.

[65] J.E. Benson, M. Boudart, Hydrogen-oxygen titration method for the measurement of supported platinum surface areas, J. Catal. 4 (1965) 704–710. doi:10.1016/0021-9517(65)90271-X.

[66] G. Jacobs, E. Chenu, P.M. Patterson, L. Williams, D. Sparks, G. Thomas, et al., Water-gas shift: comparative screening of metal promoters for metal/ceria systems and role of the metal, Appl. Catal. Gen. 258 (2004) 203–214. doi:10.1016/j.apcata.2003.09.007.

[67] K.G. Azzam, I.V. Babich, K. Seshan, L. Lefferts, Role of Re in Pt–Re/TiO2 catalyst for water gas shift reaction: A mechanistic and kinetic study, Appl. Catal. B Environ. 80 (2008) 129–140. doi:10.1016/j.apcatb.2007.11.015.

[68] Y. Sato, K. Terada, S. Hasegawa, T. Miyao, S. Naito, Mechanistic study of water–gas-shift reaction over TiO2 supported Pt–Re and Pd–Re catalysts, Appl. Catal. Gen. 296 (2005) 80–89. doi:10.1016/j.apcata.2005.08.009.

[69] K.G. Azzam, I.V. Babich, K. Seshan, B.L. Mojet, L. Lefferts, Stable and Efficient Pt–Re/TiO2 catalysts for Water-Gas-Shift: On the Effect of Rhenium, ChemCatChem. 5 (2013) 557–564. doi:10.1002/cctc.201200492.

[70] P.J. Dietrich, F.G. Sollberger, M.C. Akatay, E.A. Stach, W.N. Delgass, J.T. Miller, et al., Structural and catalytic differences in the effect of Co and Mo as promoters for Pt-based aqueous phase reforming catalysts, Appl. Catal. B Environ. 156–157 (2014) 236–248. doi:10.1016/j.apcatb.2014.03.016.

[71] C. Wang, D. van der Vliet, K.-C. Chang, H. You, D. Strmcnik, J.A. Schlueter, et al., Monodisperse Pt3Co Nanoparticles as a Catalyst for the Oxygen Reduction Reaction: Size-Dependent Activity, J. Phys. Chem. C. 113 (2009) 19365–19368. doi:10.1021/jp908203p.

[72] C. Wang, M. Chi, D. Li, D. van der Vliet, G. Wang, Q. Lin, et al., Synthesis of Homogeneous Pt-Bimetallic Nanoparticles as Highly Efficient Electrocatalysts, ACS Catal. 1 (2011) 1355–1359. doi:10.1021/cs200328z.

[73] R. Carrasquillo-Flores, J.M.R. Gallo, K. Hahn, J.A. Dumesic, M. Mavrikakis, Density Functional Theory and Reaction Kinetics Studies of the Water–Gas Shift Reaction on Pt–Re Catalysts, ChemCatChem. 5 (2013) 3690–3699. doi:10.1002/cctc.201300365.

[74] J. Knudsen, A.U. Nilekar, R.T. Vang, J. Schnadt, E.L. Kunkes, J.A. Dumesic, et al., A Cu/Pt Near-Surface Alloy for Water−Gas Shift Catalysis, J. Am. Chem. Soc. 129 (2007) 6485–6490. doi:10.1021/ja0700855.

[75] S.S. Chaugule, V.F. Kispersky, J.L. Ratts, A. Yezerets, N.W. Currier, F.H. Ribeiro, et al., Formation and removal of Ba-carbonates or carboxylates on Pt/BaO/γ-Al2O3 lean NOx traps, Appl. Catal. B Environ. 107 (2011) 26–33. doi:10.1016/j.apcatb.2011.06.029.

APPENDICES

Appendix A Appendix for Chapter 2

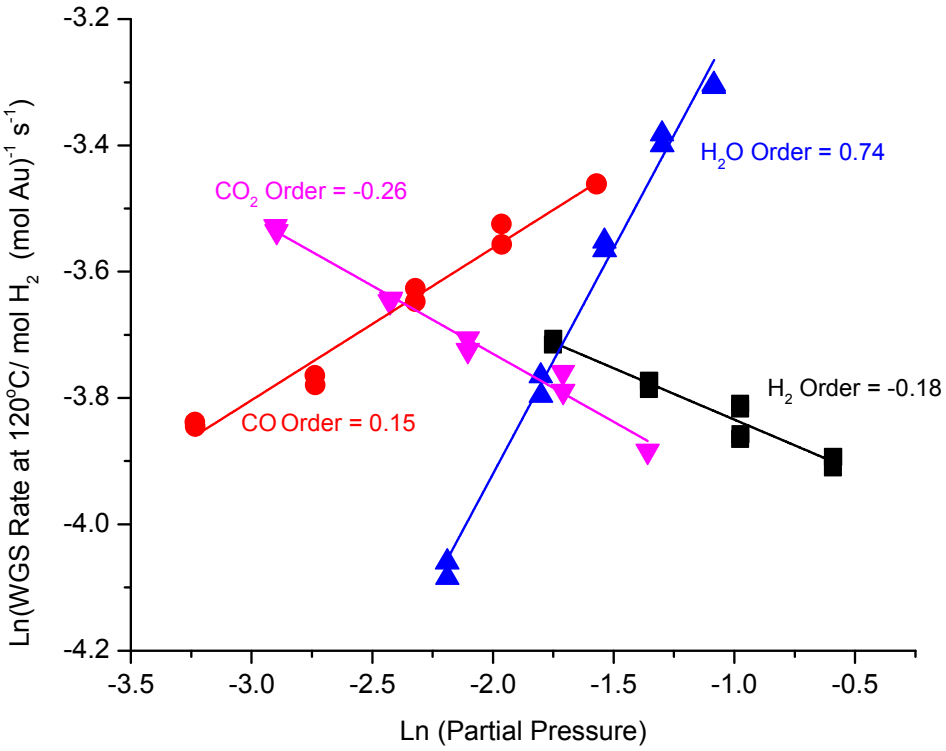

Figure A.1 Typical apparent reaction order plots of H_2O (triangles), CO (circles), CO_2 (inverted triangles) and H_2 (squares) for 1.5% Au/ Mo_2C catalyst at 120 ºC. Concentrations expressed as partial pressures (P/PT).

Table A.1 WGS kinetic data over Mo_2C and Metal/Mo_2C catalysts

Catalyst	Rate[a] /10^{-3} mol H_2 (mol metal)$^{-1}$ s^{-1}	Rate[b] /10^{-7} mol H_2 (g cat.)$^{-1}$ s^{-1}	BET Area (m^2/g)	E_a /kJ(mol)$^{-1}$ (±3)	H_2O (±0.04)	CO_2 (±0.04)	CO (±0.04)	H_2 (±0.04)
1.5 % Pt/Mo_2C	26	18	63	48	0.76	-0.02	0.06	-0.32
1.5% Pt/Mo_2C (Replicate)	27	19	--	45	0.72	-0.02	0.05	-0.33
1.5 % Au/Mo_2C	20	16	64	44	0.74	-0.26	0.15	-0.18
1.7% Pd/Mo_2C	6.8	14	62	63	0.79	-0.06	0.19	-0.51
1.8 % Ni/Mo_2C	3.4	9.5	69	70	0.59	-0.03	0.20	-0.45
1.5 % Cu/Mo_2C	2.2	5	65	84	-0.04	-0.14	0.46	-0.29
1.9% Ag/Mo_2C	1.5	3	61	87	-0.04	-0.09	0.48	-0.16
Mo_2C	-----	2	66	87	-0.09	-0.10	0.54	-0.12

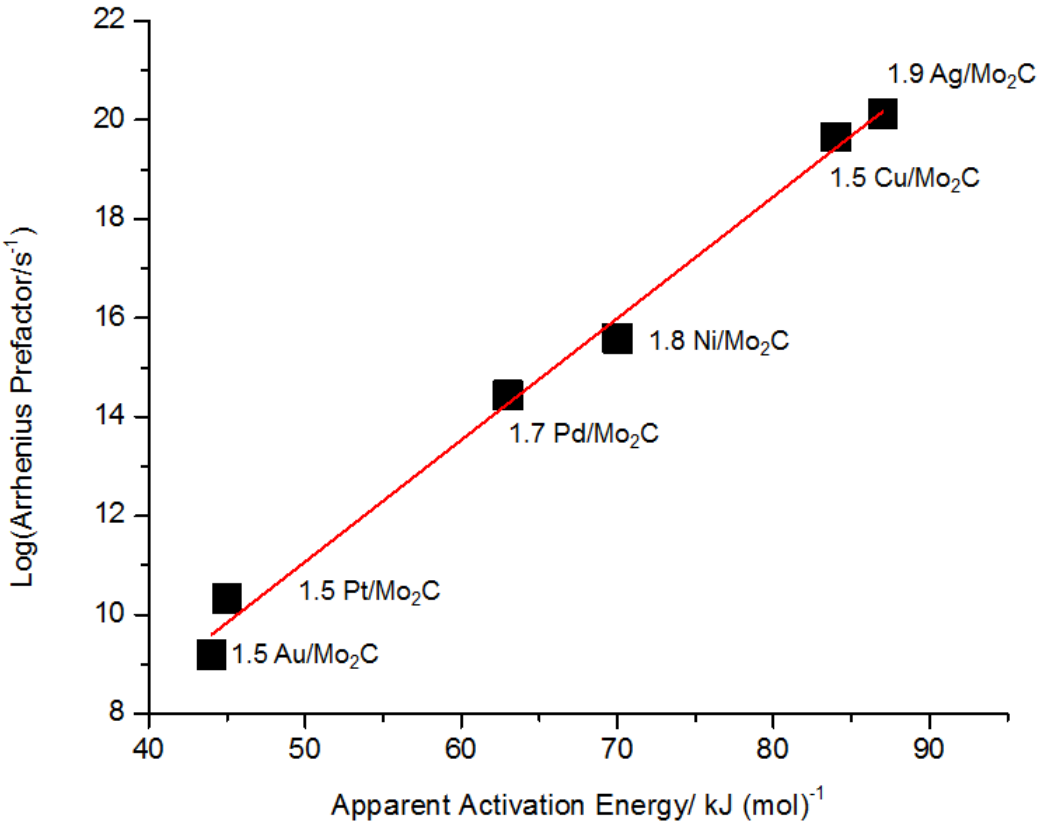

Figure A.2 Compensation plot for the Metal/Mo2C catalysts. The apparent Arrhenius Pre-factors were normalized by total moles of each metal.

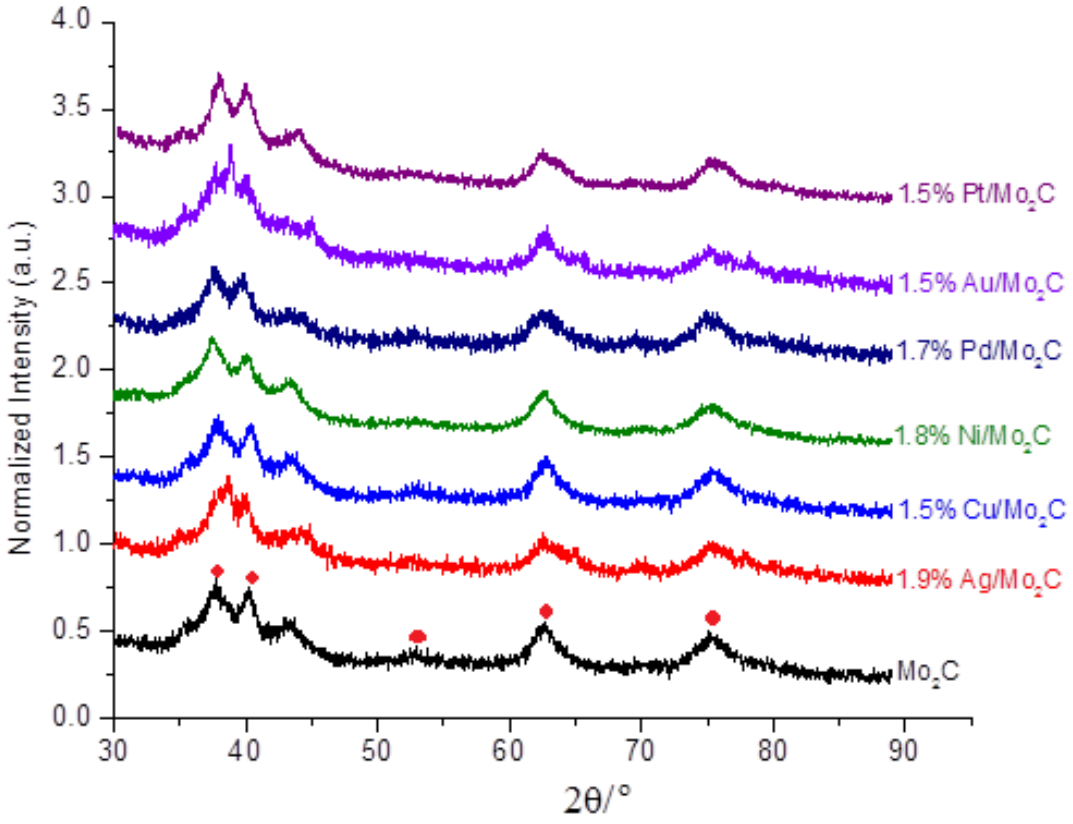

Figure A.3 X-ray diffraction patterns for Mo_2C and Metal/Mo_2C catalysts (● β-Mo_2C)

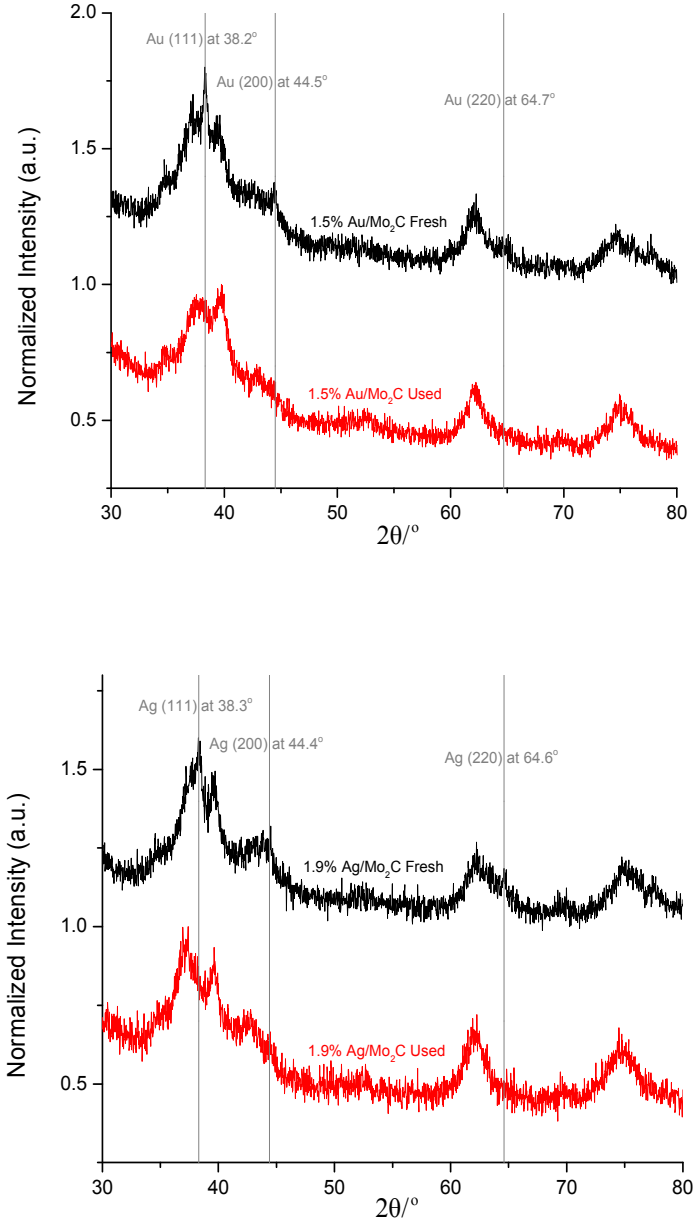

Figure A.4 (Top) the comparison of XRD patterns for fresh and used 1.5% Au/Mo_2C. The Au (111), (200) and (220) peaks are shown with the gray lines. (Bottom) the comparison of XRD patterns for fresh and used 1.9% Ag/Mo_2C. The Ag (111), (200) and (220) peaks are shown with the gray lines.

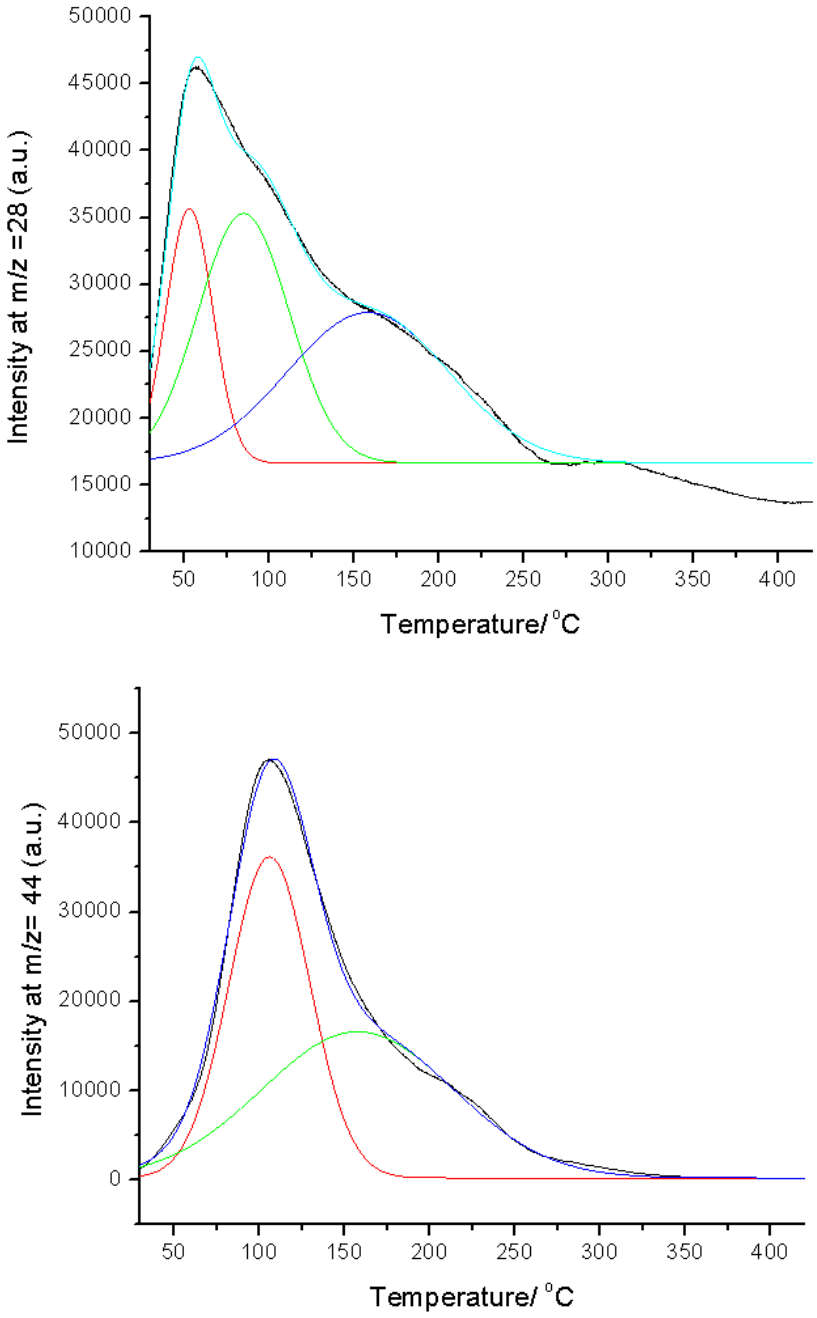

Figure A.5 Peak fitting for CO evolution (top) and CO_2 desorption (bottom) from the bulk Mo_2C support during the CO TPD experiment.

Table A.2 Quantification of CO adsorbed during static chemisorption measurement and CO+CO_2evolved during TPD. Static chemisorption was performed at 35 ^oC using Micromeritics ASAP 2020 analyzer. All catalysts were subjected to carburization at 600 ^oC prior to chemisorption measurement.

Catalyst	CO adsorbed during static measurement / µmol(g^{-1})	CO desorbed during TPD / µmol(g^{-1})	CO_2 evolved during TPD/ µmol(g^{-1})	Total (CO + CO_2 / µmol(g^{-1})
1.5%Pt/Mo_2C	378	360	35.8	395.8
1.5%Au/Mo_2C	366	357	38.2	395.2
1.7%Pd/Mo_2C	360	356	34	390
1.8%Ni/Mo_2C	371	398	5.7	403.7
1.9%Ag/Mo_2C	341	371	12.6	383.6
1.5%Cu/Mo_2C	358	370	14	384
Mo_2C	375	377	22	398

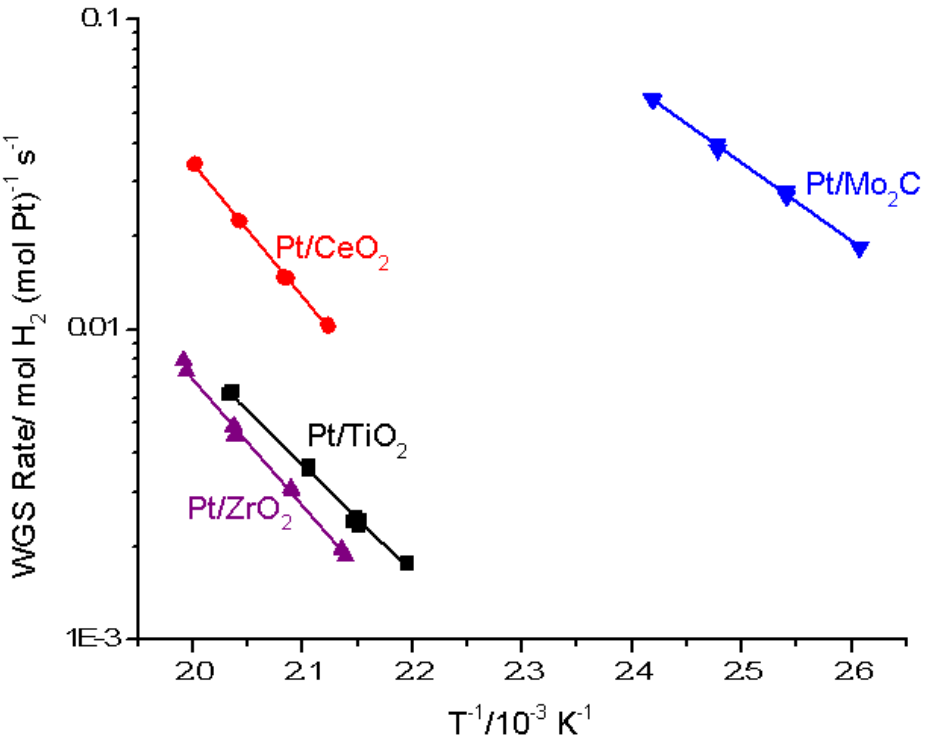

Figure A.6 Arrhenius plots for WGS over Pt/TiO_2, Pt/ZrO_2, Pt/CeO_2 and Pt/Mo_2C catalysts

Table A.3 *In situ* Au L_{III} edge EXAFS data for 1.5% Au/Mo_2C

Catalyst / (Pretreatment)/Condition	Au-Au CN	R(Å)	DWF (x 10^3)	E_o(eV)	Est. Size (nm)
Au/Mo_2C Fresh (Under Air) / RT	11.4	2.88	0.0	-0.7	9
Au/Mo_2C(carburization up to 600^0C)/ WGS at 160^0C	7.3	2.85	4.0	-1.9	2.5
Au/Mo_2C(carburization at 600^0C, WGS at 160^0C) He / RT	8.1	2.85	2.0	-1.7	3.0
Au/Mo_2C(carburization at 600^0C, WGS at 160^0C) Air / RT during passivation	8.6	2.86	2.0	-0.8	3.5

Table A.4 *In situ* Pt L_{III} edge EXAFS data for 1.5% Pt/Mo_2C

(Pretreatment) / Condition	Backscatter	CN	R(Å)	DWF (x 10^3)	E_o(eV)
(Freshly prepared Pt/Mo_2C) Air/ RT	Pt-Pt	2.2	2.32	3.0	3.0
	Pt-Cl	1.5	2.74	3.0	-3.1
Pt/Mo_2C Fresh	Pt-Pt	6.2	2.76	3.0	-4.6
(Pt/Mo_2C carburized at 600^0C)/ WGS at 160^0C	Pt-Mo	4.1	2.74	3.0	3.4
(Pt/Mo_2C carburized at 600^0C) WGS at 160^0C) He / RT	Pt-Pt	6.2	2.76	2.0	-4.1
	Pt-Mo	4.0	2.74	2.0	5.1
(Pt/Mo_2C carburized at 600^0C, WGS at 160^0C) Air / RT during passivation	Pt-Pt	5.8	2.76	2.0	-3.5
	Pt-Mo	3.7	2.74	2.0	5.1

Vibrational (infrared) spectroscopy experiment over 1.5% Pt/Mo_2C

The spectrometer used for the diffuse reflectance infrared spectroscopy experiment was a Nicolet Magna 550 FTIR and the DRIFTS cell was a Spectra-Tech Collector II with the high temperature/high pressure chamber. The details of the experimental setup can be found elsewhere [48]. The CO adsorption experiments were performed for three different dilutions of 1.5% Pt/Mo_2C with diamond dust (Catalyst: diamond dust = 1:10, 1:80 and pure Pt/Mo_2C). 100 mg of the sample was loaded in the sample holder and then subjected to reduction in presence of 25% H_2/Ar (450°C, 5 °C/min, soaked for 2 hours). The sample was then cooled to RT under Ar and then exposed to mixture of 10% CO/Ar for 2 hours. The DRIFTS spectra were recorded prior to CO adsorption, during CO adsorption and after the CO were cut off from the gas phase.

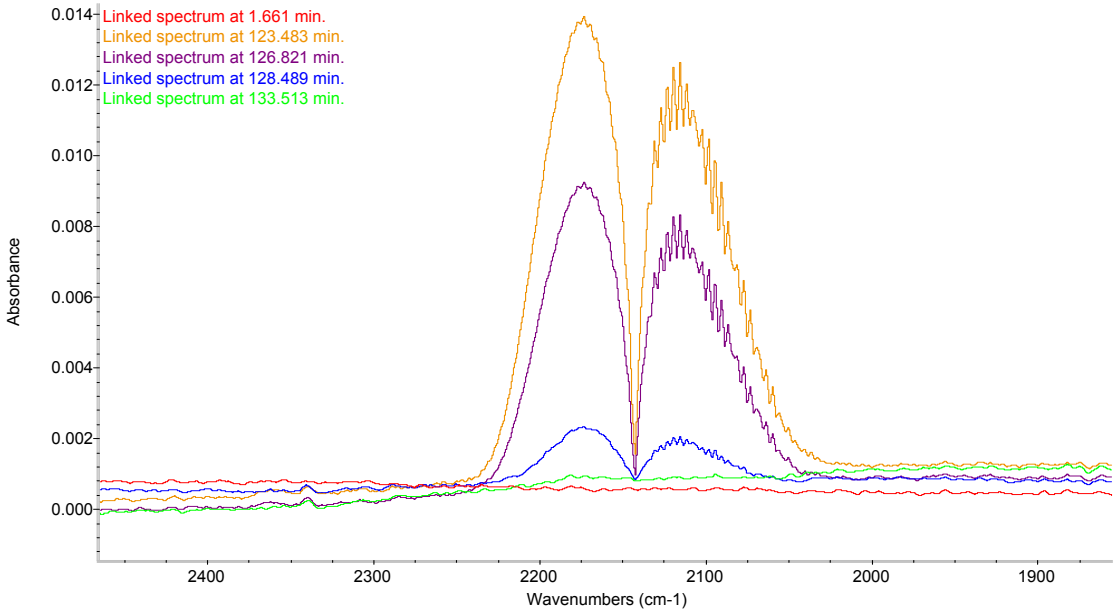

Figure A.7 Diffuse Reflectance Infrared Spectra (DRIFTS) for 1.5% Pt/Mo_2C diluted with diamond dust in the proportion 1:80.

As shown in Figure A.7, The spectrum recorded after 1.6 minutes is the background/ baseline spectrum when the sample was under inert at RT (after the reduction pretreatment). As expected, this spectrum did not show any significant peaks. The spectrum at 123 minutes was recorded shortly after the CO was cut off from the gas phase. The signature envelops corresponding to the gas phase CO can be clearly observed. Also, no peaks around the wave numbers below the gas phase CO envelop (around 2000 cm^{-1}), could be observed. The peaks for adsorbed CO are expected in this region at wavenumbers below those for the gas phase CO. The spectra collected at 126, 128 and 133 minutes show a progressive decrease in the intensity of gas phase CO. In fact, there was no gas phase CO detected at 133 minutes. At this point, a clearly discernible adsorbed CO peak should have been observed, as Pt supported on oxides exhibits a linear CO peak below 2100 cm^{-1}under WGS [42] .The absence of peaks related to adsorbed CO suggests that majority of the IR radiation was being absorbed by the black Mo_2C support.

The intensity recorded at the detector could be due solely to the reflectance occurring from the diamond dust particles in the sample. Similar results were obtained for the other dilution with diamond dust (1:10) and the pure Pt/Mo_2C sample. The adsorption of CO over this 1.5% Pt/Mo_2C sample was confirmed with a CO chemisorption experiment performed with Micrometrics ASAP 2020 instrument. The amount of CO adsorbed was 378 μmol/g at 35°C, which suggests that the CO covers about 33% of the catalyst surface (assuming 10^{19} sites/m^2).

Thus, despite the presence of a significant amount of adsorbed CO, it could not be observed with the DRIFTS experiment, which highlights the incompatibility for the Metal/Mo_2C catalysts for such experiment.

.

Appendix B Appendix for Chapter 3

Table B.1 *In situ* XANES and EXAFS Fit parameters for the Pt L_{III} edge over Pt/Mo_2C/MWCNT catalysts with varying Mo

Sample	Treatment	XANES		Edge Energy, keV (Pt = 11.5640)	Scatter	N	R, Å	$\Delta\sigma^2$ (x 10^3)	Eo, eV
		Fraction Pt^{+2}	Fraction Pt^0						
1.5% Pt, 2% Mo	Air RT	0.50	0.50	11.5646	Pt-O	1.9	2.04	4.0	-0.2
					Pt-Pt	2.6	2.65	4.0	-5.3
	H_2 600°C	-	1.0	11.5653	Pt-Mo	4.1	2.73	2.0	4.4
					Pt-Pt	4.6	2.74	2.0	-3.1
1.5% Pt, 3% Mo	Air RT	0.60	0.40	11.5649	Pt-O	2.4	2.04	4.0	-0.1
					Pt-Pt	2.3	2.65	4.0	-5.2
	H_2 600°C	-	1.0	11.5652	Pt-Mo	4.6	2.73	2.0	4.0
					Pt-Pt	4.6	2.74	2.0	-3.1
1.5% Pt, 10% Mo	Air RT	0.70	0.30	11.5649	Pt-O	2.5	2.04	4.0	0.6
					Pt-Pt	1.5	2.62	4.0	-5.4
	H_2 600°C	-	1.0	11.5652	Pt-Mo	3.8	2.73	2.0	3.5
					Pt-Pt	4.6	2.74	2.0	-3.6
1.5% Pt, 20% Mo	Air RT	0.60	0.40	11.5649	Pt-O	2.2	2.04	4.0	0.5
					Pt-Pt	1.7	2.63	4.0	-5.2
	H_2 600°C	-	1.0	11.5653	Pt-Mo	3.6	2.73	2.0	3.7
					Pt-Pt	4.6	2.74	2.0	-3.4

Table B.2 *In situ* EXAFS fit parameters over Pt/Mo_2C/MWCNT catalysts with varying Pt loading

Sample	Treatment	Edge Energy, keV (Pt = 11.5640)	Scatter	N	R, Å	$\Delta\sigma^2$ (x 10^3)	Eo, eV
0.5% Pt, 10% Mo	H_2 600°C, He RT	11.5650	Pt-Mo	4.4	2.73	2.0	2.3
			Pt-Pt	4.9	2.74	2.0	-3.9
	160°C WGS	11.5650	Pt-Mo	4.3	2.73	4.0	1.8
			Pt-Pt	5.0	2.74	4.0	-4.6
1.5% Pt, 10% Mo	H_2 600°C, He RT	11.5649	Pt-Mo	4.9	2.73	2.0	3.6
			Pt-Pt	4.9	2.74	2.0	-4.1
	160°C WGS	11.5650	Pt-Mo	4.9	2.73	4.0	3.7
			Pt-Pt	5.4	2.74	4.0	-4.3
3% Pt, 10% Mo/	H_2 600°C, He RT	11.5650	Pt-Mo	4.9	2.73	2.0	4.6
			Pt-Pt	5.4	2.74	2.0	-4.1
	160°C WGS	11.5650	Pt-Mo	4.9	2.73	4.0	5.2
			Pt-Pt	6.1	2.74	4.0	-4.1
5% Pt, 10% Mo	H_2 600°C, He RT	11.5650	Pt-Mo	4.5	2.73	2.0	1.8
			Pt-Pt	5.1	2.74	2.0	-4.9
	160°C WGS	11.5650	Pt-Mo	4.4	2.73	4.0	5.4
			Pt-Pt	6.7	2.74	4.0	-4.3

Table B.3 The linear combination XANES fits for Pt/Mo_2C/MWCNT catalysts under WGS conditions (6.8% CO, 8.5% CO_2, 22% H_2O, 37.4% H_2 and balance He).

Catalyst	% of Pt in contact with Mo_2C	% Pt in contact with MWCNT	WGS Rate at 120°C/ 10^{-2} mol H_2 (mol Pt)$^{-1}$ s^{-1}	WGS Rate at 120°C/10^{-2} mol H_2 (mol Pt on Mo_2C)$^{-1}$ s^{-1}
1.5% Pt/ 2% Mo/ MWCNT	73	27	0.9	1.2
1.5% Pt/ 3% Mo/ MWCNT	82	18	1.3	1.6
1.5% Pt/ 10% Mo/ MWCNT	92	8	1.7	1.8
1.5% Pt/ 20% Mo/ MWCNT	99	1	1.9	1.9
0.5% Pt/ 10% Mo/ MWCNT	98	2	1.5	1.6
3% Pt/ 10% Mo/ MWCNT	96	4	1.3	1.4
5% Pt/ 10% Mo/ MWCNT	99	1	1.2	1.2

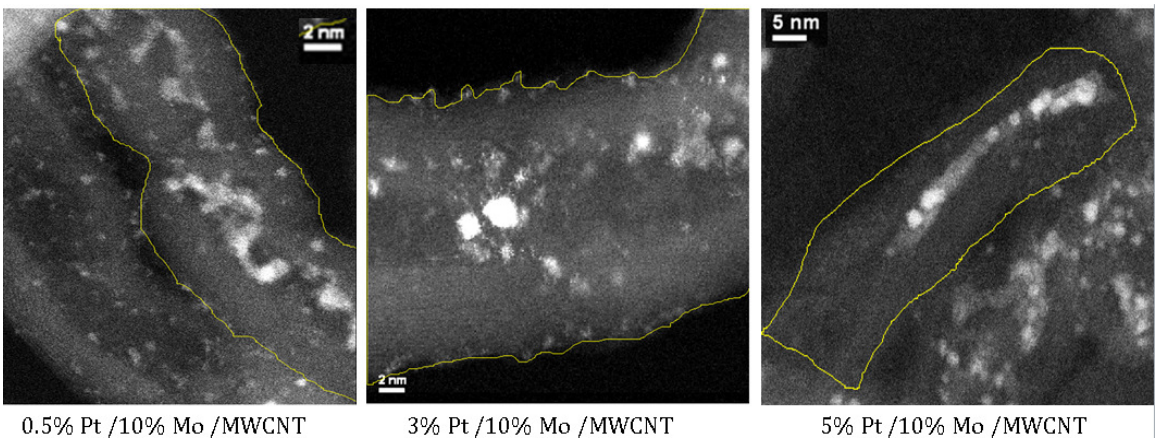

Figure B.1 HAADF-STEM micrographs of the catalysts with varying Pt loading at a fixed Mo loading

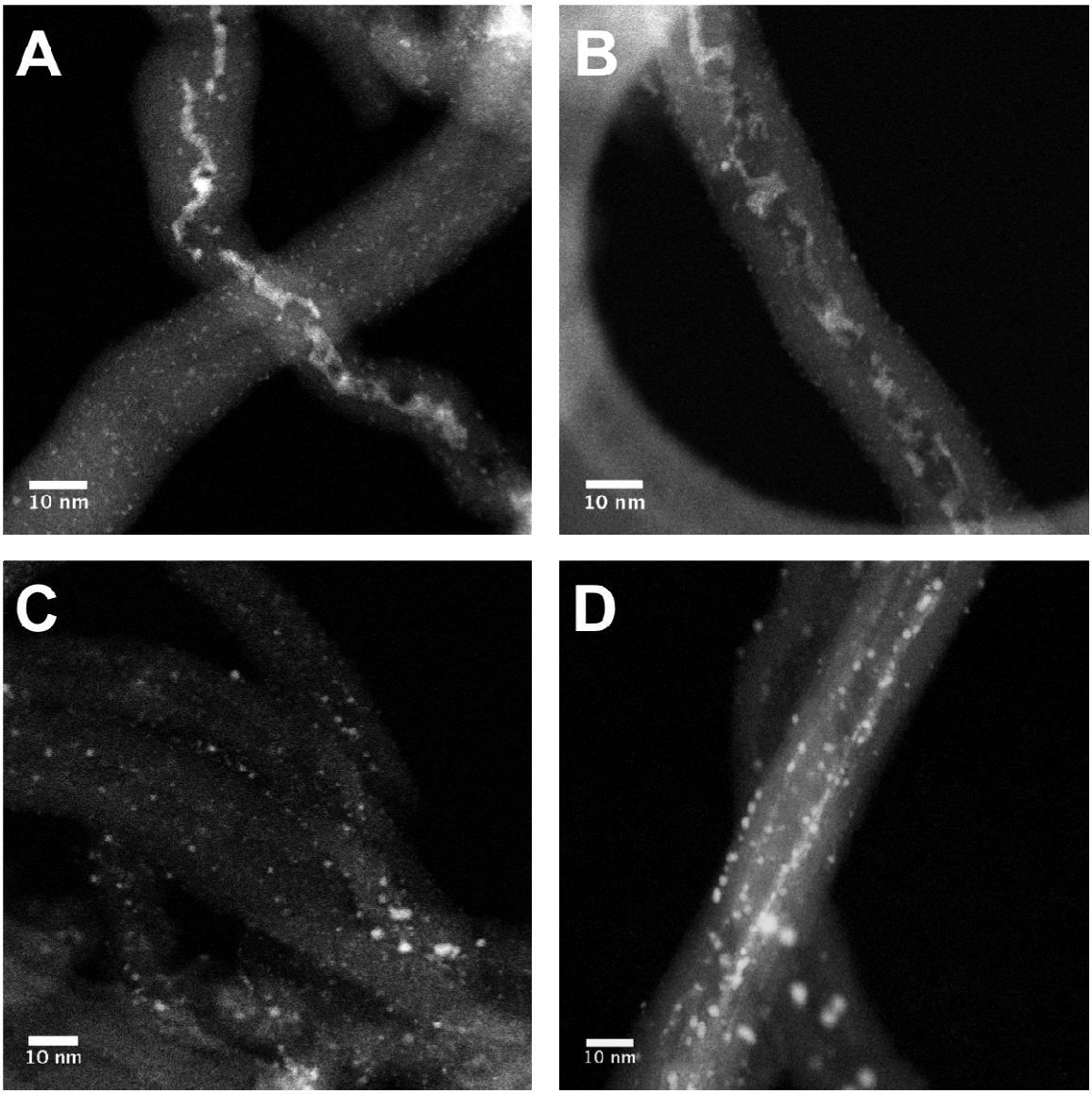

Figure B.2 HAADF-STEM micrographs of Pt / 10% Mo/ MWCNT catalysts with varied Pt loading (A) 0 wt% Pt (B) 0.5 wt% Pt (C) 3 wt% (D) 5 wt%

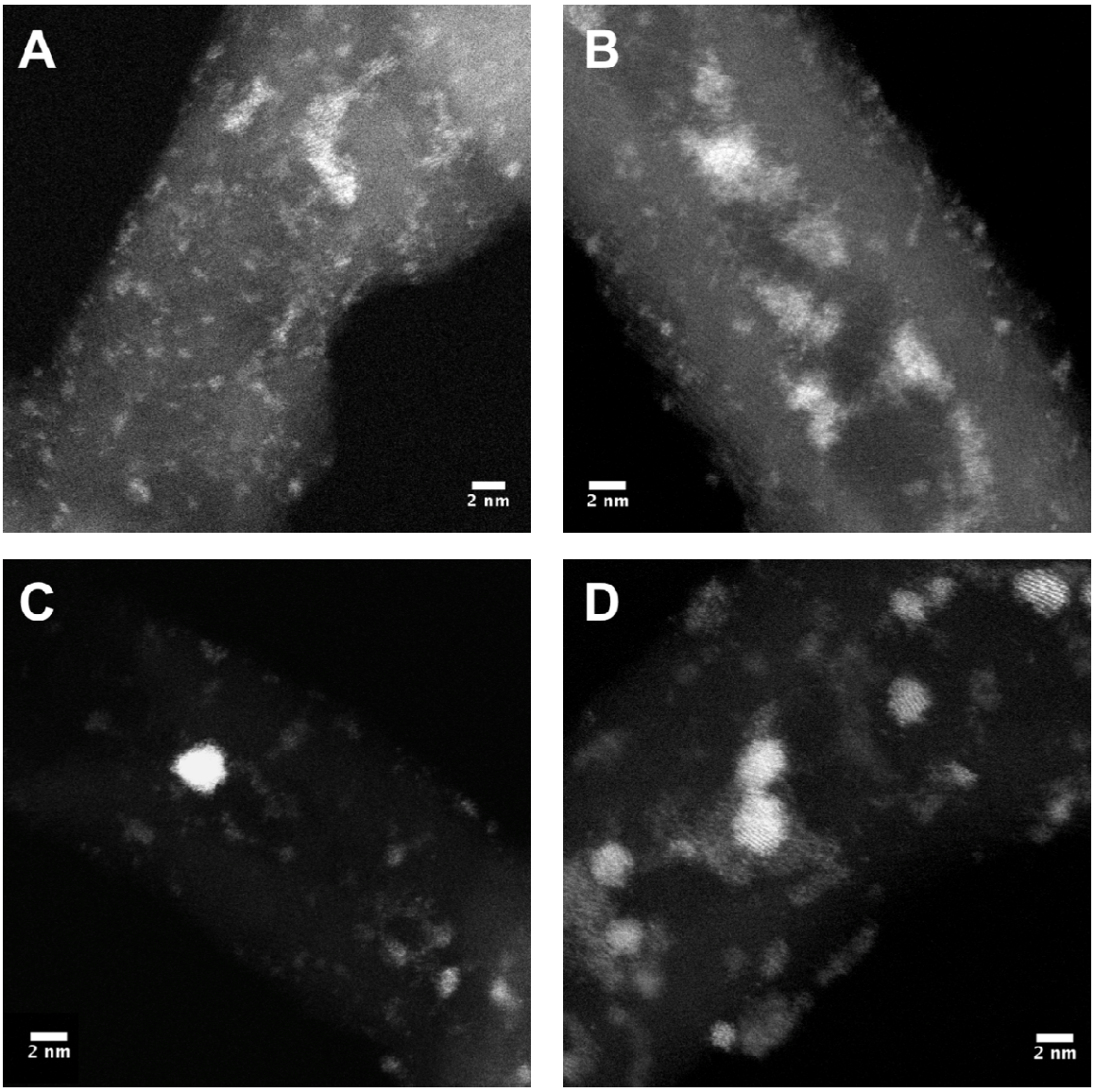

Figure B.3 High Resolution HAADF-STEM micrographs of Pt / 10% Mo/ MWCNT catalysts with varied Pt loading (A) 0 wt% Pt (B) 0.5 wt% Pt (C) 3 wt% (D) 5 wt%

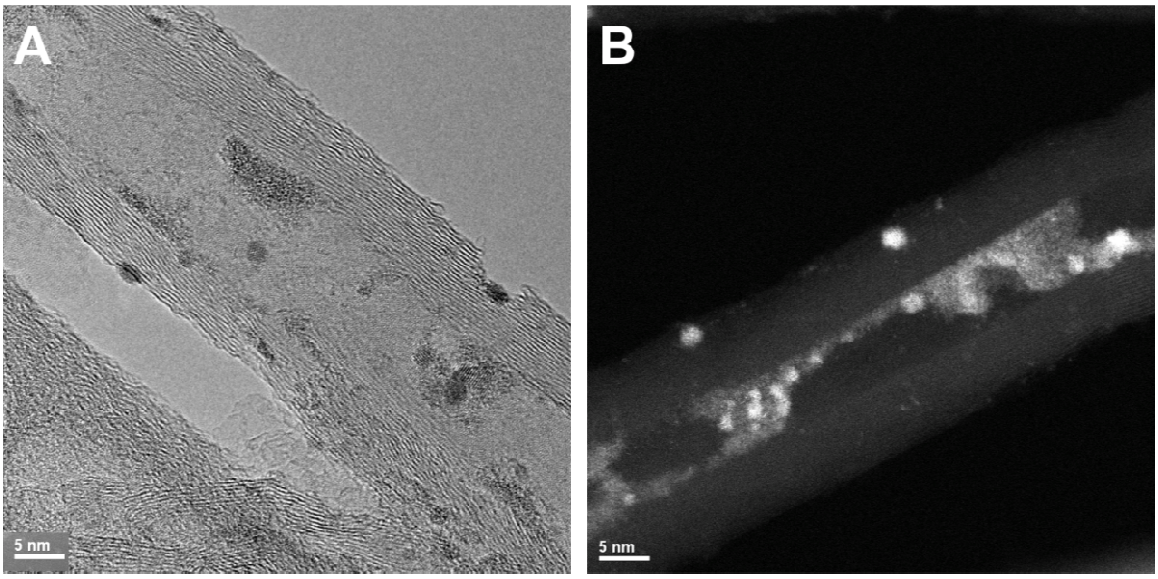

Figure B.4 Micrographs of 1.5% Pt/ 10% Mo/MWCNT catalysts (a) TEM micrograph of after WGS reaction (b) HAADF-STEM micrograph of the fresh catalyst

TEM micrograph of the 1.5% Pt/ 10% Mo/MWCNT sample is shown in Figure B.4-a. Pt and Mo species provide good contrast with the carbon nanotube and are easily detected. The mass-thickness differences creates this amplitude contrast on TEM micrographs and Pt particles provide more contrast compared to Mo species owing to their higher atomic number, Z. Accordingly, smaller and darker species are suspected to be Pt particles, whereas larger but lighter regions could be Mo-rich species, possibly Mo_2C. Amplitude contrast is not directly interpretable and element specific spectroscopy imaging is needed to identify the chemical nature of the observed species.

HAADF-STEM micrograph on the other hand, provides not only higher contrast between carbon, molybdenum and platinum species but can also be interpreted more straightforward manner. The observed contrast on HAADF-STEM scales with thickness × atomic mass^2, ($t \times Z^2$) and makes the interpretation of the micrograph easy. Carbon

nanotubes offer a structure of uniform thickness so that the contrast difference between other species is mainly due to their chemical nature. Accordingly, region of higher atomic number would appear brighter, whereas as low-Z region would appear darker. As a result three different contrast levels are recognized on the micrograph shown in Figure B.4-b and can be matched with carbon (dark regions), Mo-species (bright features) and Pt (brightest regions). Based on this assignment, the structure of the 1.5% Pt/ 10% Mo/MWCNT catalyst hosts Pt particles that are in close contact with Mo-species supported on carbon nanotube.

EELS mapping confirmed the assignment of chemical nature based on the HAADF-STEM contrast. Figure B.5 shows the HAADF-STEM micrograph of the 5% Pt/ 10% Mo/ MWCNT catalyst. STEM-EELS maps of the same region are acquired using the C K-edge, Pt $M_{4,5}$ and Mo $M_{4,5}$ edges. The brightest feature on the HAADF micrograph is confirmed to be Pt. Other structures with slightly lower brightness are identified as Mo and carbon is found to provide the lowest brightness among other elements as expected. Worth to mention is the regions where Pt and Mo co-exist hinting to the mixing of Pt and Mo.

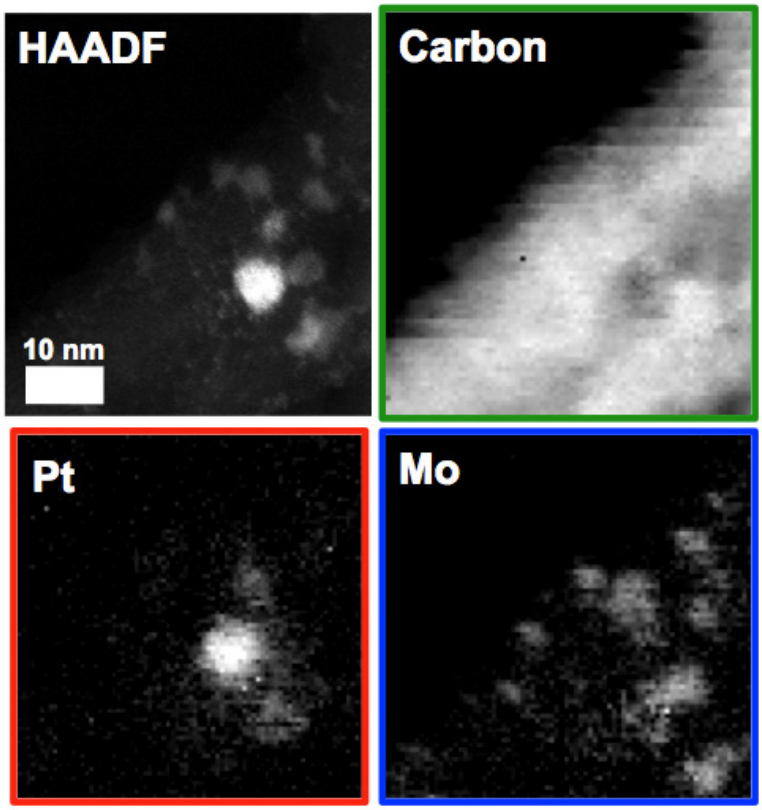

Figure B.5 HAADF STEM micrograph and elemental maps of the 5% Pt / 10% Mo /MWCNT catalyst

Appendix C Appendix for Chapter 5

Table C.1 WGS Kinetic data over the series of PtCo/MWCNT catalysts

a. Rate extrapolated to 300°C

b. Catalysts subjected to acetic acid leaching at 25°C

Catalyst	Pt	PtCo 1:1	PtCo 1:2	PtCo 1:3	PtCo 1:5	PtCo 1:8	PtCo 1:3 L[b]	PtCo 1:5 L	PtCo 1:8 L	Pt_3Co
Test Temp./°C	290	275	260	250	250	250	310	310	310	330
Rate[a]/10^{-2} mol H_2 (mol Pt.)$^{-1}$ s^{-1}	0.96	1.9	4.4	9.3	9.4	8.4	0.19	0.34	0.35	0.14
Ea /kJ(mol)$^{-1}$(±3)	86	96	114	137	142	136	118	116	118	113
H_2O (±0.04)	0.83	0.90	1.1	1.1	1.1	0.90	1.0	1.0	0.75	0.87
CO (±0.04)	0.10	-0.01	-0.03	-0.26	-0.17	-0.20	-0.10	-0.02	0.00	-0.03
CO_2 (±0.04)	-0.05	-0.11	-0.07	-0.01	-0.01	-0.01	-0.05	-0.02	-0.05	-0.04
H_2 (±0.04)	-0.38	-0.47	-0.52	-0.57	-0.47	-0.49	-0.58	-0.58	-0.59	-0.54

Table C.2 CO Chemisorption and WGS TOR data for PtCo/MWCNT Catalysts

Catalyst	CO Adsorbed at 35°C / μmol g^{-1}	WGS TOR at 300°C/ 10^{-2} mol H_2 (mol CO ads)$^{-1}$ s^{-1}
Pt/MWCNT	49	4.6
Pt/MWCNT treated with acetic acid	21	4.2
PtCo 1:1/ MWCNT	51	9.0
PtCo 1:2/ MWCNT	57	22
PtCo 1:3/ MWCNT	51	46
PtCo 1:5/ MWCNT	62	39
PtCo 1:8/ MWCNT	71	30
PtCo 1:3 /MWCNT Leached	47	2.1
PtCo 1:5/ MWCNT Leached	21	1.8
PtCo 1:8/ MWCNT Leached	52	1.7
Pt_3Co/ MWCNT	19	1.8

Table C.3 Results of linear combination XANES fits of the Co K edge for the as prepared leached PtCo/MWCNT catalysts. Co foil was used as a standard for metallic Co, while CoO powder was used a s reference for Co^{2+}

Catalyst	% Co	% Co^{2+}
PtCo 1:1/MWCNT	91	9
PtCo 1:2/MWCNT	89	11
PtCo 1:3/MWCNT	87	13
PtCo 1:5/MWCNT	86	14
PtCo 1:8/MWCNT	80	20
PtCo 1:3/MWCNT Leached with acetic acid	100	0
PtCo 1:5/MWCNT Leached with acetic acid	100	0
PtCo 1:8/MWCNT Leached with acetic acid	100	0

Table C.4 Pt L_{III} edge EXAFS data fit parameters for the PtCo/MWCNT catalysts.

Catalyst	Pt-Pt				Pt-Co				Total CN
	CN	R/Å	σ^2	E_0/eV	CN	R/Å	σ^2	E_0/eV	
PtCo(1:1)	5.9	2.71	0.002	-2.6	2.1	2.58	0.002	2.9	8
PtCo(1:2)	6	2.72	0.002	-2.7	2.8	2.59	0.002	4.3	8.8
PtCo(1:3)	5	2.71	0.002	-3.4	3.5	2.58	0.002	3.6	8.5
PtCo(1:5)	5.9	2.71	0.002	-5.4	2.9	2.58	0.002	4.9	8.8
PtCo(1:8)	5.9	2.71	0.002	-5.2	2.6	2.58	0.002	4.6	8.5
PtCo(1:3) Leached	6.7	2.74	0.002	0	2.5	2.61	0.002	3.4	9.2
PtCo(1:5) Leached	6.6	2.74	0.002	-1	1.4	2.61	0.002	0.7	8
PtCo(1:8) Leached	6.6	2.73	0.002	-2.3	1.7	2.6	0.002	2.9	8.3
Pt_3Co	6.2	2.73	0.002	-3.1	3.4	2.59	0.002	3.0	9.6

VITA

VITA

Kaiwalya D. Sabnis
Graduate School, Purdue University

Education

Bachelor of Chemical Engineering, 2010, Institute of Chemical Technology, Mumbai India
Doctor of Philosophy, Chemical Engineering, 2014, Purdue University, Indiana, USA

Experience

Graduate Research (Purdue University)

- Measured detailed water-gas shift (WGS) reaction kinetics over more than 150 catalysts.
- Prepared transition metal carbides using temperature programmed carburization and supported catalysts using incipient wetness impregnation and deposition precipitation.
- Devised a method of synthesizing thermally robust transition metal catalysts supported on molybdenum carbide, possessing higher activity compared to the commercial WGS catalyst. Characterized prepared catalysts using Transmission Electron Microscopy (TEM), X-ray Absorption Fine Structure (XAFS), Chemisorption and Temperature Programmed Reduction techniques.
- With the use of reaction kinetics, identified the CO adsorption strength as a potential descriptor for the WGS reaction rate over Metal/molybdenum carbide systems.
- Used *in situ* XAFS techniques to determine that adhesive interaction between supported metal particles and the native molybdenum carbide surface is stronger than the metal-metal cohesion. Studied and quantified the promotional effects of alkali metals over supported Pt catalysts for the WGS reaction.
- Part of the *operando* X-ray absorption characterization team for aqueous phase reforming of glycerol for hydrogen production using supported bimetallic catalysts.

Undergraduate Design Project (ICT, Mumbai, India)

- Designed a plant to manufacture 10,000 TPA of Ultrastable Y Zeolite (Faujasite, USY).
- Performed material and energy balance calculations, equipment design and process control and instrumentation design over chosen units.
- Determined the plant location and evaluated the economic feasibility of the project.

Summer Intern (Innotech Pharmaceuticals Limited, Aurangabad, India)

- Established energy balances, identified bottlenecks and designed heat exchangers for energy integration in the chloroquinone (an antimalerial drug) plant.
- Involved in the design of heat integration systems for the distillation columns to reduce the overall steam consumption by 15%.

Teaching (Purdue University)

- Teaching assistant for graduate level Advance Transport Phenomena in Fall 2011.
- Teaching assistant for the Chemical Engineering Laboratory I, Fall 2013.

Skills

- Experimental/Analytical: GC-MSD, Catalyst Synthesis, Reaction Kinetics, TEM, XAFS, Temperature Programmed Techniques (TPR/TPD), Infrared (IR) Spectroscopy, Chemisorption, XPS and XRD.
- Computational: MATLAB, Mathematica, WinXAS, CasaXPS, LabView, MS Office, JMP, SAS.

Awards and Honors

- Outstanding Poster Presentation Award, Graduate Research Symposium – School of Chemical Engineering, Purdue University, 2012.
- Invited Keynote Lecture, 2012 AIChE annual meeting Pittsburgh, PA, 2012.
- Best Presentation Award, Catalytic Hydrogen Generation Session, AIChE annual meeting, Pittsburg, PA, 2012.
- 'Best Paper' initiative invitation, AIChE Journal, 2012.
- Estus H. and Vasthti L. Magoon Award for Excellence in Teaching, College of engineering, Purdue University, 2014.

Presentations

- K.D. Sabnis, M. Shekhar, W.D. Williams, W.S.Lee,, J.T. Miller, W.N. Delgass, F.H. Ribeiro, 246th ACS National Meeting, *Catalysis of Water-Gas Shift: Effect of Oxide Support*, Indianapolis, IN, September 2013.
- K.D. Sabnis, Y. Cui, F.G Sollberger, M. Shekhar, W.S.Lee M. Cem Akatay,, J.T. Miller, W.N. Delgass, F.H. Ribeiro, 23rd North American Meeting, *Water-Gas Shift Catalysis over Transition Metals Supported on Molybdenum Carbide*, Louisville, KY, June 2013.
- K.D. Sabnis, M. Shekhar, W.D. Williams, W.S.Lee,, J.T. Miller, W.N. Delgass, F.H. Ribeiro, Michigan Catalysis Society Symposium, *Catalysis of Water-Gas Shift over Supported Au Nanoparticles*, Dearborn, MI, May 2013
- Keynote Address: K.D. Sabnis, Y. Cui, F.G Sollberger, M. Shekhar, W.S.Lee M. Cem Akatay,, J.T. Miller, W.N. Delgass, F.H. Ribeiro, AIChE Annual Meeting *Water-Gas Shift Catalysis over Transition Metals Supported on Molybdenum Carbide*, Pittsburgh, PA,, October 2012.
- K.D. Sabnis, M. Shekhar, W.S.Lee, J.T. Miller, W.N. Delgass, F.H. Ribeiro, Spring Symposium of the Catalysis Club of Chicago, *Water-Gas Shift Catalysis over Transition Metals Supported on Molybdenum Carbide*, Naperville, IL, May 2012.

Leadership and Teamwork

- ChE GSO Safety Committee Representative, Purdue University: Organized safety awareness seminars, Participated in the periodic safety reviews of the chemical engineering department building.
- Industrial Liaison Committee Head, GSO Research Symposium, Chemical Engineering, Purdue University, 2013.
- Event Coordinator, 'Exergy 2010', national level technical symposium, ICT, Mumbai.